Title
Monometallic and Bimetallic Complexes with Sulfonamido-Based Tripodal Ligands

Author
Lau, Nathanael

Publication Date
2017

UNIVERSITY OF CALIFORNIA,
IRVINE

Monometallic and Bimetallic Complexes with Sulfonamido-Based Tripodal Ligands

DISSERTATION

submitted in partial satisfaction of the requirements for the degree of

DOCTOR OF PHILOSOPHY

In Chemistry

By

Nathanael Lau

Dissertation Committee:
Professor Andrew S. Borovik, Chair
Professor William J. Evans
Professor Alan F. Heyduk

2017

DEDICATION

Where would I be without others?
No one is master of their own success
This work was impossible without my sisters and brothers
I am ever grateful to my God, family, and friends for their largesse

To Andy, my advisor, I owe the most
For the guidance that shaped me into the chemist I am today
To my labmates, the Boroviks, a toast
For the laughs, the tears, the work, the play

To my family, my firm foundation
Thank you for your support, your caring, your love
To my friends, thank you for your kindness and validation;
My community here is a gift from above

Remember others, the storms we have weathered
Remember all we have accomplished together

TABLE OF CONTENTS

LIST OF FIGURES

LIST OF SCHEMES

LIST OF TABLES

ACKNOWLEDGEMENTS

Thank you, Andy, for believing in me. Due to a long layoff in the field and my difficult undergraduate experience, I lacked confidence in my ability to do science when I first arrived at UCI. You mentored me expertly by adapting your style to suit my changing needs. By initially guiding me closely, providing perspective in hard times, encouraging me constantly, and later feeding me with difficult but achievable problems that developed my abilities, you helped forge me into the scientist I am today. I am also very grateful for your expectation that our group produce high quality scientific presentations. You are an excellent teacher, and taught the group how to effectively communicate science to many types of audiences. Also, thank you for encouraging me to pursue excellence in graphic design. Being in your supportive lab allowed me to hone my design abilities to unprecedented levels.

I must also thank the other fantastic professors in the inorganic department at UCI. Professors Alan Heyduk and Bill Evans, thank you for agreeing to be on my dissertation committee and for all your excellent feedback and instruction during my time here. Professor Jenny Yang, thank you for allowing me to teach with you for much of my time here and for the great experience that it was.

I also thank the expert facility managers at UCI for all their help with various characterization methods. Dr. Joe Ziller, Dr. Jordan Corbey, Jason Jones, and Mikey Wojnar, thank you for all your help with X-ray crystallography. Thank you, Dr. Phil Dennison, for your help in the NMR facilities. Dr. John Greaves, Dr. Felix Grun, and Dr. Dmitriy Uchenik, thank you for your help with air-free mass spectrometry, with a special mention of Dr. Beniam Berhan. My friend, you'll never walk alone, especially under a blue moon.

I would not be the scientist I am today without the support of my lab mates in the Borovik group. Our group has a friendly and collaborative atmosphere that truly makes it a special lab to work in. Everyone in the Borovik group has been a tremendous resource to me. I am particularly indebted to Dr. Yohei Sano and Dr. Nathaniel Sickerman. Thank you both for patiently training me when I first started in the lab. I learned most of the key skills that carried me through these past five years from you. Dr. Jonathan Paretsky is one of the most fun and welcoming people I know. Thank you for making it easy to want to join our group, and for all your work towards building camaraderie and coziness. I was fortunate to join the group with two fantastic scientists and gentleman, Jason Jones and Sam Mann. Thank you for soldiering with me through all the major milestones at UCI, be it classes, advancement, or graduation. You are dear friends who inspired me to constantly grow through your insight and hard work. I must also thank my seniors and postdocs for their friendship and wisdom: Dr. David Marsh, Dr. Sarah Cook, Dr. Ethan Hill, Dr. Taketo Taguchi, Dr. Noam Levi, Dr. Maisha Kamunde-Devonish, Dr. Justin Bogart, Dr. Lisa Olshansky, Dr. Suman Barman, and Dr. Deborah Brazzolotto. I am also thankful for my juniors: Victoria Oswald, Kelsey Rose Miller, Justin Lee, Dolores Ross, and Sunny Sun.

I have been blessed to have found a supportive community in Irvine outside of my lab. I thank my friends within the chemistry department, especially Dr. Ryan Langeslay, his wife Angeline, Dr. Kyle Rosenkoetter, as well as my teammates on the various iterations of the Sharks with Lasers flag football team (pew pew pew) and the Bad Life Choices softball team. I also have tremendous friends outside of the department. Winnie Chung, Timothy Johnson, Xiaoting Zheng, Justin Rowe, and Timothy Plett, thank you for your deep and impactful friendships. You stood with me through everything during my graduate experience, and I know that we will remain lifelong friends. Sarah Li, Stephen Wilke, Andrew Bartlett, Dennis Lam, Stephen and Sharon Crane, and Stephanie Hwang, thank you also for all your love and support.

Finally, I must thank my beloved family. Heavenly Father, thank you for getting me into graduate school through a non-conventional way and for always being there with me. I deeply love my parents David and Alia, who are my best friends. Mom and dad, thank you for guiding me prudently, supporting me generously, and loving me unconditionally. I thank my brother Shanan for all his support, who along with my cousins Kimbly, Viola, and Thomas, have walked with me through the many ups and downs of graduate school. I am also grateful to the rest of the Lau clan, as well as the Man family, whose love and collaboration taught me how to live well in community.

I could not have completed this work without standing on the shoulders of giants like yourselves. I am eternally grateful for you all.

CURRIVULUM VITAE

Nathanael Lau

Education

University of California, Irvine – Irvine, CA June 2017

- Doctor of Philosophy Candidate: Chemistry
- Research Advisor: Professor A. S. Borovik

Alliant International University – San Francisco, CA July 2011

- Masters of Arts in Education: Teaching

California Institute of Technology – Pasadena, CA June 2008

- Bachelor of Science: Chemistry, History

Publications and Presentations

Lau, N.; Sano, Y.; Weitz, A. C.; Ziller, J. W.; Hendrich, M. P.; Borovik, A. S. Modular Bimetallic Complexes with a Sulfonamido-Based Ligand. *In preparation*

Sano, Y.; Lau, N.; Weitz, A. C.; Ziller, J. W.; Hendrich, M. P.; Borovik, A. S. Models for Unsymmetrical Active Sites in Metalloproteins: Structural, Redox, and Magnetic, Properties of Bimetallic Complexes with M^{II}–(μ-OH)–Fe^{III} Cores (M^{III} = Mn^{II}, Fe^{II}, Co^{II}, Ni^{II}, Cu^{II}, and Zn^{II}). *In preparation*

Lau, N.; Sano, Y.; Ziller, J. W.; Borovik, A. S. Terminal Ni^{II}−OH/−OH_2 complexes in trigonal bipyramidal geometry prepared from H_2O. *Polyhedron* **2017**, *125*, 179-185

Lau, N.; Borovik, A. S. Chemical and spectroscopic characterization of a monomeric Ni(II)–OH complex derived from water, Presentation at the 251th National Meeting of the American Chemical Society, San Diego, CA, Mar 13–17, 2016; American Chemical Society: Washington, DC, 2016; INOR 1261

Lau, N.; Ziller, J. W.; Borovik, A. S. Sulfonamido tripods: tuning redox potentials via ligand modifications. *Polyhedron* **2015**, *84*, 777-782

Teaching Experience

Teacher's Assistant Sept 2012
University of California, Irvine – Irvine, CA – Present

High School Chemistry Teacher Aug 2009
Ánimo Locke #3 Charter High School – Watts, Los Angeles, CA – June 2011

High School Chemistry and Conceptual Physics Teacher Aug 2008
East Oakland School of the Arts – Oakland, CA – June 2009

High School Chemistry Summer School Teacher and Oakland Teaching Fellow June 2008
Oakland Teaching Fellows – Oakland, CA – Aug 2008

ABSTRACT OF DISSERTATION

Monometallic and Bimetallic Complexes with Sulfonamido-Based Tripodal Ligands

By

Nathanael Lau

Doctor of Philosophy in Chemistry

University of California, Irvine, 2017

Professor Andrew S. Borovik, Chair

A central tenet of chemistry is the importance of the local environments that surround molecules. Rules for how such local environments control molecular properties have been developed and form the basis for coordination chemistry, an area of chemistry devoted to the study of molecules containing metal ions. Within this context, the volume of space surrounding metal ions is divided into two regions, referred to as the primary and secondary coordination spheres. The primary coordination sphere involves covalent interactions between atoms on ligands that are directly bound to the metal center. The secondary coordination sphere, which involves non-covalent interactions, is part of the volume of space around the metal center and often interacts with the ligands of the primary coordination sphere. Together, the coordination spheres define the physical properties and reactivity of a metal ion. The importance of modulating both is seen within the active sites of metalloproteins, in which the interplay between the two coordination spheres allow these proteins to catalyze difficult reactions under ambient conditions, with selectivities and efficiencies that are currently unattainable in synthetic systems.

One approach towards understanding how the two coordination spheres affect function involves specially designed ligands that account for effects in both coordination spheres. The aim of this dissertation is to study synthetic metal complexes that incorporate these types of ligands, and explore their fundamental physical, structural, and chemical properties. The ligands used are based on the tripodal sulfonamido-based ligand *N*,*N′*,*N″*-[2,2′,2″-nitrilotris(ethane-2,1-diyl)]tris(2,4,6-trimethylbenzenesulfonamido) ($[MST]^{3-}$). This ligand contains a tris(2-aminoethyl)amine (tren) backbone that allows for the preparation of four- or five-coordinate metal complexes with local C_3 symmetry to control the primary coordination sphere. The trigonal environment leads to high-spin metal complexes, and the presence of three anionic nitrogen donors helps to stabilize relatively high oxidation states. Secondary coordination sphere effects are modulated through the sulfonamido moieties. The $[MST]^{3-}$ ligand can support monometallic metal complexes with terminal hydroxido, aqua, or ammine ligands, as the sulfonamido moieties can accept H-bonds from H-atom containing exogenous ligands. Additionally, the sulfonamido O-atoms can serve as a secondary metal binding site, allowing discrete bimetallic complexes to be prepared with $[MST]^{3-}$.

In this dissertation, new monometallic and bimetallic complexes with sulfonamido-based tripodal ligands were prepared, with the goal of understanding how the choice of ligands influences the properties of metal complexes. The first study investigated the effect of ligand modification on the physical properties of a series of $Fe^{II}–OH_2$ complexes supported by ligands related to $[MST]^{3-}$. The aryl groups of the five new *N*,*N*',*N*"-[2,2',2"-nitrilotris(ethane-2,1-diyl)]-tris-({R-Ph}-sulfonamido)) ($[RST]^{3-}$) ligands had *para*-substituents of varying electron-withdrawing and donating strengths. The physical properties of the subsequent $Fe^{II}–OH_2$

complexes were probed by various characterization methods, which revealed that the greatest impact of the ligand modification occurred in the metal complexes' electrochemical properties.

Monometallic Ni complexes with $[MST]^{3-}$ and a related urea-based ligand, $[H_3buea]^{3-}$, were then studied. The solid-state structures of these compounds showed that these ligands allowed for the preparation of Ni^{II} complexes with terminal aqua or hydroxido ligands in distorted trigonal bipyramidal geometries. Additionally, the oxidation chemistry of both Ni^{II} compounds was investigated, allowing for the preparation and characterization of uncommon Ni^{III} complexes.

Bimetallic complexes with $[MST]^{3-}$ are prepared by treating a solution of a monometallic $[MST]^{3-}$ complex, secondary metal salt, and secondary multidentate ligand with O_2. The secondary ligand serves to "cap" the secondary metal center, resulting in discretely bimetallic units. A new series of bimetallic complexes with $Fe^{II}(OH)Fe^{III}$, $Co^{II}(OH)Fe^{III}$, and $Ni^{II}(OH)Fe^{III}$ cores was prepared, using the bidentate capping ligand tetramethylethylenediamine (TMEDA). Previously, all other capping ligands used in this system had denticities of three and above. The bidentate capping ligand TMEDA allows the previously outer-sphere trifluoromethansulfonate (OTf^{-}) counter anion to become inner-sphere, occupying the sixth coordination site of the second metal center.

The ability to form heterobimetallic complexes and the presence of the weakly coordinating OTf^{-} ligand prompted an investigation of the substitution chemistry of the system. In the $Fe^{II}(OH)Fe^{III}$ species, the OTf^{-} ligand could be directly substituted for either isothiocyanate (NCS^{-}) or azide (N_3^{-}) ligands. Additionally, a Br^{-} ligand can occupy the sixth coordination site of the Fe^{II} center if the preparation of the diiron complex was modified. Furthermore, the TMEDA capping ligand can be directly substituted for two ethylenediamine (en) ligands. These results stress the importance of the choice of the capping ligand in these types of compounds, which has important implications on the substitution chemistry of this bimetallic system.

CHAPTER 1

Introduction

Basic Concepts: The Primary and Secondary Coordination Spheres

A central tenet of coordination chemistry is the importance of ligand environment to a coordinated metal center. Ligand coordination geometry and donor strength define the ligand field splitting of a metal center, which dictates the magnetic, electronic, and physical properties of the metal complex. These strong, covalent interactions between a metal center and its ligands are known as the primary coordination sphere.[1,2] Factors such as solvent molecules and counter ions, which are in the vicinity of but not directly in the primary coordination sphere, also affect the chemistry of metal centers. This microenvironment is known as the secondary coordination sphere and is dominated by weaker, non-covalent interactions, including hydrogen bonds (H-bonds). On aggregate, these weaker interactions often influence reactivity, as is demonstrated by Nature.[3–6]

In biology, metalloenzymes often have isolated active sites with amino acid functional groups that can contribute to both intermolecular and intramolecular H-bonding interactions. The interplay between the primary and secondary coordination spheres of such proteins drive their ability to catalyze difficult reactions under ambient conditions with selectivity and efficiency that are currently unattainable in synthetic systems.[7] In natural systems, productive reaction pathways are generally facilitated when highly reactive species, generated through effects from both coordination spheres, are directed towards a substrate which is often positioned within the secondary coordination sphere.[8–13] Additionally, the secondary coordination sphere further promotes productive chemistry by preventing harmful oxidative reactions to the protein host, as highly reactive ligands can be stabilized through H-bonds while sequestered into sterically protected pockets.[14–17]

A beautiful example of this balance is found in the metalloenzyme nickel superoxide dismutase (NiSOD) (Figure 1.1). This enzyme protects cells from oxidative damage by facilitating the disproportionation of superoxide ($O_2^{\bullet-}$) into dioxygen (O_2) and hydrogen peroxide (H_2O_2).[18] To do this, highly reactive $Ni^{II}–OO^{\bullet-}$ and $Ni^{III}–OO^{\bullet-}$ species are generated,[19] but such potent oxidizing species are harnessed without damage to the protein through the synergy of the primary and secondary coordination spheres.

Figure 1.1 shows the N_3S_2 primary coordination sphere of the oxidized form of NiSOD, which is derived from one histidine (His) and two cysteine (Cys) residues.[19,20] Two thiolate moieties from Cys2 and Cys6 provide the two donor S-atoms, while the three of the donor N-atoms are from the backbone amidate of Cys2, N-terminus of His1, and His1 imidazole moiety. In the resting, reduced state of NiSOD, it is unclear if His1 is bound as an axial fifth ligand.[21–23]

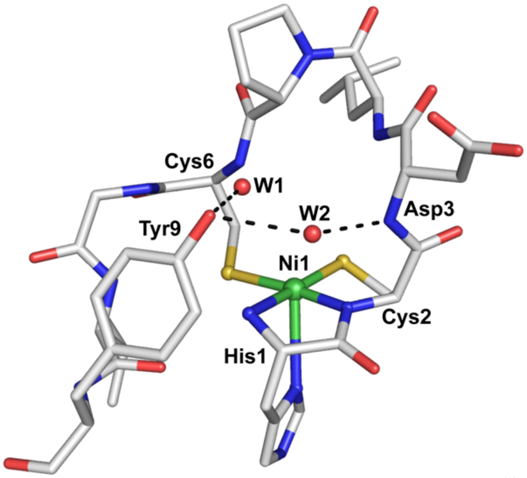

Figure 1.1. The active site of oxidized nickel superoxide dismutase. (PDB: 1Q0D)[20]

Although Ni^{II} is generally not redox-active in aqueous media,[24] the Ni center of NiSOD is still capable of accessing the Ni^{III} oxidation state. This is due to the presence of the thiolate ligands in its primary coordination sphere. Most redox-active Ni^{II}-based metalloenzymes are ligated to sulfur-based donors because these ligands tune the redox potential of the $Ni^{II/III}$ couples to potentials that are accessible by biological oxidants.[25] Additionally, the thiolate ligands of NiSOD can be protonated without S–Ni bond cleavage in the reduced state of the enzyme.[21,26–28] Protonation of the thiolate ligands reduces electron density on the donor S-atoms, and the subsequent SH moieties can further withdraw electron density by donating H-bonds. This fine tuning of S-atom electron density allows metal-based oxidations to be preferred over sulfur-based oxidations in the active site, an example of how primary and secondary coordination sphere effects can protect enzymes.[27–30] Finally, the presence of the nearby His1 residue helps to stabilize the Ni^{III} state, as its binding as a fifth ligand upon metal oxidation dramatically changes the ligand field and contributes electron density to the electron-deficient Ni^{III} center.[19,28]

The secondary coordination sphere of NiSOD is defined by nearby aspartate (Asp) and tyrosine (Tyr) residues. Asp3 H-bonds with nearby residues, helping to stabilize the “Ni-hook” structure that houses the active site of NiSOD.[19] Tyr9, which sterically encumbers access to the active site, has been implicated as the “gatekeeper” for substrate binding and product release.[20,31] Furthermore, the Tyr9 OH group helps stabilize the reactive $Ni–OO^{\bullet-}$ complexes present in the catalytic cycle of NiSOD through H-bonding to the superoxido ligand.[19] These factors clearly show that the relationship between the coordination spheres is essential to the function of NiSOD.

Understanding the primary and secondary coordination spheres is also crucial for synthetic chemistry. Many synthetic groups have turned to ligand design to tune the properties of the coordination spheres, though generally more attention is paid to modifying the primary coordination sphere.[13,32,33] Due to the large protein matrix that isolates active sites and provides amino acid functional groups capable of intermolecular and intramolecular H-bonding, relatively well-ordered secondary coordination sphere environments are observed in the solid-state structures of metalloenzymes.[34–36] In contrast, synthetic systems often involve discrete, flexible small molecules that can interact randomly with the various species present in solution. Thus, the secondary coordination spheres of these types of systems are often disordered and unpredictable.[32]

One strategy that has been used to address this issue in small molecule systems is to append functional groups that can promote intramolecular H-bonds to a rigid ligand scaffold. If designed appropriately, such ligands should allow for controlled, reproducible secondary coordination sphere interactions.

An early example of this strategy was the design of "picket-fence" porphyrins developed by Collman. In this work, the meso positions of the rigid ligand porphyrin were functionalized with various substituents, including those capable of donating H-bonds such as pivalamide groups (Figure 1.2A).[37] In the presence of 1-methylimidazole, the subsequent Fe-porphyrin complex could reversibly bind O_2. In the solid-state structure, the pivalamide moieties were all oriented towards one face of the ligand, forming a secondary coordination sphere structure that functioned similarly to a hydrophobic pocket in a protein. This positioning, in conjunction with the steric bulk of the substituents, helped to stabilize a Fe–O_2 adduct by preventing irreversible O_2 binding *via* O–O bond cleavage to form oxidized Fe^{III} oxo-bridged dimers.[37,38] The stability afforded by these secondary coordination sphere effects also allowed the Fe–O_2 species to be crystallographically characterized as the first example of its kind in either a protein or synthetic system.[39,40]

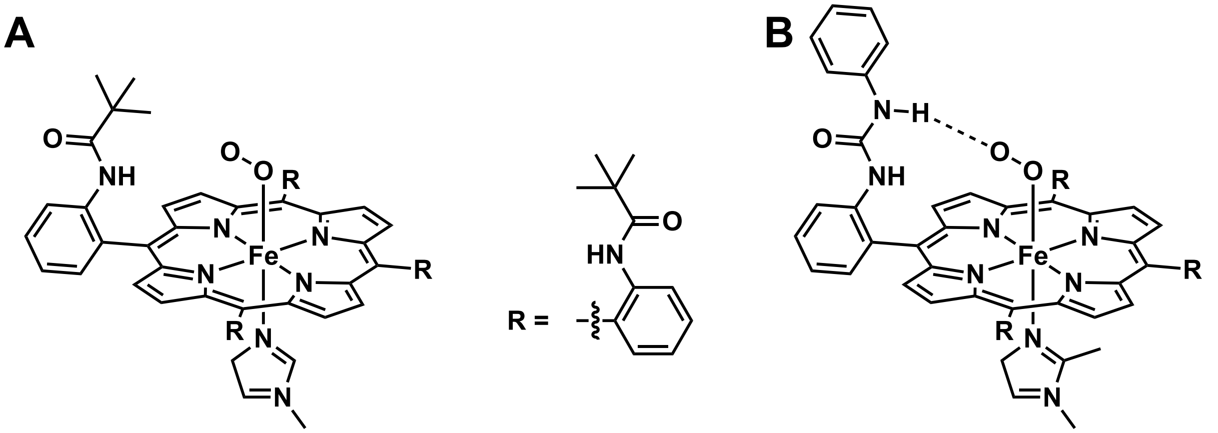

Figure 1.2. Fe–O_2 porphyrin complexes with (**A**) the original “picket-fence” porphyrin from the Collman group[37] and (**B**) the phenyl urea modified “picket-fence” porphyrin from the Reed group.[41]

The long distance of greater than 5 Å between the pivalamide NH groups and the O_2 ligand indicated that there are no intramolecular H-bonds observed in the solid-state structure. However, a later derivative of this system was successful in introducing intramolecular H-bonds, as Reed eventually developed a phenyl urea modified “picket-fence” porphyrin. In this ligand, one of the pivalamide substituents was replaced with a phenyl urea moiety (Figure 1.2B).[41] This modification brought the NH group of the urea closer to the center of the porphyrin, potentially allowing for intramolecular H-bonding between this NH group and an O_2 ligand. Indeed, O_2 binding studies showed that iron complexes with this phenyl urea modified ligand had substantially greater affinity for O_2 when compared to other iron-porphyrin complexes, illustrating the importance of intramolecular H-bonding in stabilizing reactive M–O_2 species. Note that no further structural or spectroscopic studies were done to further explore this finding.

This result demonstrated that well-ordered secondary coordination sphere effects were achievable in synthetic systems through appropriate ligand design, and paved the way for other groups to develop systems with this feature. Some early adopters of this motif include the groups of Kitajima,[42–44] Masuda,[45–47] Mareques-Rivas,[48–50] as well as our group.

Ligand Design in the Borovik Group

For over two decades, the Borovik group has specialized in designing ligands that modulate both the primary and secondary coordination spheres. An example that is particularly relevant to the research in this dissertation is the sulfonamide-based tripodal ligand *N*,*N′*,*N″*-[2,2′,2″-nitrilotris(ethane-2,1-diyl)]tris(2,4,6-trimethylbenzenesulfonamido) ($[MST]^{3-}$, Figure 1.3A).[51]

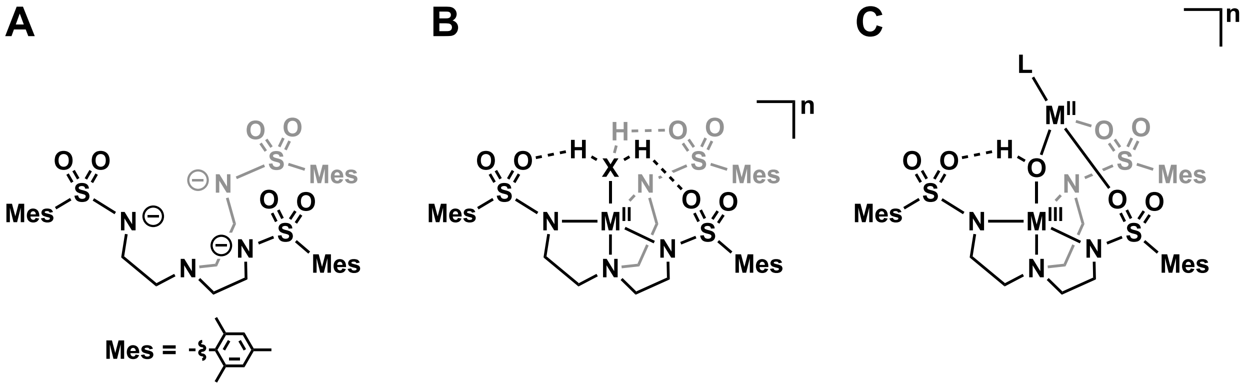

Figure 1.3. (**A**) The ligand $[MST]^{3-}$ and general examples of (**B**) monometallic $[MST]^{3-}$ complexes that can accept H-bonds from an exogenous ligand X (e.g. OH^-, OH_2, or NH_3) and (**C**) bimetallic $[MST]^{3-}$ complexes that binds a secondary M^{II} center through interactions with the electronegative sulfonamido O-atoms with a capping ligand L (e.g. crown ethers).

The ligand $[MST]^{3-}$ has several design elements that are typically used in the Borovik group to modulate the primary coordination sphere. This ligand contains a tris(2-aminoethyl)amine (tren) backbone that allows for the preparation of four- or five-coordinate metal complexes with local C_3 symmetry. The trigonal environment leads to high-spin metal complexes, while the presence of three anionic nitrogen donors allows oxidation chemistry to be investigated by helping to stabilize relatively high oxidation states.[51–57]

The design of $[MST]^{3-}$ accounts for secondary coordination sphere effects through the three sulfonamido moieties extending from the three equatorial nitrogen atoms of the tren backbone. As shown in Figure 1.3B, the three mesityl groups of typical $[MST]^{3-}$ complexes typically splay away from the metal center. This orients the O-atoms of the S=O groups towards the metal center to form a partially negatively charged pocket, a structural feature which has similarities to a protein binding pocket. Because the sulfonamido O-atoms serve as H-bond acceptors, complexes with $[MST]^{3-}$ favor binding exogenous ligands that can donate H-bonds such as hydroxido, aqua, and ammine ligands.[54–57] Note that six-membered rings are formed by these H-bonds, contributing to a well-ordered secondary coordination sphere.

Earlier ligand systems designed by our group were unable to stabilize exogenous aqua and ammine ligands, for these designs tended to feature relatively positively charged cavities through the inclusion of H-bond donating groups.[58–61] A good example of this is the urea-based tripodal ligand tris[(N)-tertbutylureaylato)-N-ethyl)]aminato ($[H_3buea]^{3-}$, Figure 1.4A).[58] The ability of the urea NH groups to donate H-bonds made this system ideal for stabilizing exogenous oxido and hydroxido ligands (Figure 1.4B). Additionally, the strong electron-donating ability of the three anionic, urea-based nitrogen donors allowed for the stabilization of higher oxidation states beyond the M^{III} state.[62–64] These features allowed our group to use this ligand system to stabilize and study biologically relevant high valent oxido species, including the first examples of a high-spin Fe^{III}–O unit[65] and a high-spin Mn^{V}=O unit.[64]

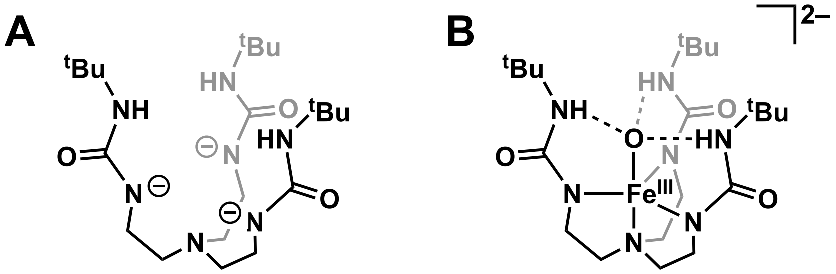

Figure 1.4. (**A**) The ligand $[H_3buea]^{3-}$ and (**B**) $[Fe^{IV}H_3buea(O)]^{-}$.[62]

The choice to reverse the polarity of cavity in $[MST]^{3-}$ had a further benefit; it reignited interest in our groups towards the study bimetallic complexes. Bimetallic complexes are of general interest to synthetic groups because of their many attractive properties. The two metal centers may cooperate to allow for the mediation of multi-electron processes with earth abundant, first row transition metals.[66,67] In catalysis, bimetallic units can provide different reaction pathways, faster reaction rates, and greater selectivity than their monometallic counterparts.[68–70] Additionally, since a second metal center provides an additional parameter to modulate, greater fine tuning of physical properties should be possible in bimetallic complexes in comparison to monometallic complexes.[71]

Previously, our group mainly prepared bimetallic complexes through the use of dinucleating ligands. Such ligand often required complicated ligand synthesis,[60,72,73] but the $[MST]^{3-}$ scaffold allowed us to prepare bimetallic complexes with a ligand that is comparatively facile to synthesize.[51] As mentioned previously, the electronegative sulfonamido O-atoms of $[MST]^{3-}$ can interact with Lewis acids, including protons but also metal ions. Early work with this system demonstrated that counter cations, such as Na^+ or K^+, could interact with the sulfonamido O-atoms to form multimetallic species, and subsequent work harnessed this property to allow discretely bimetallic complexes to be prepared. When a monometallic $NMe_4[M^{II}MST]$ salt is treated with a second metal ion in the presence of O_2, discrete bimetallic complexes can be formed if an additional multidentate ligand is present in the reaction (Figure 1.3C). The additional ligand serves as a “cap” on the second metal center, preventing aggregation. This discovery allowed for the preparation of an entire family of bimetallic complexes.[51–53,74]

Overview of Remaining Chapters

The remaining chapters of this dissertation discuss the preparation and properties of several new compounds prepared with $[MST]^{3-}$ and related systems. These studies focus on further understanding the effects of ligand design choices on the properties of metal complexes. Both monometallic (Chapters 2 and 3) and bimetallic complexes (Chapters 4 and 5) were investigated.

Work described in Chapter 2. The effect of ligand modification on the physical properties of a series of $Fe^{II}–OH_2$ complexes supported by ligands related to $[MST]^{3-}$, *N*,*N*',*N*"-[2,2',2"-nitrilotris(ethane-2,1-diyl)]-tris-({R-Ph}-sulfonamido)) ($[RST]^{3-}$, R = $–OCH_3$, – CH_3, –H, –Cl, or $–CF_3$, Figure 1.5), was investigated.[56] The aryl-groups of the various $[RST]^{3-}$ ligands contained a different *para*-substituent of varying electron-withdrawing strengths. As these substituents are relatively far away from the primary coordination sphere, this study aimed to determine if these long-range modifications would mostly influence the secondary coordination sphere over the primary coordination sphere. The effects of these modifications on the series of $Fe^{II}–OH_2$ complexes were probed by Fourier transform infrared (FTIR) spectroscopy, X-ray diffraction methods, and cyclic voltammetry (CV), and trends in the data were analyzed. These results demonstrated the difficulty of isolating effects of the two coordination spheres; in small systems changes in one coordination sphere also affect the other.

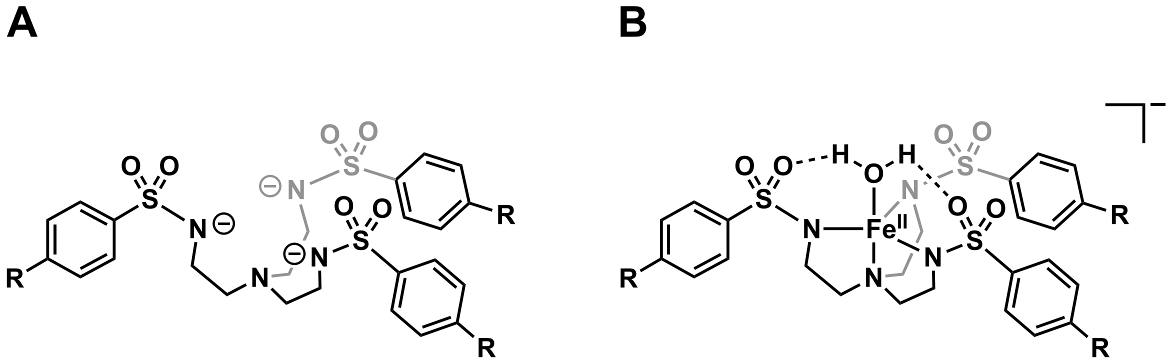

Figure 1.5. (**A**) The ligand series $[RST]^{3-}$ (R = $-OCH_3$, $-CH_3$, –H, –Cl, or $-CF_3$) and (**B**) subsequent $Fe^{II}-OH_2$ complexes.

Work described in Chapter 3. Continuing with monometallic systems, the chemistry of Ni complexes with $[MST]^{3-}$was investigated. The salt $NMe_4[Ni^{II}MST(OH_2)]$ was prepared and studied and compared to $K_2[Ni^{II}H_3buea(OH)]$ (Figure 1.6B).[57] The solid-state structures of these compounds revealed that they are rare examples of five-coordinate, trigonal bipyramidal Ni^{II} complexes with terminal aqua or hydroxido ligands.

The oxidation chemistry of both salts was investigated to prepare rare Ni^{III} complexes. Such species are proposed as intermediates in Ni enzymes catalytic cycles[75,76] and are uncommon species in synthetic systems.[77–81] Both $[MST]^{3-}$ and $[H_3buea]^{3-}$ seemed capable of stabilizing Ni^{III} complexes since these systems have previously been shown to stabilize $M^{III}-OH$ species.[62,63,82,83] CV studies on $NMe_4[Ni^{II}MST(OH_2)]$ and $K_2[Ni^{II}H_3buea(OH)]$ suggested that both complexes could be oxidized by one-electron oxidants. Such oxidation experiments were conducted, and the properties of the resulting Ni^{III} species were investigated.

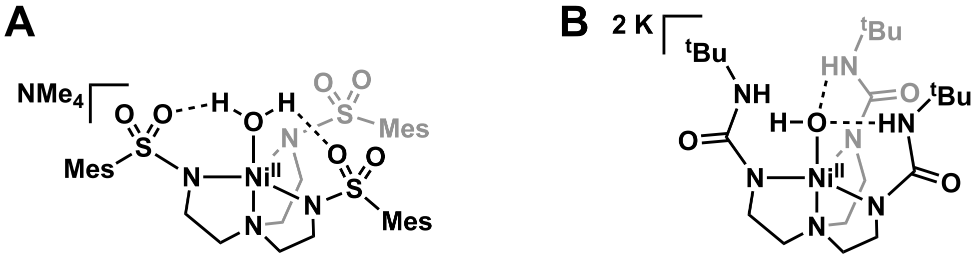

Figure 1.6. The Ni^{II} compounds (**A**) NMe$_4$[Ni^{II}MST(OH$_2$)] and (**B**) K$_2$[Ni^{II}H$_3$buea(OH)].

Work described in Chapter 4. As mentioned previously, [MST]$^{3-}$ can support bimetallic complexes through the interaction of a secondary metal center with the sulfonamido O-atoms. In order to prepare discretely bimetallic complexes with this system, it is necessary to include an additional multidentate capping ligand (L). The choice of L is important, as different capping ligands are used for the preparation of different types of bimetallic complexes. Specifically, crown ethers have been used to cap redox-inactive metal ions (Figure 1.7A),[51–53,74] while multidentate ligands containing nitrogen donors have been used to cap transition metal ions (Figure 1.7B and C).[84]

Two series of mixed-valent transition metal bimetallic complexes were compared, both containing Fe^{III} bound to [MST]$^{3-}$. The first series, previously prepared by Dr. Yohei Sano, used the tridentate ligand 1,4,7-trimethyl-1,4,7-triazacyclononane (TMTACN) to cap the first-row divalent transition metal ions Mn^{II}, Fe^{II}, Co^{II}, Ni^{II}, Cu^{II}, or Zn^{II}.[84,85] These complexes, of the formulation [(TMTACN)M^{II}–(μ-OH)–Fe^{III}MST]OTf (Figure 1.7B), were primarily studied using X-ray diffraction methods, electrospray ionization mass spectrometry (ESI-MS), and X-band electron paramagnetic resonance (EPR) spectroscopy. The solid-state structures revealed that the divalent metal ions were coordinatively saturated, having an O$_3$N$_3$ primary coordination sphere where the bridging hydroxido ligand and two sulfonamido groups donate the three oxygen atoms while TMTACN provides the three nitrogen donors.

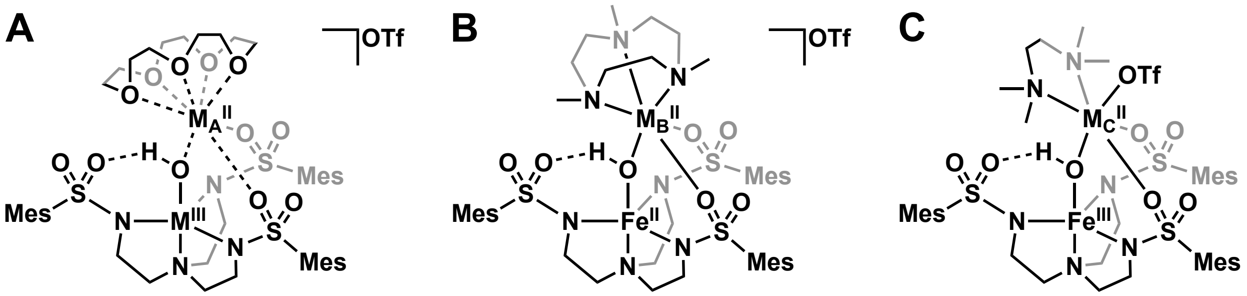

Figure 1.7. Bimetallic $[\mathrm{MST}]^{3-}$ complexes (**A**) $[(\text{15-crown-5})\supset \mathrm{M_A}^{\mathrm{II}}-(\mu\text{-OH})-\mathrm{M}^{\mathrm{III}}\mathrm{MST}]\mathrm{OTf}$ ($\mathrm{M_A}^{\mathrm{II}}\mathrm{M}^{\mathrm{III}}$ = $\mathrm{Ca^{II}Mn^{III}}$, $\mathrm{Sr^{II}Mn^{III}}$, $\mathrm{Ba^{II}Mn^{III}}$ (with 18-crown-6), $\mathrm{Ca^{II}Fe^{III}}$, $\mathrm{Sr^{II}Fe^{III}}$, or $\mathrm{Ba^{II}Fe^{III}}$ (with 18-crown-6)),[53] (**B**) $[(\mathrm{TMTACN})\mathrm{M_B}^{\mathrm{II}}-(\mu\text{-OH})-\mathrm{Fe^{III}MST}]\mathrm{OTf}$ ($\mathrm{M_B}^{\mathrm{II}}$ = $\mathrm{Mn^{II}}$, $\mathrm{Fe^{II}}$, $\mathrm{Co^{II}}$, $\mathrm{Ni^{II}}$, $\mathrm{Cu^{II}}$, or $\mathrm{Zn^{II}}$),[84,85] and (**C**) $[(\mathrm{TMEDA})\mathrm{M_C}^{\mathrm{II}}(\mathrm{OTf})-(\mu\text{-OH})-\mathrm{Fe^{III}MST}]$ ($\mathrm{M_C}^{\mathrm{II}}$ = $\mathrm{Fe^{II}}$, $\mathrm{Co^{II}}$, or $\mathrm{Ni^{II}}$).

To prepare similar complexes towards *unsaturated* divalent metal ions, a new series of bimetallic complexes using the bidentate ligand tetramethylethylenediamine (TMEDA) was prepared. These three salts had the formulation $[(\mathrm{TMEDA})\mathrm{M^{II}}(\mathrm{OTf})-(\mu\text{-OH})-\mathrm{Fe^{III}MST}]$ (Figure 1.7C), where $\mathrm{M^{II}}$ = $\mathrm{Fe^{II}}$, $\mathrm{Co^{II}}$, or $\mathrm{Ni^{II}}$. The solid-state structures of the TMEDA complexes revealed that while the divalent metal ions had a saturated pseudo-octahedral ligand environment, the sixth ligand was a weakly coordinating trifluoromethansulfonate ($\mathrm{OTf^-}$) anion.

Work described in Chapter 5. It was determined that $[(\mathrm{TMEDA})\mathrm{Fe^{II}}(\mathrm{OTf})-(\mu\text{-OH})-\mathrm{Fe^{III}MST}]$ does not react with external substrates with weak C–H bonds such as dihydroanthracene or xanthene. However, due to the presence of the weakly coordinating $\mathrm{OTf^-}$ ligand, the substitution chemistry of this salt was probed. Two preparative methods were used to produce new $[(\mathrm{TMEDA})\mathrm{Fe^{II}}(\mathrm{X})-(\mu\text{-OH})-\mathrm{Fe^{III}MST}]$ ($\mathrm{X^-}$ = $\mathrm{Br^-}$, $\mathrm{NCS^-}$, or $\mathrm{N_3^-}$) (Figure 1.8A) salts that were studied by EPR and FTIR spectroscopies as well as X-ray diffraction methods. If $\mathrm{FeBr_2}$ is used in the initial preparation instead of $\mathrm{Fe(OTf)_2\cdot 2MeCN}$, a $\mathrm{Br^-}$ anion occupies the sixth coordination site to form $[(\mathrm{TMEDA})\mathrm{Fe^{II}}(\mathrm{Br})-(\mu\text{-OH})-\mathrm{Fe^{III}MST}]$. If instead $[(\mathrm{TMEDA})\mathrm{Fe^{II}}(\mathrm{OTf})-(\mu\text{-OH})-\mathrm{Fe^{III}MST}]$ is treated with $\mathrm{NMe_4(X)}$ ($\mathrm{X^-}$ = $\mathrm{NCS^-}$ or $\mathrm{N_3^-}$), a successful metathesis reaction occurs that results in the production of diiron isothiocyanato or azido compounds.

The ability to substitute the sixth ligand motivated studies on the substitution chemistry of the capping ligand. TMEDA can be substituted in the presence of two equivalents of ethylenediamine (en). The resulting compound, [(en)$_2$Fe^{II}–(μ-OH)–Fe^{III}MST]OTf (Figure 1.8B), has a completely different primary coordination sphere in comparison to the other bimetallic complexes with [MST]$^{3-}$. These results and those from Chapter 4 show clearly that the system based on [(TMEDA)Fe^{II}(OTf)–(μ-OH)–Fe^{III}MST] is highly modular.

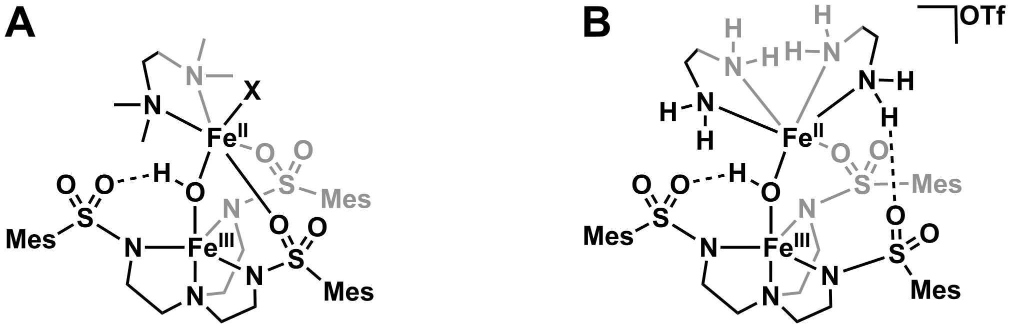

Figure 1.8. (**A**) [(TMEDA)Fe^{II}(OTf)–(μ-OH)–Fe^{III}MST] (X$^-$ = OTf$^-$, Br$^-$, NCS$^-$, or N$_3^-$)and (**B**) [(en)$_2$Fe^{II}–(μ-OH)–Fe^{III}MST]OTf.

References

(1) Werner, A. Über die raumisomeren Kobaltverbindungen. *Justus Liebig's Ann. der Chemie* **1912**, *386*, 1–272.

(2) Werner, A. Zur Kenntnis des asymmetrischen Kobaltatoms. V. *Berichte der Dtsch. Chem. Gesellschaft* **1912**, *45*, 121–130.

(3) Hwang, H. J.; Carey, J. R.; Brower, E. T.; Gengenbach, A. J.; Abramite, J. A.; Lu, Y. Blue Ferrocenium Azurin: An Organometalloprotein with Tunable Redox Properties. *J. Am. Chem. Soc.* **2005**, *127*, 15356–15357.

(4) Lu, Y.; Yeung, N.; Sieracki, N.; Marshall, N. M. Design of functional metalloproteins. *Nature* **2009**, *460*, 855–862.

(5) Marshall, N. M.; Garner, D. K.; Wilson, T. D.; Gao, Y.-G.; Robinson, H.; Nilges, M. J.; Lu, Y. Rationally tuning the reduction potential of a single cupredoxin beyond the natural range. *Nature* **2009**, *462*, 113–116.

(6) Berry, S. M.; Baker, M. H.; Reardon, N. J. Reduction potential variations in azurin through secondary coordination sphere phenylalanine incorporations. *J. Inorg. Biochem.* **2010**, *104*, 1071–1078.

(7) Holm, R. H.; Solomon, E. I. Preface: Biomimetic Inorganic Chemistry. **2004**.

(8) Sigman, J. A.; Kim, H. K.; Zhao, X.; Carey, J. R.; Lu, Y. The role of copper and protons in heme-copper oxidases: kinetic study of an engineered heme-copper center in myoglobin. *Proc. Natl. Acad. Sci. U. S. A.* **2003**, *100*, 3629–3634.

(9) Holm, R. H.; Kennepohl, P.; Solomon, E. I. Structural and Functional Aspects of Metal Sites in Biology. **1996**.

(10) Moore, C. M.; Szymczak, N. K. A tris(2-quinolylmethyl)amine scaffold that promotes hydrogen bonding within the secondary coordination sphere. *Dalt. Trans.* **2012**, *41*, 7886.

(11) Reback, M. L.; Ginovska-Pangovska, B.; Ho, M.-H.; Jain, A.; Squier, T. C.; Raugei, S.; Roberts, J. A. S.; Shaw, W. J. The Role of a Dipeptide Outer-Coordination Sphere on H_2-Production Catalysts: Influence on Catalytic Rates and Electron Transfer. *Chem. Eur. J.* **2013**, *19*, 1928–1941.

(12) Ginovska-Pangovska, B.; Dutta, A.; Reback, M. L.; Linehan, J. C.; Shaw, W. J. Beyond the Active Site: The Impact of the Outer Coordination Sphere on Electrocatalysts for Hydrogen Production and Oxidation. *Acc. Chem. Res.* **2014**, *47*, 2621–2630.

(13) Cook, S. A.; Borovik, A. S. Molecular Designs for Controlling the Local Environments around Metal Ions. *Acc. Chem. Res.* **2015**, *48*, 2407–2414.

(14) Reedy, C. J.; Gibney, B. R. Heme Protein Assemblies. **2004**.

(15) Lu, Y. Biosynthetic Inorganic Chemistry. *Angew. Chemie Int. Ed.* **2006**, *45*, 5588–5601.

(16) Petros, A. K.; Reddi, A. R.; Kennedy, M. L.; Hyslop, A. G.; Gibney, B. R. Femtomolar Zn(II) Affinity in a Peptide-Based Ligand Designed To Model Thiolate-Rich Metalloprotein Active Sites. *Inorg. Chem.* **2006**, *45*, 9941–9958.

(17) Adelhardt, M.; Chalkley, M. J.; Heinemann, F. W.; Sutter, J.; Scheurer, A.; Meyer, K. Synthesis and Characterization of Iron Trisphenolate Complexes with Hydrogen-Bonding Cavities. *Inorg. Chem.* **2014**, *53*, 2763–2765.

(18) Ryan, K. C.; Maroney, M. J. Nickel Superoxide Dismutase. *Encyclopedia of Metalloproteins*; Kretsinger, R. H., Uversky, V. N., Permyakov, E. A., Eds.; Springer New York: New York, NY, 2013; pp 1505–1515.

(19) Barondeau, D. P.; Kassmann, C. J.; Bruns, C. K.; Tainer, J. A.; Getzoff, E. D. Nickel superoxide dismutase structure and mechanism. *Biochemistry* **2004**, *43*, 8038–8047.

(20) Wuerges, J.; Lee, J.-W.; Yim, Y.-I.; Yim, H.-S.; Kang, S.-O.; Djinovic Carugo, K. Crystal structure of nickel-containing superoxide dismutase reveals another type of active site. *Proc. Natl. Acad. Sci. U. S. A.* **2004**, *101*, 8569–8574.

(21) Pelmenschikov, V.; Siegbahn, P. E. M. Nickel superoxide dismutase reaction mechanism studied by hybrid density functional methods. *J. Am. Chem. Soc.* **2006**, *128*, 7466–7475.

(22) Neupane, K. P.; Gearty, K.; Ashish, F.; Shearer, J. Probing Variable Axial Ligation in Nickel Superoxide Dismutase Utilizing Metallopeptide-Based Models: Insight into the Superoxide Disproportionation Mechanism. **2007**.

(23) Li, Y.; Zamble, D. B. Nickel Homeostasis and Nickel Regulation: An Overview. *Chem. Rev.* **2009**, *109*, 4617–4643.

(24) Zilbermann, I.; Maimon, E.; Cohen, H.; Meyerstein, D. Redox chemistry of nickel complexes in aqueous solutions. *Chem. Rev.* **2005**, *105*, 2609–2625.

(25) Maroney, M. J. Structure/function relationships in nickel metallobiochemistry. *Curr. Opin. Chem. Biol.* **1999**, *3*, 188–199.

(26) Prabhakar, R.; Morokuma, K.; Musaev, D. G. A DFT study of the mechanism of Ni superoxide dismutase (NiSOD): Role of the active site cysteine-6 residue in the oxidative half-reaction. *J. Comput. Chem.* **2006**, *27*, 1438–1445.

(27) Bryngelson, P.; Maroney, M. Nickel superoxide dismutase. In *Nickel and its surprising impact in nature*; John Wiley and Sons, 2007; pp 417–444.

(28) Shearer, J. Insight into the Structure and Mechanism of Nickel-Containing Superoxide Dismutase Derived from Peptide-Based Mimics. *Acc. Chem. Res.* **2014**, *47*, 2332–2341.

(29) Gale, E. M.; Narendrapurapu, B. S.; Simmonett, A. C.; Schaefer, H. F.; Harrop, T. C. Exploring the Effects of H-Bonding in Synthetic Analogues of Nickel Superoxide Dismutase (Ni-SOD): Experimental and Theoretical Implications for Protection of the Ni−SCys Bond. *Inorg. Chem.* **2010**, *49*, 7080–7096.

(30) Mathrubootham, V.; Thomas, J.; Staples, R.; McCraken, J.; Shearer, J.; Hegg, E. L. Bisamidate and Mixed Amine/Amidate NiN_2S_2 Complexes as Models for Nickel-Containing Acetyl Coenzyme A Synthase and Superoxide Dismutase: An Experimental and Computational Study. *Inorg. Chem.* **2010**, *49*, 5393–5406.

(31) Herbst, R. W.; Guce, A.; Bryngelson, P. A.; Higgins, K. A.; Ryan, K. C.; Cabelli, D. E.; Garman, S. C.; Maroney, M. J. Role of conserved tyrosine residues in NiSOD catalysis: a case of convergent evolution. *Biochemistry* **2009**, *48*, 3354–3369.

(32) Borovik, A. S. Bioinspired hydrogen bond motifs in ligand design: the role of noncovalent interactions in metal ion mediated activation of dioxygen. *Acc. Chem. Res.* **2005**, *38*, 54–61.

(33) Shook, R. L.; Borovik, A. S. Role of the secondary coordination sphere in metal-mediated dioxygen activation. *Inorg. Chem.* **2010**, *49*, 3646–3660.

(34) Mann, S. I.; Heinisch, T.; Weitz, A. C.; Hendrich, M. P.; Ward, T. R.; Borovik, A. S. Modular Artificial Cupredoxins. *J. Am. Chem. Soc.* **2016**, *138*, 9073–9076.

(35) Poulos, T. L.; Finzel, B. C.; Gunsalus, I. C.; Wagner, G. C.; Kraut, J. The 2.6-A Crystal Structure of Pseudomonas putida Cytochrome P-450. *J. Biol. Chem.* **1985**, *260*, 16122–16130.

(36) Fisher, S. Z.; Kovalevsky, A. Y.; Domsic, J. F.; Mustyakimov, M.; McKenna, R.; Silverman, D. N.; Langan, P. A. Neutron Structure of Human Carbonic Anhydrase II: Implications for Proton Transfer. *Biochemistry* **2010**, *49*, 415–421.

(37) Collman, J. P.; Gagne, R. R.; Halbert, T. R.; Marchon, J. C.; Reed, C. A. Reversible oxygen adduct formation in ferrous complexes derived from a picket fence porphyrin. Model for

oxymyoglobin. *J. Am. Chem. Soc.* **1973**, *95*, 7868–7870.

(38) Collman, J. P.; Gagne, R. R.; Reed, C.; Halbert, T. R.; Lang, G.; Robinson, W. T. Picket fence porphyrins. Synthetic models for oxygen binding hemoproteins. *J. Am. Chem. Soc.* **1975**, *97*, 1427–1439.

(39) Collman, J. P.; Gagne, R. T.; Reed, C. A. Paramagnetic dioxygen complex of iron(II) derived from a picket fence porphyrin. Further models for hemoproteins. *J. Am. Chem. Soc.* **1974**, *96*, 2629–2631.

(40) Collman, J. P.; Gagnet, R. R.; Reedtt, C. A.; Robinson, W. T.; Rodley, G. A. Structure of an Iron(II) Dioxygen Complex; A Model for Oxygen Carrying Hemeproteins (picket fence porphyrin/x-ray diffraction). **1974**, *71*, 1326–1329.

(41) Wuenschell, G. E.; Tetreau, C.; Lavalette, D.; Reed, C. A. Hydrogen-bonded oxyhemoglobin models with substituted picket-fence porphyrins: the model compound equivalent of site-directed mutagenesis. *J. Am. Chem. Soc.* **1992**, *114*, 3346–3355.

(42) Kitajima, N.; Tamura, N.; Amagai, H.; Fukui, H.; Moro-oka, Y.; Mizutani, Y.; Kitagawa, T.; Mathur, R.; Heerwegh, K. Monomeric Carboxylate Ferrous Complexes as Models for the Dioxygen Binding Sites in Non-Heme Iron Proteins. The Reversible Formation and Characterization of .mu.-Peroxo Diferric Complexes. *J. Am. Chem. Soc.* **1994**, *116*, 9071–9085.

(43) Kitajima, N.; Komatsuzaki, H.; Hikichi, S.; Osawa, M.; Moro-oka, Y. A Monomeric Side-On Peroxo Manganese(III) Complex: Mn(O2)(3,5-iPr2pzH)(HB(3,5-iPr2pz)3). *J. Am. Chem. Soc.* **1994**, *116*, 11596–11597.

(44) Fujisawa, K.; Tanaka, M.; Moro-oka, Y.; Kitajima, N. A Monomeric Side-On Superoxocopper(II) Complex: Cu(O2)(HB(3-tBu-5-iPrpz)3). *J. Am. Chem. Soc.* **1994**, *116*, 12079–12080.

(45) Harata, M.; Jitsukawa, K.; Masuda, H.; Einaga, H. A Structurally Characterized Mononuclear Copper(II)-Superoxo Complex. *J. Am. Chem. Soc.* **1994**, *116*, 10817–10818.

(46) Wada, A.; Harata, M.; Hasegawa, K.; Jitsukawa, K.; Masuda, H.; Mukai, M.; Kitagawa, T.; Einaga, H. Structural and Spectroscopic Characterization of a Mononuclear Hydroperoxo-Copper(II) Complex with Tripodal Pyridylamine Ligands. *Angew. Chemie Int. Ed.* **1998**, *37*, 798–799.

(47) Wada, A.; Ogo, S.; Nagatomo, S.; Kitagawa, T.; Watanabe, Y.; Jitsukawa, K.; Masuda, H. Reactivity of Hydroperoxide Bound to a Mononuclear Non-Heme Iron Site. **2002**.

(48) Mareque-Rivas, J. C.; Prabaharan, R.; Martín de Rosales, R. T.; Rentzeperis, D.; Marky, L. A.; Chin, J.; Kitagawa, T.; Einaga, H.; Noble, R. W.; Lin, S.-H.; Yu, N.-T. Relative importance of hydrogen bonding and coordinating groups in modulating the zinc–water acidity. *Chem. Commun.* **2004**, *117*, 76–77.

(49) Mareque-Rivas, J. C.; Prabaharan, R.; Parsons, S.; Masuda, H.; Patel, B.; Macchioni, A.; Crabtree, R. H.; Masuda, H.; Einaga, H. Quantifying the relative contribution of hydrogen bonding and hydrophobic environments, and coordinating groups, in the zinc(ii)–water acidity by synthetic modelling chemistry. *Dalt. Trans.* **2004**, *74*, 1648–1655.

(50) Mareque Rivas, J. C.; Hinchley, S. L.; Metteau, L.; Parsons, S. The strength of hydrogen bonding to metal-bound ligands can contribute to changes in the redox behaviour of metal centres. *Dalton Trans.* **2006**, No. 19, 2316–2322.

(51) Park, Y. J.; Ziller, J. W.; Borovik, A. S. The Effects of Redox-Inactive Metal Ions on the Activation of Dioxygen: Isolation and Characterization of a Heterobimetallic Complex Containing a Mn^{III}–(μ-OH)–Ca^{II} Core. *J. Am. Chem. Soc.* **2011**, *133*, 9258–9261.

(52) Lacy, D. C.; Park, Y. J.; Ziller, J. W.; Yano, J.; Borovik, A. S. Assembly and Properties of Heterobimetallic $Co^{II/III}/Ca^{II}$ Complexes with Aquo and Hydroxo Ligands. *J. Am. Chem. Soc.* **2012**, *134*, 17526–17535.

(53) Park, Y. J.; Cook, S. A.; Sickerman, N. S.; Sano, Y.; Ziller, J. W.; Borovik, A. S. Heterobimetallic complexes with M^{III}-(μ-OH)-M^{II} cores (M^{III} = Fe, Mn, Ga; M^{II} = Ca, Sr, and Ba): structural, kinetic, and redox properties. *Chem. Sci.* **2013**, *4*, 717–726.

(54) Sickerman, N. S.; Peterson, S. M.; Ziller, J. W.; Borovik, A. S.; Mäemets, V.; Leito, I.; Koppel, I. A.; Borovik, A. S. Synthesis, structure and reactivity of $Fe^{II}/^{III}$–NH_3 complexes bearing a tripodal sulfonamido ligand. *Chem. Commun.* **2014**, *50*, 2515.

(55) Cook, S. A.; Ziller, J. W.; Borovik, A. S. Iron(II) Complexes Supported by Sulfonamido Tripodal Ligands: Endogenous versus Exogenous Substrate Oxidation. *Inorg. Chem.* **2014**, *53*, 11029–11035.

(56) Lau, N.; Ziller, J. W.; Borovik, A. S. Sulfonamido tripods: Tuning redox potentials via ligand modifications. *Polyhedron* **2015**, *85*, 777–782.

(57) Lau, N.; Sano, Y.; Ziller, J. W.; Borovik, A. S. Terminal Ni^{II}−OH/−OH_2 complexes in trigonal bipyramidal geometries derived from H_2O. *Polyhedron* **2017**, *125*, 179–185.

(58) Hammes, B. S.; Young, Jr., V. G.; Borovik, A. S. Hydrogen-Bonding Cavities about Metal Ions: A Redox Pair of Coordinatively Unsaturated Paramagnetic Co-OH Complexes. *Angew. Chemie Int. Ed.* **1999**, *38*, 666–669.

(59) Shook, R. L.; Gunderson, W. A.; Greaves, J.; Ziller, J. W.; Hendrich, M. P.; Borovik, A. S. A monomeric Mn(III)-peroxo complex derived directly from dioxygen. *J. Am. Chem. Soc.* **2008**, *130*, 8888–8889.

(60) Ng, G. K. Y.; Ziller, J. W.; Borovik, A. S. Structural Diversity in Metal Complexes with a Dinucleating Ligand Containing Carboxyamidopyridyl Groups. *Inorg. Chem.* **2011**, *50*, 7922–7924.

(61) Sickerman, N. S.; Park, Y. J.; Ng, G. K.-Y.; Bates, J. E.; Hilkert, M.; Ziller, J. W.; Furche, F.; Borovik, A. S. Synthesis, structure, and physical properties for a series of trigonal bipyramidal M(II)-Cl complexes with intramolecular hydrogen bonds. *Dalton Trans.* **2012**, *41*, 4358–4364.

(62) Lacy, D. C.; Gupta, R.; Stone, K. L.; Greaves, J.; Ziller, J. W.; Hendrich, M. P.; Borovik, A. S. Formation, structure, and EPR detection of a high spin Fe(IV)-oxo species derived from either an Fe(III)-oxo or Fe(III)-OH complex. *J. Am. Chem. Soc.* **2010**, *132*, 12188–12190.

(63) Taguchi, T.; Gupta, R.; Lassalle-kaiser, B.; Boyce, D. W.; Yachandra, V. K.; Tolman, W. B.;

Yano, J.; Hendrich, M. P.; Borovik, a S. Preparation and Properties of a Monomeric High-Spin Mn. *J. Am. Chem. Soc.* **2012**, *134*, 1996–1999.

(64) Gupta, R.; Taguchi, T.; Lassalle-Kaiser, B.; Bominaar, E. L.; Yano, J.; Hendrich, M. P.; Borovik, A. S. High-spin Mn-oxo complexes and their relevance to the oxygen-evolving complex within photosystem II. *Proc. Natl. Acad. Sci. U. S. A.* **2015**, *112*, 5319–5324.

(65) MacBeth, C. E.; Golombek, A. P.; Young Jr., V. G.; Yang, C.; Kuczera, K.; Hendrich, M. P.; Borovik, A. S. O2 Activation by Nonheme Iron Complexes: A Monomeric Fe(III)-Oxo Complex Derived From O2. *Science* **2000**, *289*, 938–941.

(66) McCollum, D. G.; Yap, G. P. A.; Liable-Sands, L.; Rheingold, A. L. Bimetallic Reactivity . Oxo Transfer Reactions with a Heterobimetallic Complex of Iron(II) and Vanadium(III). *Inorg. Chem.* **1997**, *36*, 2230–2235.

(67) Incarvito, C.; Rheingold, A. L.; Gavrilova, A. L.; Qin, C. J.; Bosnich, B. Bimetallic reactivity. One-site addition two-metal oxidation reactions using a Di-Co(II) complex of a binucleating ligand with 5- and 6-coordinate sites. *Inorg. Chem.* **2001**, *40*, 4101–4108.

(68) Shibasaki, M.; Yamamoto, Y. Preface. In *Multimetallic Catalysts in Organic Synthesis*; Shibasaki, M., Yamamoto, Y., Eds.; Wiley-VCH, 2004; pp XI–XII.

(69) Powers, D. C.; Benitez, D.; Tkatchouk, E.; Goddard, W. A.; Ritter, T. Bimetallic Reductive Elimination from Dinuclear Pd(III) Complexes. *J. Am. Chem. Soc.* **2010**, *132*, 14092–14103.

(70) Shibasaki, M.; Kanai, M.; Matsunaga, S.; Kumagai, N. Multimetallic Multifunctional Catalysts for Asymmetric Reactions. In *Bifunctional Molecular Catalysis*; Springer Berlin Heidelberg, 2011; pp 1–30.

(71) Mankad, N. P. Selectivity Effects in Bimetallic Catalysis. *Chem. Eur. J.* **2016**, *22*, 5822–5829.

(72) Zinn, P. J.; Powell, D. R.; Day, V. W.; Hendrich, M. P.; Sorrell, T. N.; Borovik, A. S. Pyrazolate-Bridging Dinucleating Ligands Containing Hydrogen-Bond Donors: Synthesis and Structure of Their Cobalt Analogues. **2006**.

(73) Ng, G. K.-Y.; Ziller, J. W.; Borovik, A. S. Preparation and structures of dinuclear complexes containing M^{II}–OH centers. *Chem. Commun.* **2012**, *48*, 2546–2548.

(74) Sickerman, N. S.; Henry, R. M.; Ziller, J. W.; Borovik, A. S. Preparation and structural properties of In^{III}–OH complexes. *Polyhedron* **2013**, *58*, 65–70.

(75) Fontecilla-Camps, J. C.; Volbeda, A. [NiFe]-Hydrogenases. *Encyclopedia of Metalloproteins*; Springer New York, 2013; pp 1535–1544.

(76) Can, M.; Armstrong, F. A.; Ragsdale, S. W. Structure, Function, and Mechanism of the Nickel Metalloenzymes, CO Dehydrogenase, and Acetyl-CoA Synthase. *Chem. Rev.* **2014**.

(77) Pandarus, V.; Zargarian, D. New Pincer-Type Diphosphinito (POCOP) Complexes of Nickel. *Organometallics* **2007**, *26*, 4321–4334.

(78) Anderson, T. J.; Jones, G. D.; Vicic, D. A. Evidence for a Ni^{I} Active Species in the Catalytic Cross-Coupling of Alkyl Electrophiles. *J. Am. Chem. Soc.* **2004**, *126*, 8100–8101.

(79) Zultanski, S. L.; Fu, G. C. Catalytic asymmetric γ-alkylation of carbonyl compounds via stereoconvergent Suzuki cross-couplings. *J. Am. Chem. Soc.* **2011**, *133*, 15362–15364.

(80) Lee, W.-Z.; Chiang, C.-W.; Lin, T.-H.; Kuo, T.-S. A discrete five-coordinate Ni(III) complex resembling the active site of the oxidized form of nickel superoxide dismutase. *Chem. Eur. J.* **2012**, *18*, 50–53.

(81) Chiang, C.-W.; Chu, Y.-L.; Chen, H.-L.; Kuo, T.-S.; Lee, W.-Z. Synthesis and characterization of Ni(III)N_3S_2 complexes as active site models for the oxidized form of nickel superoxide dismutase. *Chem. Eur. J.* **2014**, *20*, 6283–6286.

(82) MacBeth, C. E.; Gupta, R.; Mitchell-Koch, K. R.; Young, V. G.; Lushington, G. H.; Thompson, W. H.; Hendrich, M. P.; Borovik, A. S. Utilization of hydrogen bonds to stabilize M-O(H) units: synthesis and properties of monomeric iron and manganese complexes with terminal oxo and hydroxo ligands. *J. Am. Chem. Soc.* **2004**, *126*, 2556–2567.

(83) Parsell, T. H.; Behan, R. K.; Green, M. T.; Hendrich, M. P.; Borovik, A. S. Preparation and properties of a monomeric Mn(IV)-oxo complex. *J. Am. Chem. Soc.* **2006**, *128*, 8728–8729.

(84) Sano, Y.; Weitz, A. C.; Ziller, J. W.; Hendrich, M. P.; Borovik, A. S. Unsymmetrical Bimetallic Complexes with M^{II}–(μ-OH)–M^{III} Cores ($M^{II}M^{III}$ = $Fe^{II}Fe^{III}$, $Mn^{II}Fe^{III}$, $Mn^{II}Mn^{III}$): Structural, Magnetic, and Redox Proper. *Inorg. Chem.* **2013**, *52*, 10229–10231.

(85) Sano, Y.; Lau, N.; Weitz, A. C.; Ziller, J. W.; Hendrich, M. P.; Borovik, A. S. Models for Unsymmetrical Active Sites in Metalloproteins: Structural, Redox, and Magnetic Properties of Bimetallic Complexes with M^{II}–(μ-OH)–Fe^{III} Cores. *Manuscript in preparation.*

CHAPTER 2

Sulfonamido tripods: tuning redox potentials via ligand modifications

Introduction

As discussed in Chapter 1, the relationship between the primary and secondary coordination spheres has an important effect on the properties of the metal center, particularly on its redox properties.[1–3] This is illustrated by several studies involving metalloenzymes which demonstrated that modifications in either the primary or secondary coordination spheres directly influence the electrochemical properties of metal centers. For instance, Lu showed that changes in the primary and secondary coordination spheres of a single Cu center had a large impact on the Cu^{I}/Cu^{II} redox couple in blue copper proteins.[4–6] Lowe investigated the effect of modifying the *para*-substituents of a tyrosine residue located in the secondary coordination sphere of the Fe^{III} center in rubredoxin.[7] Though only small changes in the redox potential were effected, they observed a strong correlation between the Fe^{II}/Fe^{III} redox couple and the Hammett constants (σ_p) of the non-native *para*-substituents of the tyrosine-based residues. Even larger changes were reported by Miller in a series of mutated Fe superoxide dismutases, in which a single point mutation caused a change of greater than 500 mV for the Fe^{II}/Fe^{III} redox couple.[8]

Additionally, numerous synthetic systems have shown that varying the structural features on ligands can control redox processes.[9–12] Work by Costas illustrated how physical properties of Fe complexes can be varied through modification of ring substituents of a coordinated pyridine ligand.[13] Moreover, intramolecular hydrogen bonds (H-bonds) within the secondary coordination sphere can alter the redox potential of transition metal complexes.[14–17]

Continuing on this line of inquiry, this chapter details the study of the effect of ligand modifications on the properties of a series of $Fe^{II}–OH_2$ complexes supported by ligands based on the tetradentate sulfonamide-based tripodal ligand *N,N',N''*-(nitrilotris(ethane-2,1-diyl))tris(2,4,6-trimethyl-benzenesulfonamido) ($[MST]^{3–}$).[18–24] Originally prepared by Mountford,[25,26] these types of sulfonamide-based tripodal ligands can be easily modulated by using different commercially available sulfonyl chloride in the synthesis of ligand precursors (Scheme 2.1). This method allowed for the preparation of the family of sulfonamido tripodal ligands *N*,*N*',*N*"-[2,2',2"-nitrilotris(ethane-2,1-diyl)]-tris-({R-Ph}-sulfonamido) ($[RST]^{3–}$, R = $–CF_3$, –Cl, –H, $–CH_3$, or $–OCH_3$, Figure 2.1) that contained different *para*-substituents on the aryl group of the sulfonamido arms. The physical properties of the five corresponding monomeric $Fe^{II}–OH_2$ complexes were studied to determine if trends arising from the varying electron-withdrawing or -donating properties of the different R groups could be observed. The data showed that the electrochemical properties of the complexes can be predictably tuned through the modulation of the ligands at sites that are distant from the metal center.

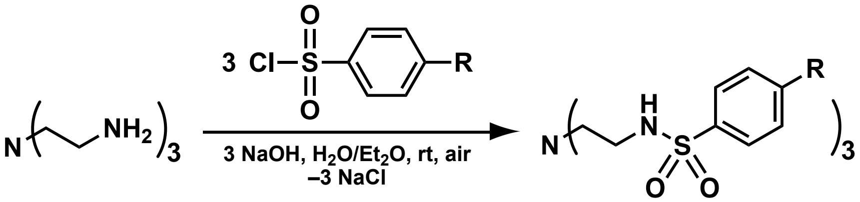

Scheme 2.1. Preparation of H_3RST ligand precursors.

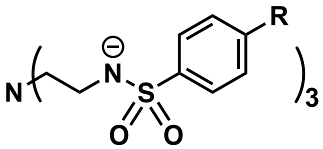

Figure 2.1. $[RST]^{3–}$ ligands (R = $–CF_3$ ($[F_3ST]^{3–}$), –Cl ($[CST]^{3–}$), –H ($[PST^{3–}]$), $–CH_3$ ($[TST]^{3–}$), or $–OCH_3$ ($[MOST]^{3–}$)).

Results and Discussion

Preparation and Properties of the $NMe_4[Fe^{II}RST(OH_2)]$ Compounds

The five $NMe_4[Fe^{II}RST(OH_2)]$ salts were prepared using the synthetic route described in Scheme 2.2, based on preparative routes for $[MST]^{3-}$ complexes.[18–24] First, the putative four-coordinate $NMe_4[Fe^{II}RST]$ salts were isolated from a dimethylacetamide (DMA) solution through precipitation with Et_2O, and their properties were consistent with a formulation of $NMe_4[Fe^{II}RST]$. For instance, vibrational features greater than 3300 cm^{-1} were not observed, suggesting that neither water molecules nor hydroxide ions were coordinated to the iron centers. However, acceptable elemental analysis for any of these salts could not be obtained, presumably because small amounts of the complexes were five-coordinate, which could arise from weakly interacting solvent molecules.

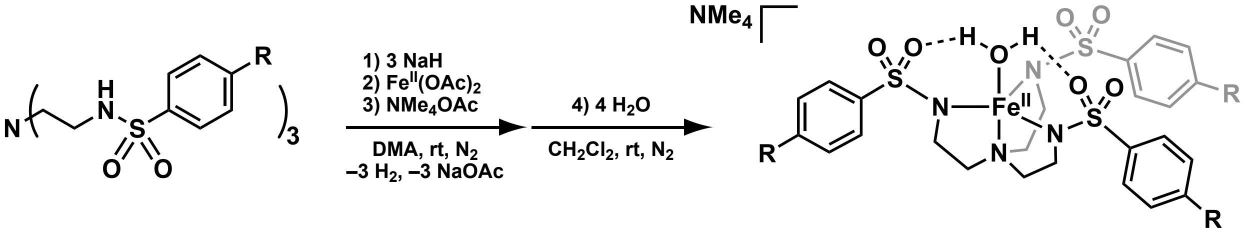

Scheme 2.2. Preparation of $NMe_4[Fe^{II}RST(OH_2)]$ compounds.

To prepare the $Fe^{II}–OH_2$ complexes, CH_2Cl_2 solutions of the $[Fe^{II}RST]^-$ complexes were treated with four equivalents of water. CH_2Cl_2 solutions of the aqua species were layered under pentane to afford crystalline products in yields ranging from 74–96%.

The $NMe_4[Fe^{II}RST(OH_2)]$ salts were characterized by X-band electron paramagnetic resonance (EPR) and Fourier transform infrared (FTIR) spectroscopies, solution effective magnetic moment measurements, and elemental analysis. The perpendicular-mode EPR spectra measured at 77 K did not contain any features, which is consistent with each complex having a high-spin Fe^{II} center. This premise is supported by the room temperature solution effective magnetic moment of the complexes determined using Evans' method.[27] The effective magnetic moments for the complexes were virtually identical and closely matched the spin-only magnetic moment value of 4.9 μ_B. These values can be attributed to an S = 2 spin ground-state from the five-coordinate Fe^{II} complexes. FTIR spectra of the complexes recorded as a Nujol mull revealed the presence of peaks that ranged between 3300 to 3250 cm^{-1}, which is consistent with O–H vibrations from a coordinated water molecule.

Solid-State Molecular Structures of $[Fe^{II}RST(OH_2)]^-$ Complexes

The molecular structures of the $NMe_4[Fe^{II}RST(OH_2)]$ salts were characterized by X-ray diffraction methods. Selected bond lengths and bond angles are given in Table 2.1 and representative thermal ellipsoid diagrams of $[Fe^{II}TST(OH_2)]^-$ and $[Fe^{II}PST(OH_2)]^-$ are shown in Figure 2.2. All the salts crystallized with their anionic complexes as monomers, with one distinct metal complex per asymmetric unit cell for three of the five salts: $NMe_4[Fe^{II}CST(OH_2)]$, $NMe_4[Fe^{II}PST(OH_2)]$, and $NMe_4[Fe^{II}TST(OH_2)]$. Two crystallographically distinct but chemically equivalent complexes were contained per asymmetric unit cell in $NMe_4[Fe^{II}F_3ST(OH_2)]$ and $NMe_4[Fe^{II}MOST(OH_2)]$.

Each $[Fe^{II}RST(OH_2)]^-$ complex had a similar N_4O primary coordination sphere around the Fe^{II} center, whereby the trigonal plane was defined by the three deprotonated nitrogen atoms (N2, N3, N4) from the sulfonamido groups. One apical position (N1) was occupied by the amine nitrogen atom of the $[RST]^{3-}$ ligands and the other site is taken by oxygen atom (O1) from the exogenous aqua ligand. The Fe^{II} center was displaced from the trigonal plane in each complex (~

0.35 Å) toward the O1. Each complex showed a modest distortion from idealized trigonal bipyramidal (tbp) coordination geometry based on the structural parameter τ_5 = 0.826 – 0.859, where τ_5 = 1 for ideal tbp geometry and τ_5 = 0 for ideal square pyramidal geometry.[28] The distortions from idealized tbp could be partially caused by the Jahn-Teller effect that should be present in high-spin d^6 metal complex having local C_3 symmetry.[29] This effect should be small because it arises from the d_{xz} and d_{yz} orbitals that are formally non-bonding. A larger contributor to the distortion is the contraction of the N1–Fe1–O1 angle, which in each complex was less than 175˚. Note that the "bend" in the angle was such that O1 is positioned towards two of the sulfonamido arms containing O2 and O4, with O1···O2 distances ranging from 2.672 – 2.763 Å and the O1···O4 distances ranging from 2.676 – 2.782 Å. Both these distances were indicative of H-bonds formed between the aqua ligand and oxygen atoms of the sulfonamido groups from two different arms of the $[RST]^{3-}$ ligands. These two intramolecular H-bonds undoubtedly assist in positioning the aqua ligand within the complexes.[30] The other metrical parameters were consistent with values found in similar Fe^{II} complexes.[31]

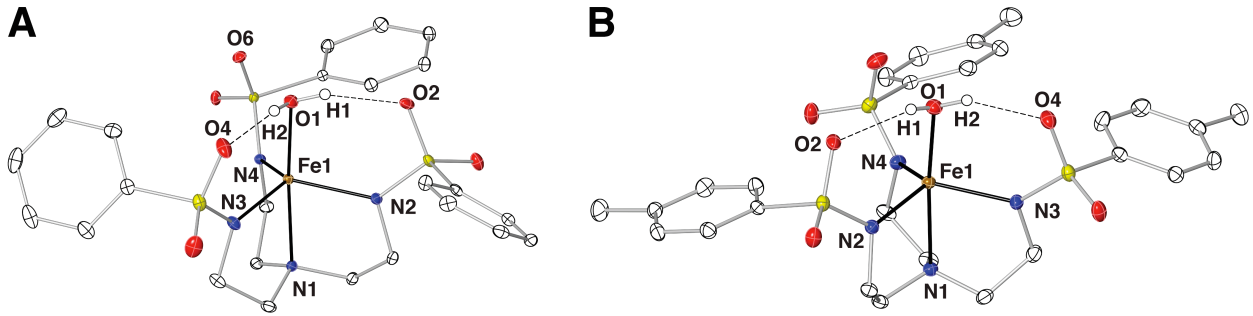

Figure 2.2. Thermal ellipsoid diagram depicting the molecular structure of (**A**) $[Fe^{II}PST(OH_2)]^-$ and (**B**) $[Fe^{II}TST(OH_2)]^-$. Ellipsoids are drawn at the 50% probability level, and only the aqua H-atoms are shown for clarity.

Table 2.1. Selected metrical parameters for the $[Fe^{II}RST(OH_2)]^-$ complexes.

$[Fe^{II}RST(OH_2)]^-$	R =				
	$-CF_3$*	–Cl	–H	$-CH_3$	$-OCH_3$*
			Bond distances (Å)		
Fe1–O1	2.120(3)	2.096(2)	2.139(1)	2.099(2)	2.164(4)
Fe1–N1	2.208(3)	2.219(2)	2.214(1)	2.227(2)	2.226(4)
Fe1–N2	2.010(3)	2.112(2)	2.107(1)	2.086(2)	2.071(4)
Fe1–N3	2.071(3)	2.094(2)	2.098(1)	2.108(2)	2.091(4)
Fe1–N4	2.082(3)	2.070(2)	2.065(1)	2.069(2)	2.041(4)
O1···O2	2.672	2.708	2.697	2.763	2.673
O1···O4	2.782	2.773	2.676	2.701	2.707
O1···O6	3.005	3.087	3.089	3.090	3.089
Average Fe–N_{eq}	2.084(3)	2.092(2)	2.090(1)	2.088(2)	2.068(4)
Bond angle (°)					
N1-Fe1-O1	174.91(1)	169.74 (6)	170.91(5)	170.25(7)	173.19(1)
N1-Fe1-N2	80.25(1)	80.11 (6)	79.08(5)	79.17(7)	80.50(1)
N1-Fe1-N3	79.75(1)	78.93 (6)	80.76(5)	80.20(7)	79.63(1)
N1-Fe1-N4	80.98(1)	80.13(6)	80.58(5)	79.85(7)	80.85(1)
N2-Fe1-N3	115.48(1)	115.57(7)	114.60(5)	115.98(7)	112.21(2)
N2-Fe1-N4	120.95(1)	120.18(7)	116.96(5)	115.70(7)	116.40(2)
N3-Fe1-N4	115.24(1)	114.93(7)	119.85(5)	119.02(8)	123.04(2)
τ_5 value	0.859	0.826	0.851	0.854	0.836

*Indicates average values, because of two crystallographically distinct but chemically equivalent complexes in the asymmetric unit cell of these structures.

Effects of the Substituents on the $[RST]^{3-}$ Ligands: Vibrational Properties

The *para*-substituents on aryl groups of the $[RST]^{3-}$ ligands varied in their electronic effects, which should cause predictable changes in the physical and chemical properties of these compounds. However, no correlations between the substituents and either the vibrational properties of the coordinated aqua ligands or the structural parameters of the complexes were observed. The energies of the ν(OH) bands would be expected to be related to ability of the primary coordination sphere to donate electron density to the Fe^{II} center, which should be influenced by the various *para-* substituents. More electron-donating substituents (e.g. R = –

OCH_3) should increase the electron density at the metal center. This effect should decrease the acidity of the protons of the aqua ligand and be observable as an increase in the energy of the ν(OH) band relative to those complexes with more electron-withdrawing substituents. Yet this analysis is complicated by the presence of intramolecular H-bonds involving the coordinated aqua ligand. The electron-donating and -withdrawing properties of the substituents on the $[RST]^{3-}$ ligands also affect their ability to act as H-bond acceptors, with the more electron-donating ligands being able to form stronger H-bonds, resulting in an increase in acidity of the aqua ligand protons. Therefore, it appears that the effect of this ligand modification on the primary and secondary coordination spheres counteract each other, which could explain the observed lack of correlations.

Effects of the Substituents on the $[RST]^{3-}$ Ligands: Structural Properties

There are no statistically significant trends between the electronic properties of the *para*-substituent on the $[RST]^{3-}$ ligand and the structural parameters of the $[Fe^{II}RST(OH_2)]^-$ complexes. For example, the Fe1–O1 bond distances should change in accordance with the effects of the substituent on the $[RST]^{3-}$ ligand, with shortest bond distance predicted to be found in $[Fe^{II}F_3ST(OH_2)]^-$. However, $[Fe^{II}TST(OH_2)]^-$ and $[Fe^{II}CST(OH_2)]^-$ had statistically equivalent Fe1–O1 bond lengths and were the shortest values in the series. In addition, the average Fe1–N_{eq} bond distances in $[Fe^{II}TST(OH_2)]^-$, $[Fe^{II}PST(OH_2)]^-$, $[Fe^{II}CST(OH_2)]^-$, $[Fe^{II}F_3ST(OH_2)]^-$ are statistically equivalent. There could be a slight correlation between ligand electron-withdrawing properties with the Fe1–N1 bond length, as marginally shorter lengths were observed with $[Fe^{II}PST(OH_2)]^-$, $[Fe^{II}CST(OH_2)]^-$, $[Fe^{II}F_3ST(OH_2)]^-$.

Effects of the Substituents on the $[RST]^{3-}$ Ligands: Redox Properties.

The electrochemical properties of the $[Fe^{II}RST(OH_2)]^{-}$ complexes were explored using cyclic voltammetry (CV) (Figure 2.3). A quasi-reversible one-electron process was observed for each complex, which was assigned as the Fe^{II}/Fe^{III} couple. In contrast to the discussion above, the redox potentials for this couple did trend with the electronic effects of the ligand, as shown by a linear Hammett plot of the $E_{1/2}$ of the Fe^{II}/Fe^{III} couple vs. the σ_p of the ligand *para*- substituents (Figure 2.4).[32] The high r^2 value of 0.99 for the linear best-fit demonstrates a high correlation between the oxidation potentials and the electronic properties of the different $[RST]^{3-}$ ligands. Complexes with ligands that contained *para*-substituents with greater electron-withdrawing ability shifted the Fe^{II}/Fe^{III} couple to more positive potentials, which is consistent with these ligands stabilizing the $Fe^{II}–OH_2$ complexes.[33]

The potential difference between the complex with the most electron-withdrawing ligand, $[F_3ST]^{3-}$, and the most electron-donating ligand, $[MOST]^{3-}$, was 157 mV or a free energy difference of 3.62 kcal mol^{-1}. This corresponds to an approximately 450-fold decrease in the rate of electron transfer between the complex with $[F_3ST]^{3-}$ and $[MOST]^{3-}$ at room temperature. Moreover, the slope of the linear trend line is 4.5 kcal mol^{-1} per Hammett unit. This is greater than the slope of the linear trend line of 0.7 kcal mol^{-1} per Hammett unit observed in the previously mentioned study by Lowe on synthetic rubredoxins that examined only secondary coordination sphere effects,[7] but less than the slope of the linear trend line of 9.9 kcal mol^{-1} per Hammett unit observed in a study by Chambers on a series of Fe^{II} bis-terpyridyl complexes that examined primary coordination sphere effects.[11]

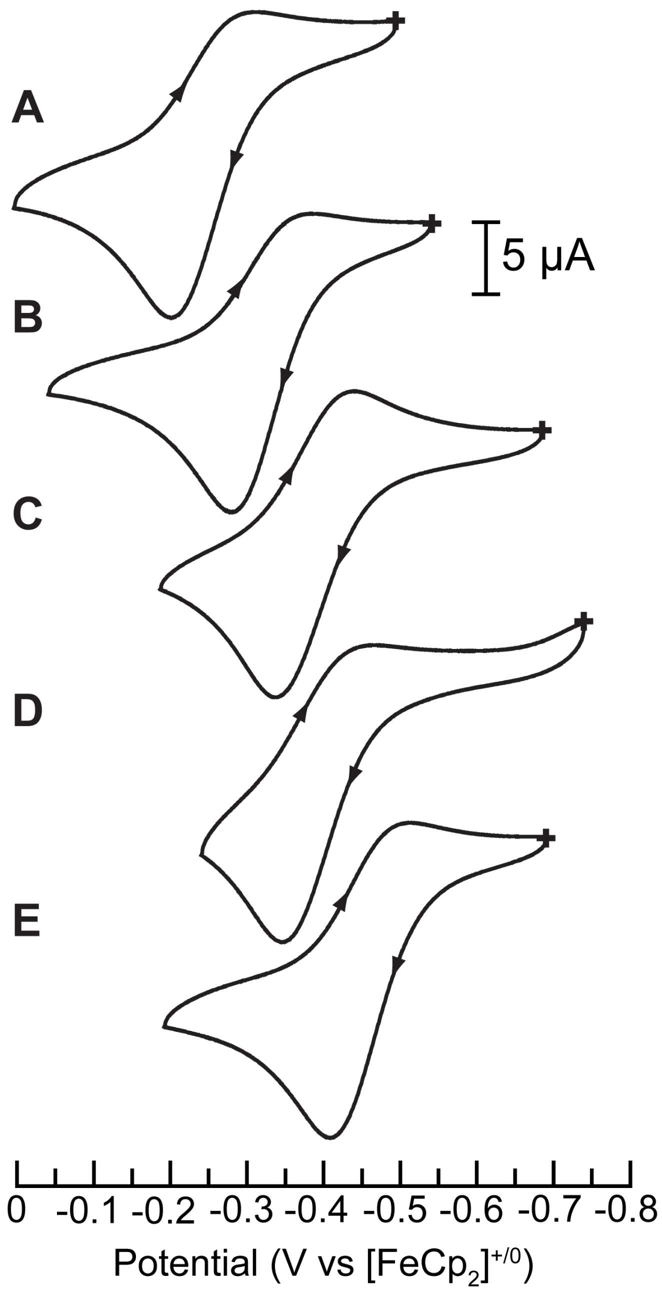

Figure 2.3. Cyclic voltammagram of (**A**) $NMe_4[Fe^{II}F_3ST(OH_2)]$, (**B**) $NMe_4[Fe^{II}CST(OH_2)]$, (**C**) $NMe_4[Fe^{II}PST(OH_2)]$, (**D**) $NMe_4[Fe^{II}TST(OH_2)]$, (**E**) $NMe_4[Fe^{II}MOST(OH_2)]$ measured in acetonitrile (MeCN, 0.1 M tetrabutylammonium hexafluorophosphate (TBAP) solution). All voltammagrams were collected at 100 mV s^{-1} and internally referenced against the cobaltocenium/cobaltocene couple ($[CoCp_2]^{0/+}$), then scaled against the ferrocene/ferrocenium couple ($[FeCp_2]^{+/0}$).[34]

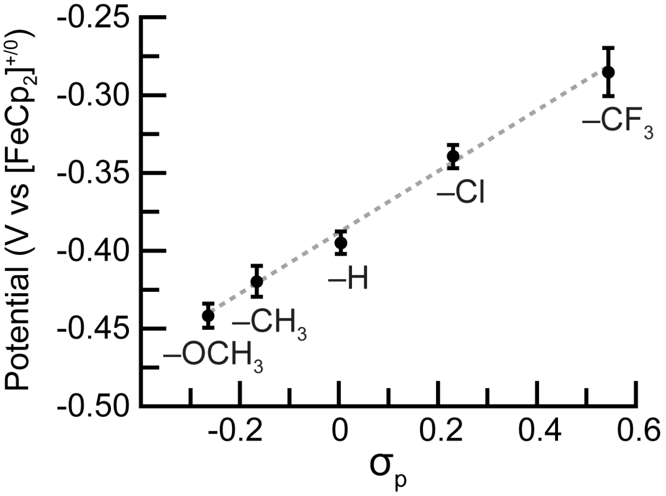

Figure 2.4. Plot of the $E_{1/2}$ of the Fe^{II}/Fe^{III} couple vs. σ_p of the ligand *para*-substituents, with the *para*-substituent R group specified.

Summary and Conclusions

This chapter presents the synthesis and characterization of a series of $Fe^{II}–OH_2$ complexes with sulfonamido tripodal ligands. These ligands were designed to vary the properties at the iron center *via* modifying the *para*-substituent of the aryl group on the ligand sulfonamido arms. The $[Fe^{II}RST(OH_2)]^-$ complexes have many similar properties despite the modulation of the ligands. Structurally, all the complexes in this series have nearly the same distorted tbp geometry with small metrical differences in their primary coordination spheres. The complexes were determined to have high-spin S = 2 Fe^{II} centers, as each of their effective magnetic moments agreed closely with the spin-only magnetic moment value of 4.9 μ_B. Moreover, the vibrational properties of the $[Fe^{II}RST(OH_2)]^-$ complexes, specifically the energies of the bands associated with the ν(OH), did not show a correlation with the substituent effects on the $[RST]^{3-}$ ligands. This lack of correlative relationships is attributed to the presence of intramolecular H-bonds within each complex. Comparing the H-bond donating properties of the $Fe–OH_2$ unit with the H-bond accepting ability of the $[RST]^{3-}$ ligands throughout the series of complexes suggests that the H-bonds mitigate the influence that the substituents may have on these properties of the complexes. However, the effect of ligand modification is strongly correlated with the redox potentials within the series of $[Fe^{II}RST(OH_2)]^{-}$ complexes. A linear trend between the redox potentials of the Fe^{II}/Fe^{III} couples and the σ_p for the ligand *para*-substituent was observed, suggesting that the electrochemical properties of the complexes can be tuned by modifying the $[RST]^{3-}$ ligands.

Experimental

General Methods

All reagents were purchased from commercial sources and used as received unless otherwise noted. Solvents were sparged with argon and dried over columns containing Q-5 and molecular sieves. The syntheses of the ligands were carried out in air and the preparations of metal complexes were conducted in a Vacuum Atmospheres, Co. drybox under nitrogen or argon atmosphere. NaH as a 60% dispersion in mineral oil was filtered with a medium porosity glass-fritted funnel and washed 5 times each with pentane and Et_2O. Solid NaH was dried under vacuum and stored under inert atmosphere. Water was degassed by five freeze-pump-thaw cycles and stored under inert atmosphere. $Fe(OAc)_2$[35] and the ligand precursors H_3PST, [36] H_3TST,[37] and H_3MOST,[38] were synthesized following literature procedures.

Preparation of Ligand Precursors

N,N',N''-(nitrilotris(ethane-2,1-diyl))tris(4-(trifluoromethyl)-benzene-sulfonamide) (H_3F_3ST). To a 250 mL round bottom flask containing tris(2-aminoethyl)amine (tren) (0.25 g, 1.7 mmol) and

NaOH (0.33 g, 8.2 mmol) in water (20 mL), 4-(trifluoromethyl)benzenesulfonyl chloride (1.3 g, 5.4 mmol) dissolved in Et_2O (10 mL) was added dropwise at room temperature with vigorous stirring. After allowing the reaction mixture to stir for 2 days, the Et_2O was removed under reduced pressure and the resulting white precipitate was collected on a medium porosity glass-fritted funnel and washed with water. The resulting white power was dried under reduced pressure overnight, then dissolved in CH_2Cl_2 (100 mL) and dried with anhydrous sodium sulfate. After filtering off the insoluble species, the solvent was removed and the residue was dried under vacuum at 45 °C for 5 h. The residue was brought into the dry box, redissolved in CH_2Cl_2 (10 mL), and precipitated with pentane to give 0.81 g (62%) of an ivory powder. FTIR (KBr disc, cm^{-1}, selected bands): 3353, 3303, 3262, 3106, 2965, 2824, 1610, 1405, 1323, 1165, 1106, 1062, 958, 846, 713, 602, 554. ^1H NMR (500 MHz, $CDCl_3$, ppm): 2.61 (t, 2H), 3.06 (t, 2H), 5.91 (br s, 1H NH), 7.79 (d, 2H), 8.08 (d, 2H). ^{13}C NMR (500 MHz, $CDCl_3$, ppm): 41.5, 54.8, 126.8, 128.0, 129.3, 143.6. HRMS (ES+, m/z): Exact mass calcd for $C_{27}H_{27}N_4O_6S_3F_9$: 771.10, Found: 771.04.

N,N',N''-(nitrilotris(ethane-2,1-diyl))tris(4-chloro-benzenesulfonamide) (H_3CST). Prepared in an analogous manner to H_3F_3ST using tren (0.26 g, 1.8 mmol), NaOH (0.34 g, 8.4 mmol), 4-chlorobenzenesulfonyl chloride (1.2 g, 5.6 mmol) to give 0.66 g (55%) product. FTIR (KBr disc, cm^{-1}, selected bands): 3291, 3093, 2957, 2850, 1587, 1477, 1396, 1327, 1162, 1094, 955, 825, 753, 618, 567. ^1H NMR (500 MHz, $CDCl_3$, ppm): 2.55 (t, 2H), 2.98 (t, 2H), 5.91 (br s, 1H NH), 7.49 (d, 2H), 7.86 (d, 2H). ^{13}C NMR (500 MHz, $CDCl_3$, ppm): 41.4, 54.7, 129.0, 129.9, 138.5, 139.6. HRMS (ES+, m/z): Exact mass calcd for $C_{24}H_{27}N_4O_6S_3Cl_3$: 669.02, Found: 669.01.

Preparation of Complexes

$NMe_4[Fe^{II}F_3ST(OH_2)]$. A solution of H_3F_3ST (300 mg, 0.39 mmol) dissolved in 6 mL of anhydrous DMA was treated with solid NaH (28 mg, 1.2 mmol). The mixture was stirred until gas evolution ceased. $Fe(OAc)_2$ (68 mg, 0.39 mmol) and NMe_4OAc (52 mg, 0.39 mmol), were added to the cloudy white reaction, and the solution was stirred. After 3 h, 5 mL of Et_2O was added to the yellow solution to aid the precipitation of NaOAc. The reaction mixture was filtered through a medium porosity glass-fritted funnel to remove the insoluble species and the filtrate was dried under vacuum. The resulting pale yellow solid was redissolved in 5 mL of MeCN, stirred for 20 min, and filtered using a fine porosity glass-fritted funnel. The filtrate was concentrated under vacuum to *ca.* 1 mL and treated with Et_2O (10 mL) then pentane (40 mL) to precipitate a pale yellow solid. This solid was collected on a medium porosity glass-fritted funnel and dried under vacuum to give 182 mg (91%) of product. FTIR (KBr disc, cm^{-1}, selected bands): 3413, 3046, 2964, 2902, 2861, 1608, 1490, 1403, 1326, 1263, 1134, 1062, 976, 821, 710, 622, 605. MS (ES-, m/z): Exact mass calcd for $C_{27}H_{24}N_4O_6S_3F_9Fe$: 823.0, Found: 823.1. This salt, presumably $NMe_4[Fe^{II}F_3ST]$ (103 mg, 0.12 mmol) in 5 mL of CH_2Cl_2, was treated with H_2O (8 µL, 0.46 mmol) in one portion *via* a syringe and the mixture was stirred. After 15 min, volatiles were removed under reduced pressure and the solid residue was redissolved in CH_2Cl_2 (6 mL), filtered through a medium porosity glass-fritted funnel, and layered under pentane. White needle crystals were collected via filtration and dried under vacuum, to give 98 mg (94%) of crystalline product. Elemental analysis calcd for $NMe_4[Fe^{II}F_3ST(OH_2)]$ $C_{31}H_{38}N_5O_7S_3F_9Fe$: C, 40.66; H, 4.18; N, 7.65%, Found: C, 40.74; H, 4.06; N, 7.32%. FTIR (KBr disc, cm^{-1}, selected bands): 3340, 3044, 2964, 2899, 2860,

1608, 1490, 1403, 1327, 1261, 1136, 1062, 977, 825, 710, 622, 605. (Nujol, cm^{-1}): 3295 (OH). μ_{eff} (μ_B): 4.7(2). $E_{1/2}$ (MeCN): –0.284 V vs. $[FeCp_2]^{0/+}$.

NMe$_4$[Fe^{II}CST(OH$_2$)]. This salt was prepared in an analogous manner to $NMe_4[Fe^{II}F_3ST(OH_2)]$ using H_3CST (180 mg, 0.27 mmol), NaH (20 mg, 0.81 mmol), $Fe(OAc)_2$ (47 mg, 0.27 mmol), NMe_4OAc (38 mg, 0.28 mmol) to isolate a pale yellow powder, which presumably was the $NMe_4[Fe^{II}CST]$ salt (141 mg, 66%). FTIR (KBr disc, cm^{-1}, selected bands): 3341, 3036, 2960, 2898, 2856, 1636, 1581, 1477, 1392, 1251, 1141, 1084, 975, 823, 751, 630, 593. MS (ES-, m/z): Exact mass calcd for $C_{24}H_{24}N_4O_6S_3Cl_3Fe$: 720.9, Found: 721.0. The isolated $NMe_4[Fe^{II}CST]$ (33 mg, 0.04 mmol) was treated with H_2O (3 µL, 0.17 mmol) in an analogous manner to $NMe_4[Fe^{II}\ F_3ST(OH_2)]$ to give 28 mg (83%) of crystalline product. Elemental analysis calcd for $NMe_4[Fe^{II}CST(OH_2)]$ $C_{28}H_{38}N_5O_7S_3Cl_3Fe$: C, 41.26; H, 4.70; N, 8.59%, Found: C, 41.09; H, 4.57; N, 8.22%. FTIR (KBr disc, cm^{-1}, selected bands): 3313, 3036, 2964, 2899, 2855, 1580, 1476, 1391, 1247, 1138, 1083, 975, 821, 751, 629, 593. (Nujol, cm^{-1}): 3303 (OH). μ_{eff} ($CDCl_3$, μ_B): 4.8(3). $E_{1/2}$ (MeCN): -0.338 V vs. $[FeCp_2]^{0/+}$.

NMe$_4$[Fe^{II}PST(OH$_2$)]. This salt was prepared in an analogous manner to $NMe_4[Fe^{II}F_3ST(OH_2)]$ using H_3PST (300 mg, 0.53 mmol), NaH (38 mg, 1.6 mmol), $Fe(OAc)_2$ (92 mg, 0.53 mmol), NMe_4OAc (71 mg, 0.53 mmol) to isolate a pale yellow powder, which presumably was the $NMe_4[Fe^{II}PST]$ salt (340 mg, 93%). FTIR (KBr disc, cm^{-1}, selected bands): 3297, 3035, 2955, 2897, 2853, 1489, 1445, 1246, 1132, 974, 821, 761, 715, 694, 608, 586. MS (ES-, m/z): Exact mass calcd for $C_{24}H_{27}N_4O_6S_3Fe$: 619.0, Found: 619.1. The isolated $NMe_4[Fe^{II}PST]$ salt (26 mg, 0.04 mmol) was treated with H_2O (3 µL, 0.14 mmol) in an analogous manner to $NMe_4[Fe^{II}F_3ST(OH_2)]$ to give 27 mg (85%) of crystalline product. Elemental analysis calcd for $NMe_4[Fe^{II}PST(OH_2)]$ $C_{28}H_{41}N_5O_7S_3Fe$: C, 47.25; H, 5.81; N, 9.84%, Found: C, 47.19; H, 5.53; N, 9.63%. FTIR (KBr disc, cm^{-1}, selected bands): 3313, 3034, 2957, 2897, 2854, 1489, 1445, 1247, 1132, 975, 821, 761, 714, 694, 608, 586. (Nujol, cm^{-1}): 3290 (OH). μ_{eff} ($CDCl_3$, μ_B): 4.9(9). $E_{1/2}$ (MeCN): -0.394 V vs. $[FeCp_2]^{0/+}$.

$NMe_4[Fe^{II}TST(OH_2)]$. This salt was prepared in an analogous manner to $NMe_4[Fe^{II}F_3ST(OH_2)]$ using H_3TST (300 mg, 0.49 mmol), NaH (30 mg, 1.2 mmol), $Fe(OAc)_2$ (71 mg, 0.41 mmol), NMe_4OAc (55 mg, 0.41 mmol) to isolate a pale yellow powder which presumably was the $NMe_4[Fe^{II}TST]$ salt (310 mg, 86%). FTIR (KBr disc, cm^{-1}, selected bands): 3264, 3037, 2958, 2896, 2850, 1599, 1492, 1325, 1246, 1138, 975, 818, 664, 600, 555. MS (ES-, m/z): Exact mass calcd for $C_{27}H_{33}N_4O_6S_3Fe$: 661.1, Found: 661.2. The isolated solid $NMe_4[Fe^{II}TST]$ salt (56 mg, 0.08 mmol) was treated with H_2O (5 µL, 0.30 mmol) in an analogous manner to $NMe_4[Fe^{II}F_3ST(OH_2)]$ to give 42 mg (74%) of crystalline product. Elemental analysis calcd for $NMe_4[Fe^{II}TST(OH_2)]$ $C_{31}H_{47}N_5O_7S_3Fe$: C, 49.40; H, 6.28; N, 9.29%, Found: C, 49.21; H, 6.04; N, 9.02%. FTIR (KBr disc, cm^{-1}, selected bands): 3281, 3036, 2957, 2896, 2852, 1599, 1491, 1244, 1138, 975, 817, 664, 599, 554. (Nujol, cm^{-1}): 3249 (OH). μ_{eff} ($CDCl_3$, μ_B): 4.8(1). $E_{1/2}$ (MeCN): -0.419 V vs. $[FeCp_2]^{0/+}$.

$NMe_4[Fe^{II}MOST(OH_2)]$. This salt was prepared in an analogous manner to $NMe_4[Fe^{II}F_3ST(OH_2)]$ using H_3MOST (200 mg, 0.30 mmol), NaH (22 mg, 0.91 mmol), $Fe(OAc)_2$ (53 mg, 0.30 mmol), NMe_4OAc (41 mg, 0.30 mmol) to isolate a pale yellow powder ($NMe_4[Fe^{II}MOST]$) in 76% yield. FTIR (KBr disc, cm^{-1}, selected bands): 3264, 3036, 2958, 2898, 2847, 1597, 1496, 1304, 1250,

1134, 1013, 975, 818, 667, 601, 564. MS (ES-, m/z): Exact mass calcd for $C_{27}H_{33}N_4O_9S_3Fe$ 709.1, Found 709.1. The isolated solid $NMe_4[Fe^{II}MOST]$ (62 mg, 0.08 mmol) was treated with H_2O (6 µL, 0.31 mmol) in an analogous manner to $NMe_4[Fe^{II} F_3ST(OH_2)]$ to give 61 mg (96%) of crystalline product. Elemental analysis calcd for $NMe_4[Fe^{II}MOST(OH_2)]$ $C_{31}H_{47}N_5O_{10}S_3Fe$: C, 46.44; H, 5.91; N, 8.73%, Found: C, 46.34; H, 5.62; N, 8.66%. FTIR (KBr disc, cm^{-1}, selected bands): 3302, 3039, 2961, 2897, 2843, 1597, 1496, 1306, 1254, 1134, 1025, 972, 832, 667, 603, 564. (Nujol, cm^{-1}): 3247 (OH). μ_{eff} ($CDCl_3$, μ_B): 4.9(3). $E_{1/2}$ (MeCN): -0.441 V vs. $[FeCp_2]^{0/+}$.

Physical Methods

Elemental analyses were performed on a Perkin-Elmer 2400 CHNS analyzer. ^1H-NMR and ^{13}C-NMR were recorded on a Bruker DRX500 spectrometer. FTIR spectra were collected on a Varian 800 Scimitar Series FTIR spectrometer. High-resolution mass spectra were collected using Waters Micromass LCT Premier Mass Spectrometer. Perpendicular-mode X-band EPR spectra were collected using a Bruker EMX spectrometer at 77K using liquid nitrogen. Solution effective magnetic moments were measured by the Evans' method on a Bruker DRX500 spectrometer using flame sealed standard cores of 1:1 $CHCl_3$:$CDCl_3$.[27] CV experiments were conducted using a CH1600C electrochemical analyzer. A 2.0 mm glassy carbon electrode was used as the working electrode at scan velocities 0.1 Vs^{-1} unless otherwise noted. $[CoCp_2]^{0/+}$ was used as an internal reference then scaled against $[FeCp_2]^{+/0}$.[34] TBAP was use as the supporting electrolyte at a concentration of 0.1 M. Electrochemical values are reported as the average of three independent measurements.

Crystallography

A Bruker SMART APEX II diffractometer and the APEX2 program package was used to determine the unit-cell parameters and for data collection. Crystallographic details are summarized in Appendix A.

References

(1) Colquhoun, H. M.; Stoddart, J. F.; Williams, D. J. Second-Sphere Coordination–a Novel Role for Molecular Receptors. *Angew. Chemie Int. Ed. English* **1986**, *25*, 487–507.

(2) Borovik, A. S. Bioinspired hydrogen bond motifs in ligand design: the role of noncovalent interactions in metal ion mediated activation of dioxygen. *Acc. Chem. Res.* **2005**, *38*, 54–61.

(3) Shook, R. L.; Borovik, A. S. Role of the secondary coordination sphere in metal-mediated dioxygen activation. *Inorg. Chem.* **2010**, *49*, 3646–3660.

(4) Garner, D. K.; Vaughan, M. D.; Hwang, H. J.; Savelieff, M. G.; Berry, S. M.; Honek, J. F.; Lu, Y. Reduction potential tuning of the blue copper center in Pseudomonas aeruginosa azurin by the axial methionine as probed by unnatural amino acids. *J. Am. Chem. Soc.* **2006**, *128*, 15608–15617.

(5) Marshall, N. M.; Garner, D. K.; Wilson, T. D.; Gao, Y.-G.; Robinson, H.; Nilges, M. J.; Lu, Y. Rationally tuning the reduction potential of a single cupredoxin beyond the natural range. *Nature* **2009**, *462*, 113–116.

(6) Farver, O.; Marshall, N. M.; Wherland, S.; Lu, Y.; Pecht, I. Designed azurins show lower reorganization free energies for intraprotein electron transfer. *Proc. Natl. Acad. Sci. U. S. A.* **2013**, *110*, 10536–10540.

(7) Low, D. W.; Hill, M. G. Rational Fine-Tuning of the Redox Potentials in Chemically Synthesized Rubredoxins. *J. Am. Chem. Soc.* **1998**, *120*, 11536–11537.

(8) Yikilmaz, E.; Rodgers, D. W.; Miller, A.-F. The crucial importance of chemistry in the structure-function link: manipulating hydrogen bonding in iron-containing superoxide dismutase. *Biochemistry* **2006**, *45*, 1151–1161.

(9) Hong, S.; Hill, L. M. R.; Gupta, A. K.; Naab, B. D.; Gilroy, J. B.; Hicks, R. G.; Cramer, C. J.; Tolman, W. B. Effects of electron-deficient beta-diketiminate and formazan supporting ligands on copper(I)-mediated dioxygen activation. *Inorg. Chem.* **2009**, *48*, 4514–4523.

(10) Sjödin, M.; Gätjens, J.; Tabares, L. C.; Thuéry, P.; Pecoraro, V. L.; Un, S. Tuning the redox properties of manganese(II) and its implications to the electrochemistry of manganese and iron superoxide dismutases. *Inorg. Chem.* **2008**, *47*, 2897–2908.

(11) Chambers, J.; Eaves, B.; Parker, D.; Claxton, R.; Ray, P. S.; Slattery, S. J. Inductive influence

of 4′-terpyridyl substituents on redox and spin state properties of iron(II) and cobalt(II) bis-terpyridyl complexes. *Inorganica Chim. Acta* **2006**, *359*, 2400–2406.

(12) Buttafava, A.; Fabbrizzi, L.; Perotti, A.; Poggi, A.; Poli, G.; Seghi, B. Trivalent nickel bis(triaza macrocyclic) complexes. Ligand ring size and medium effects on the nickel(III)/nickel(II) redox couple potential. *Inorg. Chem.* **1986**, *25*, 1456–1461.

(13) Prat, I.; Company, A.; Corona, T.; Parella, T.; Ribas, X.; Costas, M. Assessing the impact of electronic and steric tuning of the ligand in the spin state and catalytic oxidation ability of the Fe(II)(Pytacn) family of complexes. *Inorg. Chem.* **2013**, *52*, 9229–9244.

(14) Mukherjee, J.; Lucas, R. L.; Zart, M. K.; Powell, D. R.; Day, V. W.; Borovik, A. S. Synthesis, structure, and physical properties for a series of monomeric iron(III) hydroxo complexes with varying hydrogen-bond networks. *Inorg. Chem.* **2008**, *47*, 5780–5786.

(15) Mareque Rivas, J. C.; Hinchley, S. L.; Metteau, L.; Parsons, S. The strength of hydrogen bonding to metal-bound ligands can contribute to changes in the redox behaviour of metal centres. *Dalton Trans.* **2006**, No. 19, 2316–2322.

(16) Tani, F.; Matsu-ura, M.; Nakayama, S.; Ichimura, M.; Nakamura, N.; Naruta, Y. Synthesis and Characterization of Alkanethiolate-Coordinated Iron Porphyrins and Their Dioxygen Adducts as Models for the Active Center of Cytochrome P450: Direct Evidence for Hydrogen Bonding to Bound Dioxygen. *J. Am. Chem. Soc.* **2001**, *123*, 1133–1142.

(17) Suzuki, N.; Higuchi, T.; Urano, Y.; Kikuchi, K.; Uekusa, H.; Ohashi, Y.; Uchida, T.; Kitagawa, T.; Nagano, T. Novel Iron Porphyrin−Alkanethiolate Complex with Intramolecular NH···S Hydrogen Bond: Synthesis, Spectroscopy, and Reactivity. *J. Am. Chem. Soc.* **1999**, *121*, 11571–11572.

(18) Park, Y. J.; Ziller, J. W.; Borovik, A. S. The Effects of Redox-Inactive Metal Ions on the Activation of Dioxygen: Isolation and Characterization of a Heterobimetallic Complex Containing a Mn^{III}–(μ-OH)–Ca^{II} Core. *J. Am. Chem. Soc.* **2011**, *133*, 9258–9261.

(19) Lacy, D. C.; Park, Y. J.; Ziller, J. W.; Yano, J.; Borovik, A. S. Assembly and Properties of Heterobimetallic $Co^{II/III}/Ca^{II}$ Complexes with Aquo and Hydroxo Ligands. *J. Am. Chem. Soc.* **2012**, *134*, 17526–17535.

(20) Park, Y. J.; Cook, S. A.; Sickerman, N. S.; Sano, Y.; Ziller, J. W.; Borovik, A. S. Heterobimetallic complexes with M^{III}-(μ-OH)-M^{II} cores (M^{III} = Fe, Mn, Ga; M^{II} = Ca, Sr, and Ba): structural, kinetic, and redox properties. *Chem. Sci.* **2013**, *4*, 717–726.

(21) Sano, Y.; Weitz, A. C.; Ziller, J. W.; Hendrich, M. P.; Borovik, A. S. Unsymmetrical Bimetallic Complexes with M^{II}–(μ-OH)–M^{III} Cores ($M^{II}M^{III}$ = $Fe^{II}Fe^{III}$, $Mn^{II}Fe^{III}$, $Mn^{II}Mn^{III}$): Structural, Magnetic, and Redox Proper. *Inorg. Chem.* **2013**, *52*, 10229–10231.

(22) Sickerman, N. S.; Henry, R. M.; Ziller, J. W.; Borovik, A. S. Preparation and structural properties of In^{III}–OH complexes. *Polyhedron* **2013**, *58*, 65–70.

(23) Sickerman, N. S.; Peterson, S. M.; Ziller, J. W.; Borovik, A. S.; Mäemets, V.; Leito, I.; Koppel, I. A.; Borovik, A. S. Synthesis, structure and reactivity of $Fe^{II}/^{III}$–NH_3 complexes bearing a tripodal sulfonamido ligand. *Chem. Commun.* **2014**, *50*, 2515.

(24) Cook, S. A.; Ziller, J. W.; Borovik, A. S. Iron(II) Complexes Supported by Sulfonamido Tripodal Ligands: Endogenous versus Exogenous Substrate Oxidation. *Inorg. Chem.* **2014**, *53*, 11029–11035.

(25) Schwarz, A. D.; Chu, Z.; Mountford, P. Sulfonamide-Supported Aluminum Catalysts for the Ring-Opening Polymerization of *rac*-Lactide. *Organometallics* **2010**, *29*, 1246–1260.

(26) Schwarz, A. D.; Herbert, K. R.; Paniagua, C.; Mountford, P. Ligand Variations in New Sulfonamide-Supported Group 4 Ring-Opening Polymerization Catalysts. *Organometallics* **2010**, *29*, 4171–4188.

(27) Evans, D. F. 400. The determination of the paramagnetic susceptibility of substances in solution by nuclear magnetic resonance. *J. Chem. Soc.* **1959**, 2003–2005.

(28) Addison, A. W.; Rao, T. N.; Reedijk, J.; van Rijn, J.; Verschoor, G. C. Synthesis, structure, and spectroscopic properties of copper(II) compounds containing nitrogen–sulphur donor ligands; the crystal and molecular structure of aqua[1,7-bis(N-methylbenzimidazol-2'-yl)-2,6-dithiaheptane]copper(II) perchlorate. *J. Chem. Soc. Dalt. Trans.* **1984**, No. 7, 1349.

(29) Sickerman, N. S.; Park, Y. J.; Ng, G. K.-Y.; Bates, J. E.; Hilkert, M.; Ziller, J. W.; Furche, F.; Borovik, A. S. Synthesis, structure, and physical properties for a series of trigonal bipyramidal M(II)-Cl complexes with intramolecular hydrogen bonds. *Dalton Trans.* **2012**, *41*, 4358–4364.

(30) Emsley, J. Very strong hydrogen bonding. *Chem. Soc. Rev.* **1980**, *9*, 91.

(31) Matson, E. M.; Bertke, J. A.; Fout, A. R. Isolation of iron(II) aqua and hydroxyl complexes featuring a tripodal H-bond donor and acceptor ligand. *Inorg. Chem.* **2014**, *53*, 4450–4458.

(32) Leffler, J. E.; Grunwald, E. Rates and Equilibria of Organic Reactions as Treated by Statistical, Thermodynamic, and Extrathermodynamic Methods. *Rates and Equilibria of Organic Reactions as Treated by Statistical, Thermodynamic, and Extrathermodynamic Methods*, Reprint.; Dover Publications: New York, 1989.

(33) Tustin, G. J.; Lafitte, V. G. H.; Banks, C. E.; Jones, T. G. J.; Smith, R. B.; Davis, J.; Lawrence, N. S. Synthesis and characterisation of water soluble ferrocenes: Molecular tuning of redox potentials. *J. Organomet. Chem.* **2007**, *692*, 5173–5182.

(34) Connelly, N. G.; Geiger, W. E. Chemical Redox Agents for Organometallic Chemistry. *Chem. Rev.* **1996**, *96*, 877–910.

(35) Weber, B.; Betz, R.; Bauer, W.; Schlamp, S. Crystal Structure of Iron(II) Acetate. *Z. Anorg. Allg. Chem.* **2011**, *637*, 102–107.

(36) Boon, J. M.; Lambert, T. N.; Smith, B. D.; Beatty, A. M.; Ugrinova, V.; Brown, S. N. Structure/Activity Study of Tris(2-aminoethyl)amine-Derived Translocases for Phosphatidylcholine. *J. Org. Chem.* **2002**, *67*, 2168–2174.

(37) Chen, D.; Motekaitis, R. J.; Murase, I.; Martell, A. E. The synthesis of binucleating polyaza macrocyclic and macrobicyclic ligands and the dioxygen affinities of their cobalt

complexes. *Tetrahedron* **1995**, *51*, 77–88.

(38) Warr, R. J.; Westra, A. N.; Bell, K. J.; Chartres, J.; Ellis, R.; Tong, C.; Simmance, T. G.; Gadzhieva, A.; Blake, A. J.; Tasker, P. A.; Schröder, M. Selective extraction and transport of the $[PtCl_6]^{2-}$ anion through outer-sphere coordination chemistry. *Chem. Eur. J.* **2009**, *15*, 4836–4850.

CHAPTER 3

Terminal $Ni^{II}–OH/–OH_2$ complexes in trigonal bipyramidal geometry prepared from H_2O

Introduction

Monomeric metal complexes of first-row transition metal ions with terminal hydroxido and aqua ligands are often difficult to prepare because of the strong tendency of these ligands to bridge between metal centers.[1–10] However, hydroxido and aqua bridging may be prevented using steric effects, as evidenced by the ubiquity of terminal metal hydroxido and aqua units in biology.[11–15] Using steric effects in this manner is also effective in synthetic systems, as most synthetic terminal nickel hydroxido and aqua complexes use sterically encumbered ligand frameworks around the metal center to prevent bridging. Cámpora prepared the earliest examples of monomeric square planar terminal $Ni^{II}–OH$ moieties,[16,17] and a number of similar 4-coordinate terminal $Ni^{II}–OH$ complexes have been developed for catalysis.[18–21] To date, there are only two examples of crystallographically characterized monometallic five-coordinate $Ni^{II}–OH$ complexes. Riordan prepared a square pyramidal complex with a 1,4,8,11-tetramethyl-1,4,8,11-tetraazadodecane ligand in which the exogenous hydroxido ligand is derived from dioxygen,[22] and Levy prepared a trigonal bipyramidal complex with a bulky Schiff base ligand where the exogenous hydroxido ligand is derived from adventitious water.[23] The earliest structurally characterized five-coordinate terminal $Ni^{II}–OH_2$ complex was reported by Stucky in 1969,[24] and since then many other structurally characterized terminal $Ni^{II}–OH_2$ complexes have been prepared.[25–27]

The Borovik group has also successfully used this approach to prepare many terminal metal hydroxido and aqua complexes, including a pair of terminal $Ni^{II}–OH$ complexes using sterically bulky tridentate ligands (Figure 3.1A).[28] Such ligands were derived from the previously mentioned urea based tripodal ligand tris[(N)-tertbutylureaylato)-N-ethyl)]aminato ($[H_3buea]^{3-}$) (Figure 3.1B).[29] Various monometallic terminal metal hydroxido and oxido complexes have been stabilized with $[H_3buea]^{3-}$, as the three bulky *tert*-butyl groups of $[H_3buea]^{3-}$ hinders access to the hydroxido or oxido ligand.[30–32] An additional feature of $[H_3buea]^{3-}$ is its ability to promote the formation of intramolecular hydrogen bonds (H-bonds). For instance, in our previously prepared M–OH complexes the terminal hydroxido ligand was further stabilized through intramolecular H-bonding networks that are formed between the urea N−H groups of $[H_3buea]^{3-}$ and the oxygen atom of the hydroxido ligand.

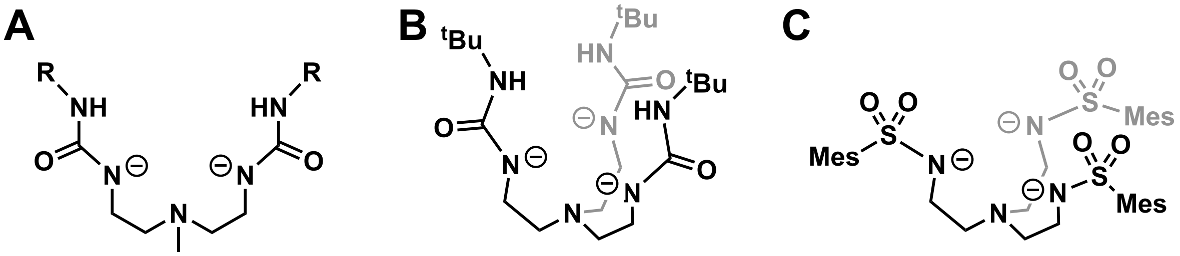

Figure 3.1. The ligands (**A**) $[H_21^R]^{2-}$ (R = iPr, ^{t}Bu), (**B**) $[H_3buea]^{3-}$,and (**C**) $[MST]^{3-}$.

Our group has also designed systems that can accept H-bonds from an apical exogenous ligand. The sulfonamido-based tripodal ligand *N*,*N'*,*N''*-[2,2',2"-nitrilotris(ethane-2,1-diyl)]tris(2,4,6-trimethylbenzenesulfonamido) ($[MST]^{3-}$) (Figure 3.1C) can stabilize hydroxido or aqua ligands through intramolecular H-bonds involving the O–H groups and the sulfonamido oxygen atoms.[33–35] Several examples of monomeric species with terminal hydroxido or aqua ligands exist with this system, and the steric bulk $[MST]^{3-}$ S=O and mesityl groups aid in preventing bridging.[36–38] However, this bulk is less significant than in $[H_3buea]^{3-}$), for as mentioned in Chapter 1 bimetallic complexes with bridging hydroxido or aqua ligands may also be prepared with $[MST]^{3-}$.[33–36]

The following work describes the synthesis and characterization of a Ni^{II}–OH complex with the ligand $[H_3buea]^{3-}$ and a Ni^{II}–OH_2 complex with the ligand $[MST]^{3-}$, where the hydroxido and aqua ligands were both derived from water. Previous work with other metals suggested that these ligands would be logical candidates to stabilize monomeric Ni^{II} complexes with terminal hydroxido and aqua ligands. Their oxidative chemistry was explored, with the goal of establishing the properties of Ni^{III}–OH species. Such species are believed to be a key intermediate in Ni based oxidations,[39–43] but to date, Ni^{III}–OH species have not been structurally characterized. While new oxidized Ni^{III} species can be detected for both systems, the data does not conclusively show that a Ni^{III}–OH unit remained intact.

Results and Discussion

Preparation and properties of $K_2[Ni^{II}H_3buea(OH)]$

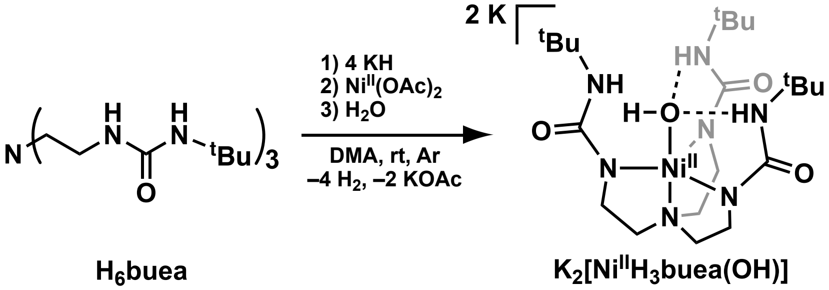

Scheme 3.1. Preparation of $K_2[Ni^{II}H_3buea(OH)]$.

The preparation of $K_2[Ni^{II}H_3buea(OH)]$ followed literature methods reported for other M^{II}–OH with $[H_3buea]^{3-}$ (Scheme 3.1).[44] A dimethylacetamide (DMA) solution of H_6buea was deprotonated with 4 equivalents of KH and treated with $Ni^{II}(OAc)_2$ and H_2O to form a green-yellow solution of $K_2[Ni^{II}H_3buea(OH)]$. Green crystals of this salt suitable for X-ray diffraction were obtained by slow diffusion of Et_2O vapors into a DMA or dimethylformamide (DMF) solution of the compound.

The absorbance spectrum of $[Ni^{II}H_3buea(OH)]^{2-}$ displayed peaks in the visible region at λ_{max} = 424 (ε_M = 61), 493 (ε_M = 35), and 677 nm (ε_M = 23). These absorbance features are similar to those of other Ni^{II} centers in local C_3 symmetry.[45,46] The X-band perpendicular-mode electronic paramagnetic resonance (EPR) spectrum collected at 77 K had no signals, which is expected for a d^8 metal center of integer spin. Evans' method was used to determine the solution effective magnetic moment of 3.1 μ_B.[47] This value is consistent with the spin-only value for an S = 1 system of 2.8 μ_B, indicating that the Ni^{II} metal center is high-spin. The Fourier transform infrared (FTIR) spectra of $K_2[Ni^{II}H_3buea(OH)]$, recorded both with ATR-IR and as a Nujol mull, did not show peaks corresponding to an O−H vibration from the hydroxido ligand. Note that all other M^{II}–OH complexes with $[H_3buea]^{3-}$ also fail to reveal any peaks for the ν(OH);[44] the reason for the absence of these signals in not known.

Preparation and properties of $NMe_4[Ni^{II}MST(OH_2)]$

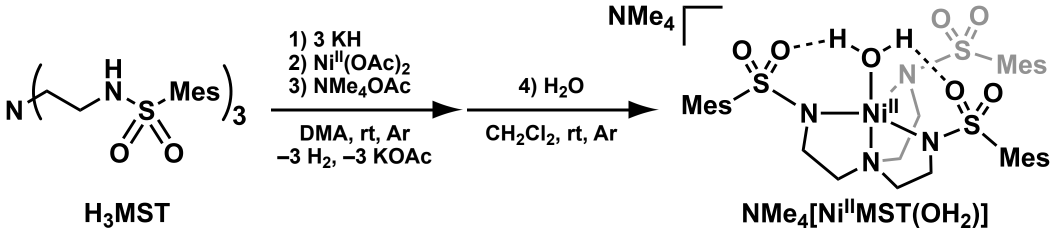

Scheme 3.2. Preparation of $NMe_4[Ni^{II}MST(OH_2)]$.

The preparation of $NMe_4[Ni^{II}MST(OH_2)]$ also followed a previously reported route from our group (Scheme 3.2).[38] A dimethylacetamide solution of H_3MST was deprotonated with 3 equivalents of KH and treated with $Ni^{II}(OAc)_2$ and NMe_4OAc form a green-yellow solution of the putative four-coordinate $NMe_4[Ni^{II}MST]$. This product was isolated as a yellow solid, then redissolved in CH_2Cl_2 and treated with four equivalents of water. Green crystals of the aqua complex suitable for X-ray diffraction were obtained by layering a CH_2Cl_2 solution of the compound under pentane.

The absorbance spectrum of $[Ni^{II}MST(OH_2)]^-$ was characterized by peaks in the visible region at λ_{max} = 431 (ε_M = 110), 506 (ε_M = 33), and 724 nm (ε_M = 52) and had no EPR features in perpendicular-mode. The solution effective magnetic moment was 3.2 μ_B, supporting an S = 1 spin ground-state.[47] The FTIR spectrum of $NMe_4[Ni^{II}MST(OH_2)]$, recorded as a Nujol mull, revealed a peak at 3241 cm^{-1} that is assigned to the O−H vibration from the aqua ligand.[37,38]

Solid-state molecular structure of $[Ni^{II}H_3buea(OH)]^{2-}$ and $[Ni^{II}MST(OH_2)]^-$

The molecular structure of $[Ni^{II}H_3buea(OH)]^{2-}$ was determined by X-ray diffraction methods and the thermal ellipsoid diagram of the complex is shown in Figure 3.2A, with selected metrical parameters shown in Table 3.1. The $[Ni^{II}H_3buea(OH)]^{2-}$ complex crystallized as a monomer, with trigonal bipyramidal (tbp) coordination geometry. The N_4O primary coordination sphere around the Ni^{II} center is defined by a trigonal plane derived from three deprotonated urea nitrogen atoms with the amine nitrogen and the oxygen atoms from the exogenous hydroxido ligand occupying the axial positions.

The complex shows a distortion from idealized tbp geometry based on the structural parameter τ_5 = 0.81, in which an ideal tbp geometry has τ_5 = 1 and ideal square pyramidal geometry has τ_5 = 0.[48] This distortion is partially caused by the Jahn-Teller effect that should be present in a high-spin d^8 metal complex having local C_3 symmetry.[49] Another possible contributor to this distortion is the presence of intramolecular H-bonds formed between the urea hydrogen atoms of $[H_3buea]^{3-}$ and O-atom from the Ni^{II}–OH unit. Two relatively short H-bonds are formed, as gauged by the N···O distances: N6···O1 and N7···O1 distance of 2.789 and 2.786 Å that are statistically shorter than the N5···O1 distance of 2.829 Å. All three interactions may be considered H-bonds because the N···O distances are under 3.07 Å. However, the two shorter distances are in the region often associated with strong H-bonding[50] and could reflect the fact that the hydroxido ligand only has two available lone pairs.

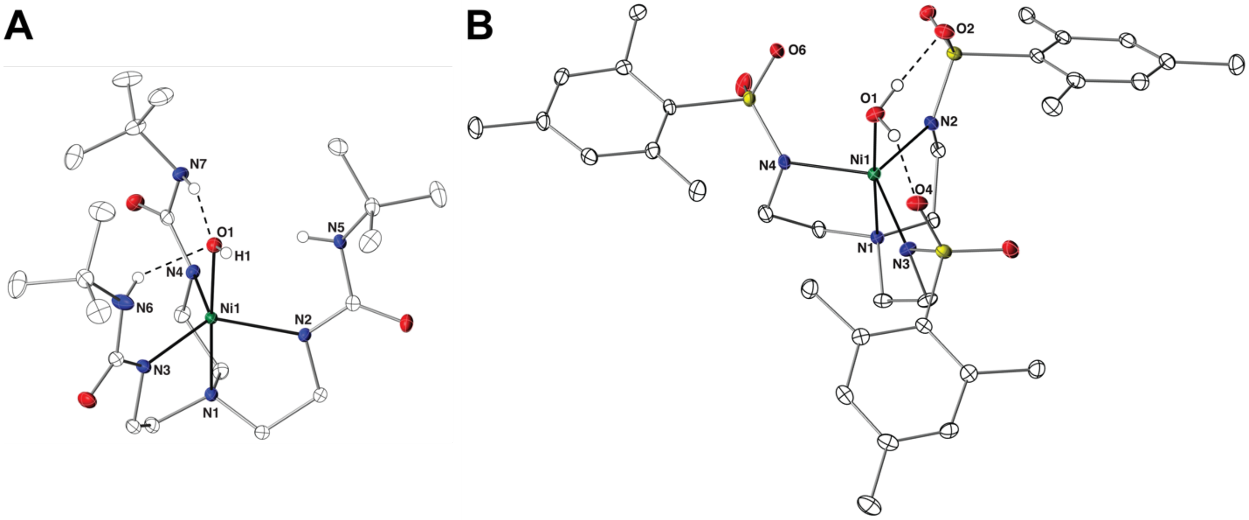

Figure 3.2. Thermal ellipsoid diagram depicting the molecular structure of (**A**) [Ni^{II}H$_3$buea(OH)]$^{2-}$ and (**B**) [NiMST(OH$_2$)]$^{-}$. Ellipsoids are drawn at the 50% probability level, and only urea, hydroxido, and aqua H-atoms are shown for clarity.

The molecular structure of [Ni^{II}H$_3$buea(OH)]$^{2-}$ represents only the third example of a structurally characterized, five-coordinate monometallic Ni^{II}–OH unit. Riordan was the first report of such a species, but that Ni^{II}–OH complex has a square planar primary coordination sphere coordination with a τ_5 value of 0.0.[22] Levy's nickel-hydroxido complex has a τ_5 value of 0.86, and is thus the only other Ni^{II}–OH complex with tbp geometry.[23] The Ni1–O1 bond distance of 2.018(1) Å is significantly longer in [Ni^{II}H$_3$buea(OH)]$^{2-}$ than in either Riordan's or Levy's complexes, which have Ni1–O1 bond distances of 1.955(2) and 1.911(4) Å, respectively. This difference is because [H$_3$buea]$^{3-}$ contains anionic nitrogen donors as well as intramolecular H-bonds to the hydroxido ligand, both of which are absent in the other complexes. Anionic nitrogen donors should provide greater electron density to the Ni^{II} center relative to neutral nitrogen donors, leading to a reduced Ni^{II}–OH interaction that lengthens the Ni–O bond. Similarly, intramolecular H-bonding should decrease the electron density on the hydroxido ligand, also leading to a reduced Ni^{II}–OH interaction that lengthens the Ni–O bond.

The molecular structure of $[Ni^{II}MST(OH_2)]^{-}$ was also determined by X-ray diffraction methods (Figure 3.2B, Table 3.1). The $[Ni^{II}MST(OH_2)]^{-}$ complex crystallized as a monomer, with the N_4O donors around the Ni^{II} center adopting a tbp primary coordination sphere. The three deprotonated sulfonamido nitrogen atoms define the trigonal plane with the amine nitrogen atom and the oxygen atom from the exogenous aqua ligand occupying the apical positions. The complex shows a slight distortion from tbp geometry based on the structural parameter $\tau_5 = 0.86$. As with $[Ni^{II}H_3buea(OH)]^{2-}$, this distortion is expected to be caused by a combination of Jahn-Teller effect and the intramolecular H-bonding network that surrounds the Ni^{II}–OH_2 unit. Two H-bonds are formed between the aqua ligand to the sulfonamido oxygen atom on two of the ligand arms, as gauged by the O···O atom distances of 2.686 and 2.679 Å.

Five-coordinate terminal Ni^{II}–OH_2 complexes tend to having τ_5 values closer to 0.0 and thus having distorted square pyramidal primary coordination spheres. $[Ni^{II}MST(OH_2)]^{-}$ currently has the highest τ_5 value among reported five-coordinate terminal Ni^{II}–OH_2 complexes, and is therefore the closest to having tbp coordination geometry. For comparison, the N-methyl-1,4-diazabicyclo[2.2.2]octane based complex of Stucky[24] and the scorpionate based complex of Yap[51] have τ_5 values of 0.73 and 0.66, representing higher limits for τ_5 values. The Ni1–O1 distance of 2.074(1) Å is shorter in $[Ni^{II}MST(OH_2)]^{-}$ than in either Stucky's or Yap's complexes, which have

Ni1–O1 distances of 2.100(6) and 2.092(2) Å respectively. This difference is also attributed to the presence of intramolecular H-bonds involving the aqua ligand.

Table 3.1. Selected metrical parameters for $[Ni^{II}H_3buea(OH)]^{2-}$, $[Ni^{II}MST(OH_2)]^{-}$ complexes

	$[Ni^{II}H_3buea(OH)]^{2-}$	$[Ni^{II}MST(OH_2)]^{-}$
Bond distances (Å)		
Ni1–O1	2.018(1)	2.074(2)
Ni1–N1	2.106(1)	2.114(2)
Ni1–N2	2.089(1)	2.027(2)
Ni1–N3	2.055(1)	2.051(2)
Ni1–N4	2.059(1)	2.026(2)
Ave. $Ni–N_{eq}$	2.068(1)	2.035(2)
N5···O1	2.829	
N6···O1	2.789	
N7···O1	2.786	
O1···O2		2.686
O1···O4		2.679
O1···O6		2.998
Bond angles (˚)		
N1–Ni1–O1	177.9(5)	176.8(8)
N1–Ni1–N2	80.5(5)	82.9(8)
N1–Ni1–N3	82.1(6)	82.6(8)
N1–Ni1–N4	83.0(6)	83.8(8)
N2–Ni1–N3	129.1(6)	120.5(9)
N2–Ni1–N4	104.6(5)	109.8(9)
N3–Ni1–N4	120.2(6)	125.4(9)
τ_5 value	0.81	0.86

Electrochemical properties of $[Ni^{II}H_3buea(OH)]^{2-}$ and $[Ni^{II}MST(OH_2)]^{-}$

The cyclic voltammogram (CV) of $K_2[Ni^{II}H_3buea(OH)]$ in a 0.1 M tetrabutylammonium hexafluorophosphate (TBAP) solution in DMF (Figure 3.3A) showed an irreversible oxidative event at −830 mV versus the ferrocene/ferrocenium couple ($[FeCp_2]^{+/0}$). In addition, the CV for $NMe_4[Ni^{II}MST(OH_2]$ measured in a 0.1 M TBAP solution in CH_2Cl_2 showed a quasi-reversible one-electron oxidation event at +370 mV versus $[FeCp_2]^{+/0}$ (Figure 3.3B). This positive shift in redox potential for the complex made with $[\mathrm{MST}]^{3-}$ versus analogous $[\mathrm{H_3buea}]^{3-}$ complex is expected, as the N-atoms of the sulfonamido groups of $[\mathrm{MST}]^{3-}$ are weaker donors to the metal center than the ureido N atoms of $[\mathrm{H_3buea}]^{3-}$.[52,53] Moreover, the $[\mathrm{Ni^{II}MST(OH_2)}]^{-}$ complex is a mono-anion while the $[\mathrm{Ni^{II}H_3buea(OH)}]^{2-}$ is a di-anion, and thus $[\mathrm{Ni^{II}MST(OH_2)}]^{-}$ should be more difficult to oxidize. As these results suggested that the $\mathrm{Ni^{II}}$ complexes could be oxidized to $\mathrm{Ni^{III}}$ species, attempts to chemically prepare these products were undertaken.

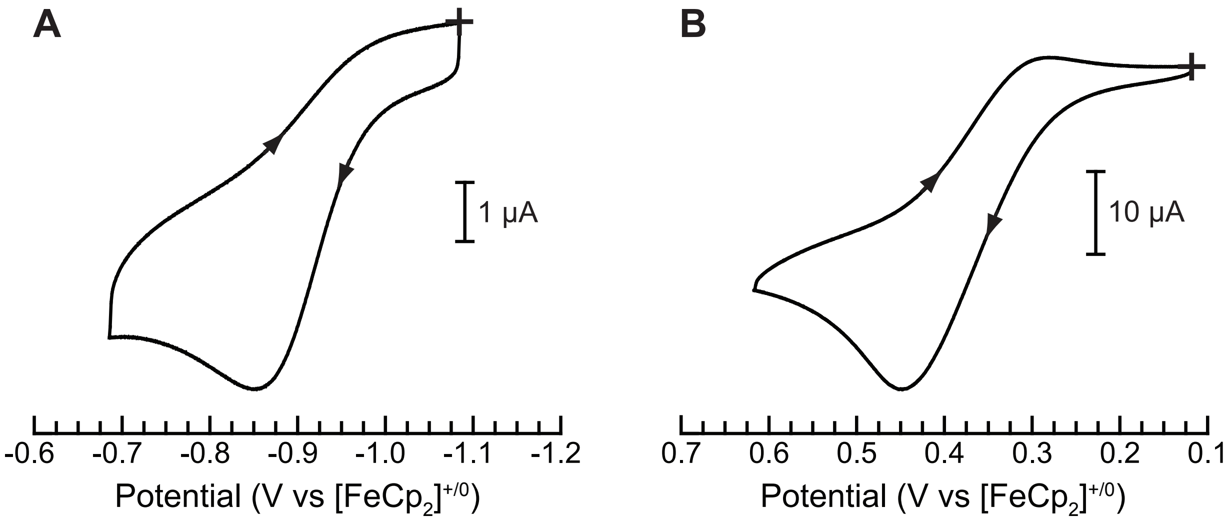

Figure 3.3. Cyclic voltammogram of (**A**) $\mathrm{K_2[Ni^{II}H_3buea(OH)]}$, collected at 100 mV $\mathrm{s^{-1}}$ in a 0.1 M TBAP solution in DMF using $[\mathrm{CoCp_2}]^{0/+}$ as an internal reference, then scaled to $[\mathrm{FeCp_2}]^{+/0}$, and of (**B**) $\mathrm{NMe_4[Ni^{II}MST(OH_2)]}$, collected at 100 mV $\mathrm{s^{-1}}$ in a 0.1 M TBAP solution in $\mathrm{CH_2Cl_2}$ using $[\mathrm{FeCp_2}]^{+/0}$ as an internal reference.

Preparation and characterization of a $\mathrm{Ni^{III}}$ *species with* $[\mathrm{H_3buea}]^{3-}$

The addition of elemental iodine ($\mathrm{I_2}$) to a sample of $\mathrm{K_2[Ni^{II}H_3buea(OH)]}$ in DMF resulted in an immediate color change from yellow-green to purple-red. Monitoring this reaction with UV-visible (UV-vis) spectroscopy at room temperature showed the growth of an intense peak at λ_{max} = 326 nm (ε_M ~ 2000) and a peak at λ_{max} = 502 nm (ε_M ~ 570) (Figure 3.4A). The perpendicular-mode EPR spectrum collected at 10 K of the purple-red solution contained a rhombic EPR signal with *g*-values at 2.29, 2.17, and 2.04 (Figure 3.4B). This spectrum is consistent with a complex containing a d^7 Ni^{III} center with an S = 1/2 spin ground-state.[45,54,55] Nearly identical EPR spectra were obtained when the oxidation of $K_2[Ni^{II}H_3buea(OH)]$ was performed in DMA, acetonitrile (MeCN), and tetrahydrofuran (THF), or when ferrocenium ($[Fe^{III}(C_5H_5)_2]^+$) was used as the oxidant.

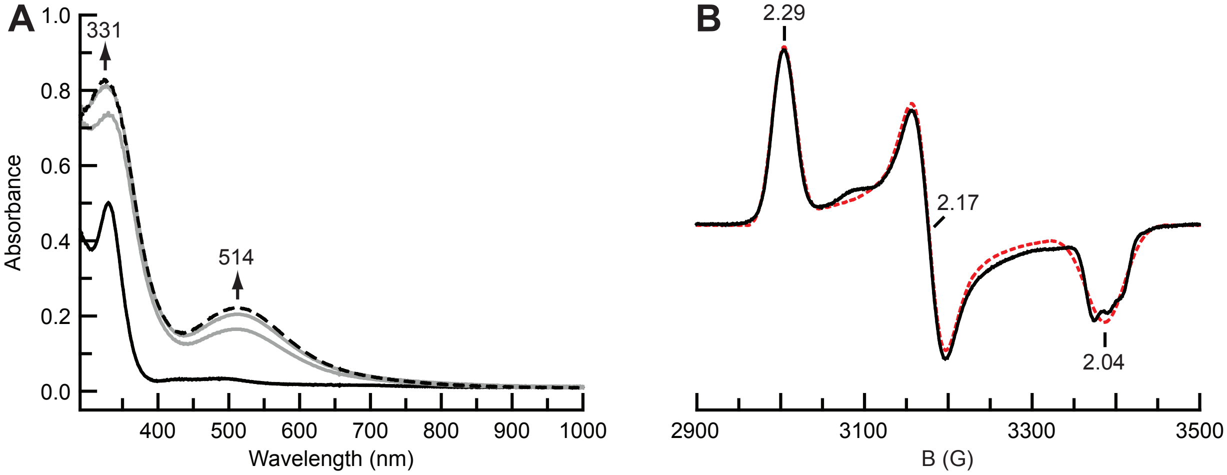

Figure 3.4. (**A**) UV-vis spectrum for oxidation of a 0.4 mM DMF solution of $K_2[Ni^{II}H_3buea(OH)]$ by I_2 at 25 ˚C, showing the conversion of the initial Ni^{II}–OH species (solid black) to a Ni^{III} species (dashed black) after 5 min. (**B**) Perpendicular-mode X-band EPR spectra collected at 10 K of the putative Ni^{III} species with $[H_3buea]^{3-}$ prepared in DMF with I_2 as the oxidant (solid black) and simulated spectrum (dashed red).

The Ni^{III} species derived from $[Ni^{II}H_3buea(OH)]^{2-}$ is unstable at room temperature and reacts further to form species with no perpendicular-mode EPR signals. This reaction followed first-order kinetics with respect to the Ni^{III} species in DMF and a half-life of 10 h was determined for the oxidized species at 25 ˚C. The Ni^{III} species is more stable at lower temperatures: solution samples stored at –30˚C retained their rhombic EPR spectra even after several months. In addition, this oxidized product was also stable in the solid state and could be stored under an inert atmosphere at room temperature. Attempts at crystallizing the Ni^{III} species at −80 ˚C, −30 ˚C, and room temperature were unsuccessful, with only light yellow powders being isolated. UV-vis spectra of this species indicated that it was not $[Ni^{II}H_3buea(OH)]^{2-}$. ^1H-NMR spectra of the powder revealed that it was identical to that of H_6buea, suggesting some amount of the ligand precursor was present. The oxidized Ni^{III} species also does not reconvert to $[Ni^{II}H_3buea(OH)]^{2-}$

upon reduction. Treating the Ni^{III} complex immediately after its formation with cobaltocene ($[Co^{II}(C_5H_5)_2]$) led to a product that had different optical properties to those of $[Ni^{II}H_3buea(OH)]^{2-}$. The reactivity of the Ni^{III} species with external substrates including 9,10-dihydroanthracene (DHA) and xanthene was also probed, yet no reaction was observed with these species.

The one-electron oxidations of $[M^{II}H_3buea(OH)]^{2-}$ complexes (M^{II} = Fe^{II}, Mn^{II}, Co^{II}) have previously been shown to produce the corresponding M^{III}–OH analogs.[56] The combined spectroscopic data for the oxidized product of $[Ni^{II}H_3buea(OH)]^{2-}$ does not allow for a similar assignment. While these results support the initial formation of a Ni^{III} species, there is no data that confirms that the hydroxido ligand is still coordinated. In particular, a characteristic peak associated with the O–H vibration has not been observed in the FTIR spectrum. A new peak appears in the FTIR spectrum at 3320 cm^{-1} after oxidation, but its shape and energy do not correspond to bands for O–H vibrations previously observed for other M^{III}–OH complexes with $[H_3buea]^{3-}$. The energy of this peak is also in the same region of observed NH signals from H_6buea, suggesting the possibility that the ligand has been protonated, as found from our NMR studies above.

Preparation and characterization of a Ni^{III} species with $[MST]^{3-}$

The oxidation of $[Ni^{II}MST(OH_2)]^{-}$ was also explored under similar conditions to $[Ni^{II}H_3buea(OH)]^{2-}$. The Ni^{II}–OH_2 complex could be oxidized with $[TBPA]PF_6$ to induce a clear color change from lime-green to orange. When the reaction was monitored by UV-vis spectroscopy at room temperature, the growth of a peak at λ_{max} = 312 nm (ε_M > 12000) and shoulders at 440 nm and 530 nm are observed (Figure 3.5A). The perpendicular-mode EPR spectrum (Figure 3.5B) at

10 K showed a rhombic signal with *g* = 2.29, 2.17, and 2.04. Attempts at crystallization yielded only green crystals, which is likely a Ni^{II} species as this compound has no signals in its perpendicular-mode EPR spectrum.

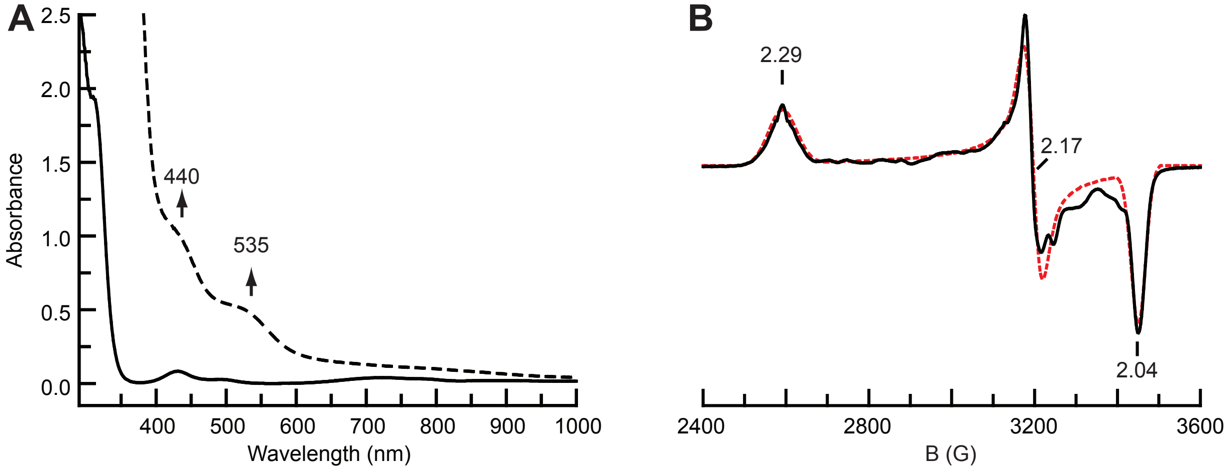

Figure 3.5. (**A**) UV-vis spectrum for oxidation of a 0.4 mM CH_2Cl_2 solution of $NMe_4[Ni^{II}MST(OH_2)]$ by $[TBPA]PF_6$ at 25 ˚C, showing the conversion of the initial $Ni^{II}–OH_2$ species (solid black) to some Ni^{III} species after 30 s. (**B**) Perpendicular-mode X-band EPR spectra collected at 77 K of the putative Ni^{III} species with $[MST]^{3-}$ prepared in CH_2Cl_2 with $[TBPA]PF_6$ as the oxidant (solid black) and simulated spectrum (dashed red).

The properties of the Ni^{III} species with $[MST]^{3-}$ are similar to those of the analogous $[H_3buea]^{3-}$ species. It reacts further to form a species with perpendicular-mode EPR signals at room temperature, which occurs within hours. Attempts at crystallizing the oxidized species at −80˚C, −30˚C, and room temperature were also unsuccessful, with only a light-yellow powder again being isolated from the reaction mixture. The UV-vis spectrum of this species is like that of the original $Ni^{II}–OH_2$ compound. However, attempts to immediately reduce the putative Ni^{III} species using $CoCp_2$ led to a species that is different from the starting $Ni^{II}–OH_2$ compound, and its formulation is still unknown.

We have previously shown that $[Fe^{III}MST(OH)]^-$ is prepared by the one-electron oxidation of $[Fe^{II}MST(OH_2)]^-$.[37] However, as with $[Ni^{II}H_3buea(OH)]^{2-}$, the spectroscopic data for the oxidized product of $[Ni^{II}MST(OH_2)]^-$ does not allow us to make a similar assignment. An O−H vibration at

3463 cm^{-1} was observed for $[\text{Fe}^{\text{III}}\text{MST(OH)}]^{-}$, but a similar feature was not found in FTIR spectra of the oxidized $[\text{Ni}^{\text{II}}\text{MST(OH}_2\text{)}]^{-}$. Moreover, we did not observe any further reactivity with the Ni^{III} species with external substrates that would support a high valent Ni–OH species.

Summary and Conclusions

This work described the preparation and characterization of $\text{K}_2[\text{Ni}^{\text{II}}\text{H}_3\text{buea(OH)}]$ and $\text{NMe}_4[\text{Ni}^{\text{II}}\text{MST(OH}_2\text{)}]$, complexes containing terminal Ni^{II}–OH and Ni^{II}–OH_2 moieties. These complexes adopt a distorted tbp geometry, as determined by the τ_5 value, which is an uncommon geometry for these types of complexes. Both complexes were oxidized by one-electron oxidants to form high-valent Ni^{III} species, as determined by perpendicular-mode EPR spectroscopy. The oxidation reactions revealed rhombic perpendicular-mode EPR spectra at 10 K, consistent with an $S = 1/2$ spin-state derived from a low-spin Ni^{III} metal center. Additional characterization by UV-vis spectroscopy and FTIR spectroscopy were performed, but single crystals have yet to be grown for either compound. Moreover, the lack of detectable vibration peaks for Ni^{III} O–H bonds prevents the definitive assignment of these complexes as high valent Ni–OH species.

Experimental

General Methods

All reagents were purchased from commercial sources and used as received, unless otherwise noted. Solvents were sparged with argon and dried over columns containing Q-5 and molecular sieves. The tripodal compounds H_6buea and H_3MST were synthesized following literature procedures.[29,33] The preparations of metal complexes were conducted in a Vacuum

Atmospheres, Co. drybox under argon atmosphere. Potassium hydride (KH) as a 60% dispersion in mineral oil was filtered with a medium porosity glass-fritted funnel and washed 5 times each with pentane and diethyl ether (Et_2O). Solid KH was dried under vacuum and stored under inert atmosphere. $Ni(OAc)_2$ was prepared by literature procedures.[57] I_2 was sublimed under vacuum and stored under inert atmosphere. Water was degassed by five freeze-pump-thaw cycles and stored under inert atmosphere.

Preparation of Complexes

Preparation of $K_2[Ni^{II}H_3buea(OH)]$. A solution of H_6buea (300 mg, 0.69 mmol) in anhydrous DMA (20 mL) was treated with solid KH (110 mg, 2.9 mmol). The mixture was stirred until gas evolution ceased. $Ni(OAc)_2$ (120 mg, 0.69 mmol) was added to the clear pale yellow reaction mixture, and the solution was stirred. After 2 h, H_2O (13 µL, 0.72 mmol) was added to the red solution *via* syringe, and the mixture was stirred for 15 min. After the addition of DMF (4 mL), the reaction mixture was filtered through a medium porosity glass-fritted funnel to remove the insoluble KOAc. The green-yellow filtrate was concentrated under vacuum to *ca.* 1 mL and treated with Et_2O (20 mL) followed by pentane (20 mL) to precipitate a green solid. The green solid was collected on a fine porosity glass-fritted funnel and dried under vacuum. After 1 h, the solid was washed with MeCN to remove an orange filtrate. The green solid was redissolved in DMA (20 mL) and recrystallized by slow diffusion with Et_2O. After 2 d, green crystals were collected to give 360 mg (87%) of product. Elemental Anal. Calc. for $K_2[Ni^{II}H_3buea(OH)]\cdot2DMF$, $K_2NiC_{29}H_{61}N_9O_6$: C, 45.31; H, 8.00; N, 16.40. Found: C, 45.01; H, 8.19; N, 16.15%. FTIR (KBr disc, cm^{-1}, selected bands): 3233, 3146, 2962, 2921, 2849, 1592, 1509, 1447, 1388, 1357, 1247, 1223, 1149, 1118, 1034, 971, 796, 731. λ_{max} (DMF, nm, ε $M^{-1}cm^{-1}$): 324 (1400), 424 (61), 493 (35), 677 (23). μ_{eff} (DMSO, μ_B): 3.1. E_a (DMF): −0.830 V versus $[FeCp_2]^{0/+}$.

Oxidation of $K_2[Ni^{II}H_3buea(OH)]$. A solution of $K_2[Ni^{II}H_3buea(OH)]$ (50 mg, 0.085 mmol) in DMF (2 mL) was treated with solid I_2 (11 mg, 0.045 mmol). The yellow-green solution immediately turned purple-red and was allowed to stir for 5 min. The solution was concentrated under vacuum until near dryness and Et_2O (5 mL) was added to precipitate a purple-red powder. After decanting the liquid, the powder was redissolved in THF (2 mL). The reaction mixture was filtered through a fine porosity glass-fritted funnel to remove the insoluble KI. The filtrate was concentrated under vacuum until near dryness then treated with Et_2O (5mL). The resulting red powder was collected on a medium porosity glass-fritted funnel. EPR (DMF, 77 K): *g* = 2.29, 2.17, 2.04. FTIR (ATR, cm^{-1}, selected bands): 3308, 2958, 2888, 1587, 1474, 1451, 1386, 1351, 1259, 1223, 1151, 1103, 1032, 961, 837, 777, 754. λ_{max} (DMF, nm, ε $M^{-1}cm^{-1}$): 326 (~ 2000), 502 (~ 570).

Preparation of $NMe_4[Ni^{II}MST(OH_2)]$. A solution of H_3MST (210 mg, 0.30 mmol) in anhydrous DMA (4 mL) was treated with solid KH (37 mg, 0.91 mmol). The mixture was stirred until gas evolution ceased. $Ni(OAc)_2{\cdot}4H_2O$ (73 mg, 0.29 mmol) and NMe_4OAc (40 mg, 0.30 mmol) were added to the clear pale yellow reaction, and the solution was stirred. After 3 h, Et_2O (5 mL) was added to the green-yellow solution to aid the precipitation of KOAc. The reaction mixture was filtered through a medium porosity glass-fritted funnel to remove the insoluble species. The filtrate was concentrated under vacuum to *ca.* 1 mL and treated with Et_2O (10 mL) followed by pentane (40 mL) to precipitate a yellow solid. The yellow solid was collected on a medium porosity glass-fritted funnel and dried under vacuum to give 207 mg (85%) of product. FTIR (KBr disc, cm^{-1}, selected bands): 3259, 3030, 2973, 2937, 2854, 1603, 1563, 1490, 1468, 1254, 1128, 1054, 977, 830, 815, 742, 656, 610. MS (ES-, m/z): Exact mass calcd for $NiC_{33}H_{45}N_4O_6S_3$: 747.2. Found: 747.2. This salt, presumably $NMe_4[Ni^{II}MST]$ (77 mg, 0.092 mmol) was redissolved in CH_2Cl_2 (10 mL) and treated with H_2O (2 µL, 0.10 mmol) in one portion *via* a syringe, and the mixture was stirred. After 15 min the green solution was filtered through a medium porosity glass-fritted funnel to remove any insoluble species and the filtrate was layered under pentane. After 2 d, green and yellow needle crystals were collected via filtration and dried very briefly under vacuum, to give 74 mg (94%) of crystalline product. Elemental Anal. Calc. for $NMe_4[Ni^{II}MST(OH_2)]$ $NiC_{37}H_{59}N_5O_7S_3$: C, 52.86; H, 7.07; N, 8.33. Found: C, 52.95; H, 7.16; N, 8.18%. FTIR (KBr disc, cm^{-1}, selected bands): 3266, 3025, 2970, 2934, 2855, 1604, 1562, 1490, 1468, 1405, 1377, 1342, 1258, 1230, 1132, 1054, 977, 813, 742, 657, 607. (Nujol, cm^{-1}): 3241 (OH). (CH_2Cl_2, 20 mM, cm^{-1}): 3280. λ_{max} (DMF, nm, ε M^{-1}cm^{-1}): 312 (3300) 431 (120), 506 (39), 724 (33). μ_{eff} (μ_B): 3.22. $E_{1/2}$ (MeCN): 0.370 V versus $[FeCp_2]^{0/+}$

Preparation of tris-(4-bromophenyl)ammoniumyl hexafluorophosphate ($[TBPA]PF_6$). $[TBPA]PF_6$ was prepared according to literature procedures with the following modifications.[58,59] A solution of tris-(4-bromophenyl)amine (200 mg, 0.42 mmol) in CH_2Cl_2 (2 mL) was cooled to –30 °C. Upon addition of nitrosonium hexafluorophosphate ($[NO][PF_6]$, 74 mg, 0.41 mmol), the clear solution immediately became dark blue. After 1 h of stirring at –30 °C, pentane (20 mL) was added to precipitate a dark blue solid. The solid was collected by filtering through a medium porosity glass-fritted funnel, washed with pentane (20 mL), dried under vacuum to yield 211 mg (81%) dark blue powder, and stored at –30°C. EPR (CH_2Cl_2, 77 K): $g = 2.00$. λ_{max} (CH_2Cl_2, nm, ε $M^{-1}cm^{-1}$): 309 (6.4×10^4), 367 (7.2×10^4), 725 (1.1×10^5).

Oxidation of *$NMe_4[Ni^{II}MST(OH_2)]$*. A solution of $NMe_4[Ni^{II}MST(OH_2)]$ (25 mg, 0.030 mmol) in CH_2Cl_2 (2 mL) was cooled to –30°C, then treated with a solution of $[TBPA]PF_6$ (21 mg, 0.033 mmol) in CH_2Cl_2 (1 mL) at –30°C. The yellow-green solution immediately turned orange-red, and was allowed to stir at –30°C for 5 min. The solution was concentrated under vacuum until near dryness, washed with Et_2O (5mL), and collected on a medium porosity glass-fritted funnel. EPR (CH_2Cl_2, 77 K): $g = 2.66, 2.15, 1.99$. FTIR (ATR, cm^{-1}, selected bands): 3250, 3021, 2968, 2934, 2853, 1602, 1579, 1485, 1415, 1380, 1311, 1265, 1184, 1152, 1098, 1071, 1054, 1006, 976, 950, 830, 734, 654, 609. λ_{max} (CH_2Cl_2, nm, ε $M^{-1}cm^{-1}$): 312 (>12000), 440(sh), 530(sh)

Physical Methods

Elemental analyses were performed on a Perkin-Elmer 2400 CHNS analyzer. ^1H NMR and ^{13}C NMR were recorded on a Bruker DRX500 spectrometer. FTIR spectra were collected on a Varian 800 Scimitar Series FTIR spectrometer in air or a Thermo Scientific Nicolet iS5 spectrophotometer with an iD5 Attenuated Total Reflectance (ATR) attachment in a nitrogen filled glovebox. High-resolution mass spectra were collected using Waters Micromass LCT Premier Mass Spectrometer. UV-vis spectra were recorded with a Cary 50 or an Agilent 8453 spectrophotometer using a 1.00 cm quartz cuvette. Perpendicular-mode X-band EPR spectra were collected using a Bruker EMX spectrometer at 10K using liquid helium. Solution effective magnetic moments were measured by Evans' method on a Bruker DRX500 spectrometer using flame sealed standard cores of 1:1 DMSO:DMSO-d_6 or 1:1 $CHCl_3$:$CDCl_3$.[47] Cyclic voltammetry experiments were conducted using a CH1600C electrochemical analyzer. A 2.0 mm glassy carbon electrode was used as the working electrode at scan velocities 0.5 Vs^{-1} unless otherwise noted. A cobaltocenium/cobaltocene couple ($[CoCp_2]^{+/0}$) was used as an internal reference then scaled against $[FeCp_2]^{0/+}$.[60] TBAP was use as the supporting electrolyte at a concentration of 0.1 M.

Crystallography

A Bruker SMART APEX II diffractometer and the APEX2 program package was used to determine the unit-cell parameters and for data collection. Crystallographic details are summarized in Appendix A.

References

(1) Du Bois, J.; Mizoguchi, T. J.; Lippard, S. J. Understanding the dioxygen reaction chemistry of diiron proteins through synthetic modeling studies. *Coord. Chem. Rev.* **2000**, *200–202*, 443–485.

(2) Merkx, M.; Kopp, D. A.; Sazinsky, M. H.; Blazyk, J. L.; Müller, J.; Lippard, S. J. Dioxygen Activation and Methane Hydroxylation by Soluble Methane Monooxygenase: A Tale of Two Irons and Three Proteins. *Angew. Chemie Int. Ed.* **2001**, *40*, 2782–2807.

(3) Que, Jr., L.; Tolman, W. B. Bis(μ-oxo)dimetal “Diamond” Cores in Copper and Iron Complexes Relevant to Biocatalysis. *Angew. Chemie Int. Ed.* **2002**, *41*, 1114–1137.

(4) Hikichi, S.; Yoshizawa, M.; Sasakura, Y.; Akita, M.; Moro-oka, Y. First Synthesis and Structural Characterization of Dinuclear M(III) Bis(μ-oxo) Complexes of Nickel and Cobalt with Hydrotris(pyrazolyl)borate Ligand. *J. Am. Chem. Soc.* **1998**, *120*, 10567–10568.

(5) Hikichi, S.; Yoshizawa, M.; Sasakura, Y.; Komatsuzaki, H.; Moro-oka, Y.; Akita, M. Structural Characterization and Intramolecular Aliphatic C−H Oxidation Ability of $M^{III}(\mu\text{-}O)_2M^{III}$ Complexes of Ni and Co with the Hydrotris(3,5-dialkyl-4-X-pyrazolyl)borate Ligands $TpMe_2$,X (X=Me, H, Br) and TpiPr. *Chem. Eur. J.* **2001**, *7*, 5011–5028.

(6) Mandimutsira, B. S.; Yamarik, J. L.; Brunold, T. C.; Gu, W.; Cramer, S. P.; Riordan, C. G. Dioxygen Activation by a Nickel Thioether Complex: Characterization of a $Ni^{III}_2(\mu\text{-}O)_2$ Core. *J. Am. Chem. Soc.* **2001**, *123*, 9194–9195.

(7) Benson, D. E.; Haddy, A. E.; Hellinga, H. W. Converting a Maltose Receptor into a Nascent Binuclear Copper Oxygenase by Computational Design. *Biochemistry* **2002**, *41*, 3262–3269.

(8) Itoh, S.; Bandoh, H.; Nakagawa, M.; Nagatomo, S.; Kitagawa, T.; Karlin, K. D.; Fukuzumi, S. Formation, Characterization, and Reactivity of Bis(μ-oxo)dinickel(III) Complexes Supported by A Series of Bis[2-(2-pyridyl)ethyl]amine Ligands. *J. Am. Chem. Soc.* **2001**, *123*, 11168–11178.

(9) Rodríguez, L.; Labisbal, E.; Sousa-Pedrares, A.; García-Vázquez, J. A.; Romero, J.; Durán, M. L.; Real, J. A.; Sousa, A. Coordination Chemistry of Amine Bis(phenolate) Cobalt(II), Nickel(II), and Copper(II) Complexes. *Inorg. Chem.* **2006**, *45*, 7903–7914.

(10) Biswas, R.; Kar, P.; Song, Y.; Ghosh, A. The importance of an additional water bridge in making the exchange coupling of bis(μ-phenoxo) dinickel(II)complexes ferromagnetic. *Dalt. Trans.* **2011**, *40*, 5324.

(11) Dixon, N. E.; Riddles, P. W.; Gazzola, C.; Blakeley, R. L.; Zerner, B. Jack bean urease (EC 3.5.1.5). V. On the mechanism of action of urease on urea, formamide, acetamide, *N*-methylurea, and related compounds. *Can. J. Biochem.* **1980**, *58*, 1335–1344.

(12) Jabri, E.; Carr, M.; Hausinger, R.; Karplus, P. The crystal structure of urease from Klebsiella aerogenes. *Science* **1995**, *268*, 998–1004.

(13) Lipscomb, W. N.; Sträter, N. Recent Advances in Zinc Enzymology. *Chem. Rev.* **1996**, *96*, 2375–2434.

(14) Christianson, D. W.; Cox, J. D. Catalysis by metal-activated hydroxide in zinc and manganese metalloenzymes. *Annu. Rev. Biochem.* **1999**, *68*, 33–57.

(15) Christianson, D. W.; Fierke, C. A. Carbonic Anhydrase: Evolution of the Zinc Binding Site by Nature and by Design. *Acc. Chem. Res.* **1996**, *29*, 331–339.

(16) Cámpora, J.; Palma, P.; del Río, D.; Álvarez, E. CO Insertion Reactions into the M−OH Bonds of Monomeric Nickel and Palladium Hydroxides. Reversible Decarbonylation of a Hydroxycarbonyl Palladium Complex. *Organometallics* **2004**, *23*, 1652–1655.

(17) Cámpora, J.; Matas, I.; Palma, P.; Graiff, C.; Tiripicchio, A. Fluoride Displacement by Lithium Reagents. An Improved Method for the Synthesis of Nickel Hydroxo, Alkoxo, and Amido Complexes. *Organometallics* **2005**, *24*, 2827–2830.

(18) Adhikari, D.; Mossin, S.; Basuli, F.; Dible, B. R.; Chipara, M.; Fan, H.; Huffman, J. C.; Meyer, K.; Mindiola, D. J. A dinuclear Ni(I) system having a diradical Ni_2N_2 diamond core resting state: synthetic, structural, spectroscopic elucidation, and reductive bond splitting reactions. *Inorg. Chem.* **2008**, *47*, 10479–10490.

(19) Huang, D.; Makhlynets, O. V; Tan, L. L.; Lee, S. C.; Rybak-Akimova, E. V; Holm, R. H. Fast carbon dioxide fixation by 2,6-pyridinedicarboxamidato-nickel(II)-hydroxide complexes: influence of changes in reactive site environment on reaction rates. *Inorg. Chem.* **2011**, *50*, 10070–10081.

(20) Zhang, Y.-P.; Li, W.-W.; Li, B.-X.; Mu, H.-L.; Li, Y.-S. Well-defined phosphino-phenolate

neutral nickel(II) catalysts for efficient (co)polymerization of norbornene and ethylene. *Dalt. Trans.* **2015**, *44*, 7382–7394.

(21) Czerny, F.; Döhlert, P.; Weidauer, M.; Irran, E.; Enthaler, S. Synthesis, characterization and application of nickel(II) complexes modified with *N,N′,N″*-pincer ligands. *Inorganica Chim. Acta* **2015**, *425*, 118–123.

(22) Kieber-Emmons, M. T.; Schenker, R.; Yap, G. P. A.; Brunold, T. C.; Riordan, C. G. Spectroscopic Elucidation of a Peroxo $Ni_2(\mu\text{-}O_2)$ Intermediate Derived from a Nickel(I) Complex and Dioxygen. *Angew. Chemie Int. Ed.* **2004**, *43*, 6716–6718.

(23) Prema, D.; Oshin, K.; Desper, J.; Levy, C. J. Mono- and dinuclear nickel(II) complexes of resolved Schiff-base ligands with extended quinoline substituents. *Dalton Trans.* **2012**, *41*, 4998–5009.

(24) Ross, F. K.; Stucky, G. D. Crystal and molecular structure of N-methyl-1,4-diazabicyclo[2.2.2]octonium trichloroaquonickelate(II). A high-spin five-coordinate complex of nickel(II) with monodentate ligands. *Inorg. Chem.* **1969**, *8*, 2734–2740.

(25) Evans, D. A.; Downey, C. W.; Hubbs, J. L. Ni(II) bis(oxazoline)-catalyzed enantioselective syn aldol reactions of N-propionylthiazolidinethiones in the presence of silyl triflates. *J. Am. Chem. Soc.* **2003**, *125*, 8706–8707.

(26) Santillan, G. A.; Carrano, C. J. Nickel(II), copper(II), and cobalt(II) solid-state structures formed through hydrogen bonding with ditopic heteroscorpionate ligands. *Dalton Trans.* **2008**, No. 30, 3995–4005.

(27) Kunishita, A.; Doi, Y.; Kubo, M.; Ogura, T.; Sugimoto, H.; Itoh, S. Ni(II)/H_2O_2 reactivity in bis[(pyridin-2-yl)methyl]amine tridentate ligand system. aromatic hydroxylation reaction by bis(mu-oxo)dinickel(III) complex. *Inorg. Chem.* **2009**, *48*, 4997–5004.

(28) Powell-Jia, D.; Ziller, J. W.; DiPasquale, A. G.; Rheingold, A. L.; Borovik, A. S. A structure and reactivity analysis of monomeric Ni(II)–hydroxo complexes prepared from water. *Dalt. Trans.* **2009**, No. 16, 2986.

(29) Hammes, B. S.; Young, Jr., V. G.; Borovik, A. S. Hydrogen-Bonding Cavities about Metal Ions: A Redox Pair of Coordinatively Unsaturated Paramagnetic Co-OH Complexes. *Angew. Chemie Int. Ed.* **1999**, *38*, 666–669.

(30) MacBeth, C. E.; Golombek, A. P.; Young Jr., V. G.; Yang, C.; Kuczera, K.; Hendrich, M. P.; Borovik, A. S. O2 Activation by Nonheme Iron Complexes: A Monomeric Fe(III)-Oxo Complex Derived From O2. *Science* **2000**, *289*, 938–941.

(31) Gupta, R.; MacBeth, C. E.; Young, V. G.; Borovik, A. S. Isolation of Monomeric $Mn^{III/II}$−OH and Mn^{III}−O Complexes from Water: Evaluation of O−H Bond Dissociation Energies. *J. Am. Chem. Soc.* **2002**, *124*, 1136–1137.

(32) Lacy, D. C.; Gupta, R.; Stone, K. L.; Greaves, J.; Ziller, J. W.; Hendrich, M. P.; Borovik, A. S. Formation, structure, and EPR detection of a high spin Fe(IV)-oxo species derived from either an Fe(III)-oxo or Fe(III)-OH complex. *J. Am. Chem. Soc.* **2010**, *132*, 12188–12190.

(33) Park, Y. J.; Ziller, J. W.; Borovik, A. S. The Effects of Redox-Inactive Metal Ions on the

Activation of Dioxygen: Isolation and Characterization of a Heterobimetallic Complex Containing a Mn^{III}–(μ-OH)–Ca^{II} Core. *J. Am. Chem. Soc.* **2011**, *133*, 9258–9261.

(34) Park, Y. J.; Cook, S. A.; Sickerman, N. S.; Sano, Y.; Ziller, J. W.; Borovik, A. S. Heterobimetallic complexes with M^{III}-(μ-OH)-M^{II} cores (M^{III} = Fe, Mn, Ga; M^{II} = Ca, Sr, and Ba): structural, kinetic, and redox properties. *Chem. Sci.* **2013**, *4*, 717–726.

(35) Sano, Y.; Weitz, A. C.; Ziller, J. W.; Hendrich, M. P.; Borovik, A. S. Unsymmetrical Bimetallic Complexes with M^{II}–(μ-OH)–M^{III} Cores ($M^{II}M^{III}$ = $Fe^{II}Fe^{III}$, $Mn^{II}Fe^{III}$, $Mn^{II}Mn^{III}$): Structural, Magnetic, and Redox Proper. *Inorg. Chem.* **2013**, *52*, 10229–10231.

(36) Lacy, D. C.; Park, Y. J.; Ziller, J. W.; Yano, J.; Borovik, A. S. Assembly and Properties of Heterobimetallic $Co^{II/III}$/Ca^{II} Complexes with Aquo and Hydroxo Ligands. *J. Am. Chem. Soc.* **2012**, *134*, 17526–17535.

(37) Cook, S. A.; Ziller, J. W.; Borovik, A. S. Iron(II) Complexes Supported by Sulfonamido Tripodal Ligands: Endogenous versus Exogenous Substrate Oxidation. *Inorg. Chem.* **2014**, *53*, 11029–11035.

(38) Lau, N.; Ziller, J. W.; Borovik, A. S. Sulfonamido tripods: Tuning redox potentials via ligand modifications. *Polyhedron* **2015**, *85*, 777–782.

(39) Pandarus, V.; Zargarian, D. New Pincer-Type Diphosphinito (POCOP) Complexes of Nickel. *Organometallics* **2007**, *26*, 4321–4334.

(40) Anderson, T. J.; Jones, G. D.; Vicic, D. A. Evidence for a Ni^{I} Active Species in the Catalytic Cross-Coupling of Alkyl Electrophiles. *J. Am. Chem. Soc.* **2004**, *126*, 8100–8101.

(41) Zultanski, S. L.; Fu, G. C. Catalytic asymmetric γ-alkylation of carbonyl compounds via stereoconvergent Suzuki cross-couplings. *J. Am. Chem. Soc.* **2011**, *133*, 15362–15364.

(42) Lee, W.-Z.; Chiang, C.-W.; Lin, T.-H.; Kuo, T.-S. A discrete five-coordinate Ni(III) complex resembling the active site of the oxidized form of nickel superoxide dismutase. *Chem. Eur. J.* **2012**, *18*, 50–53.

(43) Chiang, C.-W.; Chu, Y.-L.; Chen, H.-L.; Kuo, T.-S.; Lee, W.-Z. Synthesis and characterization of Ni(III)N_3S_2 complexes as active site models for the oxidized form of nickel superoxide dismutase. *Chem. Eur. J.* **2014**, *20*, 6283–6286.

(44) MacBeth, C. E.; Hammes, B. S.; Young, V. G.; Borovik, A. S. Hydrogen-Bonding Cavities about Metal Ions: Synthesis, Structure, and Physical Properties for a Series of Monomeric M−OH Complexes Derived from Water. *Inorg. Chem.* **2001**, *40*, 4733–4741.

(45) Pfaff, F. F.; Heims, F.; Kundu, S.; Mebs, S.; Ray, K. Spectroscopic capture and reactivity of S = 1/2 nickel(III)-oxygen intermediates in the reaction of a Ni(II)-salt with mCPBA. *Chem. Commun.* **2012**, *48*, 3730–3732.

(46) Ma, H.; Petersen, J. L.; Young, V. G.; Yee, G. T.; Jensen, M. P. Solid-state spin crossover of Ni(II) in a bioinspired N_3S_2 ligand field. *J. Am. Chem. Soc.* **2011**, *133*, 5644–5647.

(47) Evans, D. F. 400. The determination of the paramagnetic susceptibility of substances in solution by nuclear magnetic resonance. *J. Chem. Soc.* **1959**, 2003–2005.

(48) Addison, A. W.; Rao, T. N.; Reedijk, J.; van Rijn, J.; Verschoor, G. C. Synthesis, structure,

and spectroscopic properties of copper(II) compounds containing nitrogen–sulphur donor ligands; the crystal and molecular structure of aqua[1,7-bis(N-methylbenzimidazol-2′-yl)-2,6-dithiaheptane]copper(II) perchlorate. *J. Chem. Soc. Dalt. Trans.* **1984**, No. 7, 1349.

(49) Sickerman, N. S.; Park, Y. J.; Ng, G. K.-Y.; Bates, J. E.; Hilkert, M.; Ziller, J. W.; Furche, F.; Borovik, A. S. Synthesis, structure, and physical properties for a series of trigonal bipyramidal M(II)-Cl complexes with intramolecular hydrogen bonds. *Dalton Trans.* **2012**, *41*, 4358–4364.

(50) Emsley, J. Very strong hydrogen bonding. *Chem. Soc. Rev.* **1980**, *9*, 91.

(51) Oseback, S. N.; Shim, S. W.; Kumar, M.; Greer, S. M.; Gardner, S. R.; Lemar, K. M.; DeGregory, P. R.; Papish, E. T.; Tierney, D. L.; Zeller, M.; Yap, G. P. A. Crowded bis ligand complexes of TtzPh,Me with first row transition metals rearrange due to ligand field effects: structural and electronic characterization (TtzPh,Me = tris(3-phenyl-5-methyl-1,2,4-triazolyl)borate). *Dalt. Trans.* **2012**, *41*, 2774.

(52) Bordwell, F. G. Equilibrium acidities in dimethyl sulfoxide solution. *Acc. Chem. Res.* **1988**, *21*, 456–463.

(53) Jones, J. R.; Ziller, J. W.; Borovik, A. S. Modulating the Primary and Secondary Coordination Spheres within a Series of Co ^{II} —OH Complexes. *Inorg. Chem.* **2017**, *56*, 1112–1120.

(54) Cho, J.; Sarangi, R.; Annaraj, J.; Kim, S. Y.; Kubo, M.; Ogura, T.; Solomon, E. I.; Nam, W. Geometric and electronic structure and reactivity of a mononuclear “side-on” nickel(III)-peroxo complex. *Nat. Chem.* **2009**, *1*, 568–572.

(55) Xiao, Z.; Patrick, B. O.; Dolphin, D. Ni(III) complex of an N-confused porphyrin inner C-oxide. *Inorg. Chem.* **2003**, *42*, 8125–8127.

(56) MacBeth, C. E.; Gupta, R.; Mitchell-Koch, K. R.; Young, V. G.; Lushington, G. H.; Thompson, W. H.; Hendrich, M. P.; Borovik, A. S. Utilization of hydrogen bonds to stabilize M-O(H) units: synthesis and properties of monomeric iron and manganese complexes with terminal oxo and hydroxo ligands. *J. Am. Chem. Soc.* **2004**, *126*, 2556–2567.

(57) Tappmeyer, W. P.; Davidson, A. W. Cobalt and Nickel Acetates in Anhydrous Acetic Acid. *Inorg. Chem.* **1963**, *2*, 823–825.

(58) Eberson, L.; Larsson, B.; Moberg, C.; Krautwurst, K. D.; Krogsgaard-Larsen, P.; Ryhage, R.; Isaksson, R. Electron Transfer Reactions in Organic Chemistry. IX. Acyloxylation and/or Debromodimerization Instead of Electron Transfer in the Reaction between Tris(4-bromophenyl)ammoniumyl and Aliphatic Carboxylates. *Acta Chem. Scand.* **1986**, *40b*, 210–225.

(59) Eberson, L.; Larsson, B. Electron transfer reactions in organic chemistry. XII: Reactions of 4-substituted triarylaminium radical cations with nucleophiles; polar vs. Electron transfer pathways. *Acta Chem. Scand.* **1987**, *41B*, 367–378.

(60) Connelly, N. G.; Geiger, W. E. Chemical Redox Agents for Organometallic Chemistry.

Chem. Rev. **1996**, *96*, 877–910.

CHAPTER 4

Unsymmetrical heterobimetallic complexes with TMEDA and $[MST]^{3-}$

Introduction

Metalloenzymes containing bimetallic transition metal active sites perform many important functions in biology. Examples of such active sites include the MnFe site of ribonucleoide reductase which mediates the synthesis of deoxyribonucleotides,[1] the FeFe site of hemerytherin which transports O_2 in certain invertebrates,[2] the NiFe site of [NiFe] hydrogenase which reversibly forms H_2 from protons,[3] and the ZnFe site of purple acid phosphatase which degrades organophosphates.[4] The two metal centers in bimetallic active sites often have different primary coordination spheres and are bridged by one or more oxido or hydroxido ligands. Synthetic bimetallic species have been prepared as structural or functional models for these types of metalloenzymes. Though many of these synthetic bimetallic compounds contain symmetrical coordination sites for the two metals centers due to the use of symmetric dinucleating ligands,[5–16] several groups have been able to prepare synthetically more challenging bimetallic complexes with unsymmetrical coordination sites.[17–29]

As discussed in the previous two chapters, our group has used the tripodal ligand *N*,*N'*,*N''*-[2,2',2''-nitrilotris(ethane-2,1-diyl)]tris(2,4,6-trimethylbenzenesulfonamido) ($[MST]^{3-}$) and related ligands to prepare a variety of monometallic complexes.[30–35] The monomeric complexes can be oxidized with O_2 in the presence of a second metal ion (M^{II}) and a capping ligand (L) to form bimetallic species with the formulation $[(L)M^{II}-(\mu\text{-}OH)-M^{III}MST]^+$ (Figure 4.1).[30,31,36–39] The two metal centers have different coordination environments and are bridged by a hydroxido ligand formed *via* the activation of O_2. The five-coordinate site always contains an N_4O primary coordination sphere, composed of the bridging OH^{-} ligand and N-donors of [MST]$^{3-}$. The secondary site is composed of the bridging OH^{-} ligand, sulfonamido O-atoms of the [MST]$^{3-}$ arms, and the donor atoms of the capping ligands, and it ranges from six to ten-coordinate depending on the identity of the metal ion.[37–39]

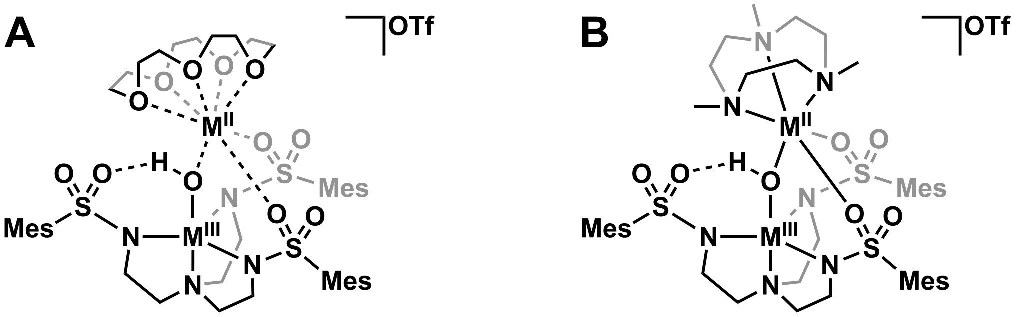

Figure 4.1. Specific examples of [MST]$^{3-}$ bimetallic complexes with (**A**) one transition metal ion (M^{III} = Mn^{III}, Fe^{III}) and one redox inactive metal ion (M^{II} = Ca^{II}, Sr^{II}, Ba^{II} (with 18-crown-6))[37] and (**B**) two transition metal ions (M^{III} = Fe^{III}, M^{II} = Mn^{II}, Fe^{II}, Co^{II}, Ni^{II}, Cu^{II}, Zn^{II}).

Our initial report detailed the preparation and characterization of a heterobimetallic complex of the formulation [15-crown-5⊃Ca^{II}–(μ-OH)–Mn^{III}MST]$^{+}$ (denoted as [C⊃M^{II}(OH)Fe^{III}]$^{+}$), which has biological relevance to the oxygen evolving complex of photosystem II (Figure 4.1A).[36] Later work demonstrated that several heterobimetallic combinations of redox-inactive metal ions and transition metal ions could be synthesized: M^{n}M^{III} = Ca^{II}Co^{III}, Sr^{II}Mn^{III}, Ba^{II}Mn^{III}, Ca^{II}Fe^{III}, Sr^{II}Fe^{III}, Ba^{II}Fe^{III}, and Na^{I}In^{III}.[30,31,37]

This system was expanded to include biologically relevant bimetallic complexes with two transition metal ions.[38,39] The capping ligand 1,4,7-trimethyl-1,4,7-triazacyclononane (TMTACN) was used for these types of compounds, enabling the preparation of an entire series of mixed-valent, unsymmetrical bimetallic complexes of formulation [(TMTACN)M^{II}–(μ-OH)–M^{III}MST]$^{+}$ (denoted as [TMTACN-M^{II}(OH)Fe^{III}]$^{+}$), where M^{II}M^{III} = Mn^{II}Mn^{III}, Mn^{II}Fe^{III}, Fe^{II}Fe^{III}, Co^{II}Fe^{III}, Ni^{II}Fe^{III}, Cu^{II}Fe^{III}, and Zn^{II}Fe^{III}) (Figure 4.1B).[38,39]

Both classes of compounds used capping ligands with denticities of three or above, and the resulting complexes contained secondary metal ions that were in coordinatively saturated environments. Bimetallic complexes with lower denticity capping ligands were pursued to determine if such a modification could affect complex reactivity. It was hypothesized that a bidentate ligand such as *N,N,N′,N′*-tetramethylethane-1,2-diamine (TMEDA) would change the primary coordination sphere of the secondary metal center, allowing it to be five-coordinate with an open coordination site that could facilitate the binding of an additional, external ligand.

In this chapter, the preparation of a new bimetallic compound with the formulation [(TMEDA)Fe^{II}(OTf)–(μ-OH)–Fe^{III}MST] (denoted as [TMEDA-Fe^{II}(OTf)(OH)Fe^{III}]) (Figure 4.2) is described. Despite the presence of the bidentate capping ligand TMEDA, the Fe^{II} center remains six-coordinate in the solid-state. However, the primary coordination sphere of the Fe^{II} center in [TMEDA-Fe^{II}(OTf)(OH)Fe^{III}] compound is notably different from that of [TMTACN-Fe^{II}(OH)Fe^{III}]OTf. Specifically, the trifluoromethanesulfonate (OTf$^-$) counter anion is bound directly to the Fe^{II} center as the sixth ligand [TMEDA-Fe^{II}(OTf)(OH)Fe^{III}], whereas in [TMTACN-Fe^{II}(OH)Fe^{III}]OTf the OTf$^-$ is outer sphere, not coordinated to any metal center.

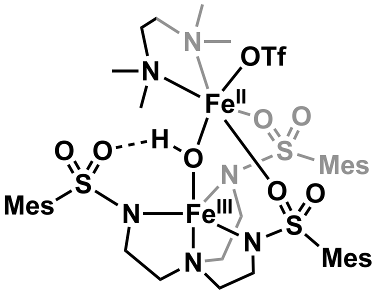

Figure 4.2. The new diiron complex prepared with L = TMEDA, [TMEDA-Fe^{II}(OTf)(OH)Fe^{III}].

Two other related heterobimetallic compounds were prepared, [TMEDA-Co^{II}(OTf)(OH)Fe^{III}] and [TMEDA-Ni^{II}(OTf)(OH)Fe^{III}], and this series of three bimetallic complexes mirrors the previously reported work with the six [TMTACN-M^{II}(OH)Fe^{III}]$^+$ complexes.[39]

Regardless of the capping ligand or secondary metal center, all the complexes had similar electronic absorbance and Fourier transform infrared (FTIR) spectra, as well as solid-state structures. However, the magnetic properties vary for the different combinations of metal centers, shown clearly by perpendicular mode X-band electronic paramagnetic (EPR) spectroscopy. Antiferromagnetic coupling is observed between the high-spin, $S = 5/2$ Fe^{III} centers to the high-spin divalent metal centers, resulting in a stepwise series of different ground-state spin-states. For the [TMEDA-M^{II}(OTf)(OH)Fe^{III}] compounds, $S = 1/2–3/2$ were achieved, while for the [TMTACN-M^{II}(OH)Fe^{III}]$^{+}$ complexes $S = 0–5/2$ were found. These magnetic studies, coupled with electrospray ionization-mass spectrometry (ESI-MS) results, strongly suggest that the series of complexes retain their discretely bimetallic cores.

Results and Discussion

Preparation of [TMEDA-M^{II}(OTf)(OH)Fe^{III}] compounds

The series of three [TMEDA-M^{II}(OTf)(OH)Fe^{III}] complexes were prepared *via* the synthetic route outlined in Scheme 4.1, which is derived from the synthesis of the series of six [TMTACN-M^{II}(OH)Fe^{III}]OTf compounds.[38,39] In a typical reaction, a CH_2Cl_2 or tetrahydrofuran (THF) suspension of NMe_4[Fe^{II}MST], TMEDA, and $M^{II}(OTf)_2·xMeCN$ (M^{II} (x) = Fe^{II} (2), Co^{II} (2), or Ni^{II} (5)) was treated with 0.5 equivalents of O_2 for 1 h. Crystals suitable for X-ray diffraction were obtained by layering either a CH_2Cl_2 or THF solution of the resulting product under pentane, resulting in either block or needle-shaped crystals in yields ranging from 60–87%.

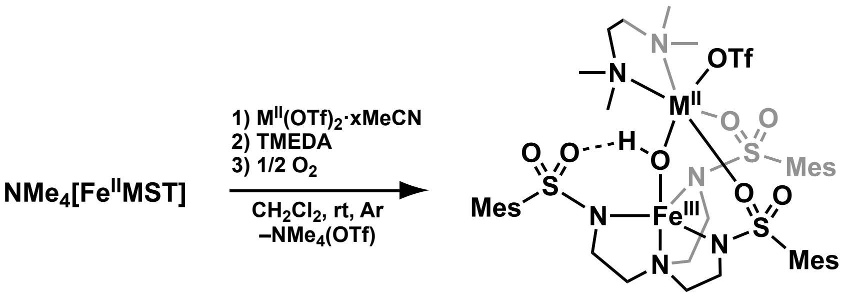

Scheme 4.1. Preparation of [TMEDA-M^{II}(OTf)(OH)Fe^{III}] complexes (M^{II} (x) = Fe^{II} (2), Co^{II} (2), Ni^{II} (5)).

The bimetallic formulation of both series of was supported by ESI-MS, in which the m/z of the molecular ion and experimental isotope patterns matched those calculated for [TMEDA-M^{II}(OH)Fe^{III}]$^+$ (Figure 4.3). All the complexes had similar optical properties with a characteristic absorbance band around λ_{max} = 380 nm and extinction coefficients ranging from 4700–6800 $M^{-1}cm^{-1}$ (Figure 4.4). These bands were similar to previously reported features observed for the related [L⊃M^{II}–(μ-OH)–Fe^{III}MST]$^+$ complexes (L⊃M^{II} = 15-crown-5⊃Ca^{II}, 15-crown-5⊃Sr^{II}, or 18-crown-6⊃Ba^{II}) (λ_{max} = 383–386 nm, ε = 4750–5250 $M^{-1}cm^{-1}$)[37] and [TMTACN-M^{II}(OH)Fe^{III}]OTf complexes (λ_{max} = 381–391 nm, ε = 4170–7480 $M^{-1}cm^{-1}$).[38,39] These bands are all similar regardless of the identity of the second metal center, suggesting this peak involves the Fe^{III} center.

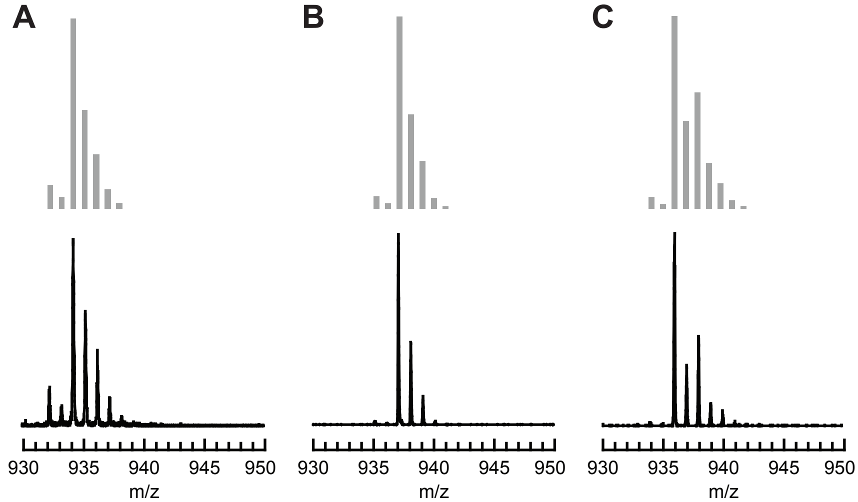

Figure 4.3. ESI-MS spectra of (**A**) [TMEDA-Fe^{II}(OH)Fe^{III}]$^+$, **B**) [TMEDA-Co^{II}(OTf)(OH)Fe^{III}]$^+$ or (**C**) [TMEDA-Ni^{II}(OTf)(OH)Fe^{III}]$^+$. Simulated spectra are in grey.

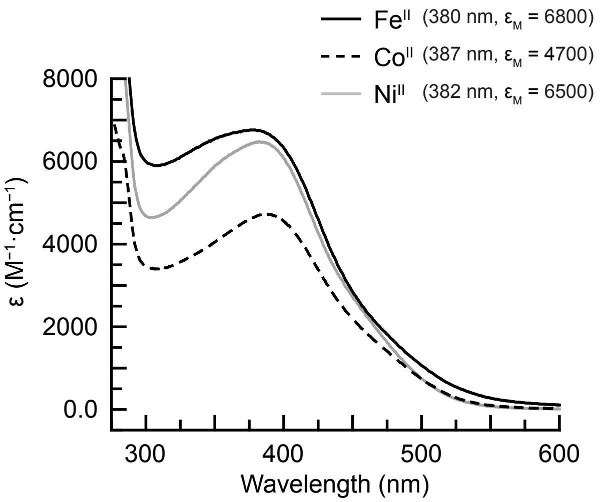

Figure 4.4. UV-visible (UV-vis) spectra for bimetallic compounds [TMEDA-M^{II}(OTf)(OH)Fe^{III}] with M^{II} center specified. All spectra were collected on 0.1 mM CH_2Cl_2 solutions at 25 ˚C.

Vibrational properties of [TMEDA-M^{II}(OTf)(OH)Fe^{III}] and [TMTACN-M^{II}(OH)Fe^{III}]OTf compounds

Similar vibrational properties for all the [TMEDA-M^{II}(OTf)(OH)Fe^{III}] compounds were observed by FTIR spectroscopy (Figure 4.5). Broad ν(OH) bands were observed between 3272–3341 cm^{-1}, where the energies and relative broadness of the bands suggests the presence of intramolecular H-bonds between the bridging hydroxido ligands and one of the sulfonamido oxygen atoms from [MST]$^{3-}$.[40,41] While no significant change in the shape of this band was observed across the series of compounds, a small trend in the energies of ν(OH) was present. The highest energy ν(OH), and thus the strongest O–H bond, was present in [TMEDA-Ni^{II}(OTf)(OH)Fe^{III}] (3341 cm^{-1}), while the lowest energy ν(OH) occurred in [TMEDA-Fe^{II}(OTf)(OH)Fe^{III}] (3272 cm^{-1}). This trend runs counter to expected effect of divalent metal center ionic radii on ν(OH). As Ni^{II} is the smallest ion of the series,[42] it was expected to have the greatest Lewis acidity and thus result in the weakest O–H bond. A similar trend between metal center ionic radii and ν(OH) was also present in the series of six [TMTACN-M^{II}(OH)Fe^{III}]$^{+}$ complexes.

These results may partially be explained by trends in the metrical parameters of the solid-state structures (see below).

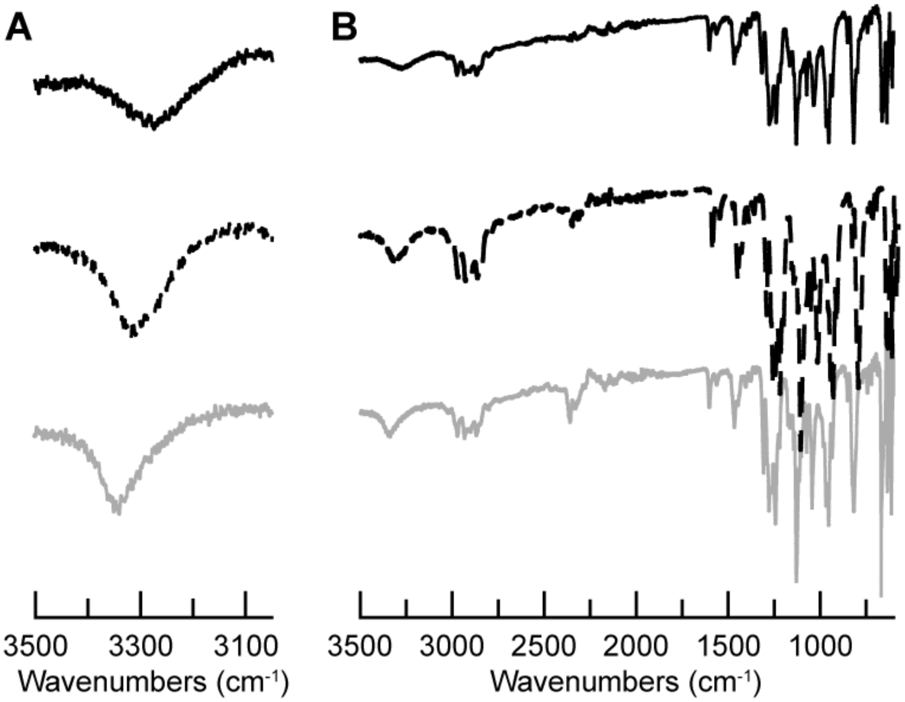

Figure 4.5. FTIR spectra of [TMEDA-Fe^{II}(OTf)(OH)Fe^{III}] (solid black), [TMEDA-Co^{II}(OTf)(OH)Fe^{III}] (dashed black), and [TMEDA-Ni^{II}(OTf)(OH)Fe^{III}] (solid grey), showing (**A**) the expanded region around ν(OH) and (**B**) the full spectra. All spectra were collected by attenuated total reflectance (ATR).

Solid-state molecular structures of [TMEDA-M^{II}(X)(OH)Fe^{III}] compounds

The molecular structures of the [TMEDA-M^{II}(X)(OH)Fe^{III}] complexes were determined by X-ray diffraction methods and revealed the expected bimetallic structures (Figure 4.6). Selected metrical parameters and calculated values are shown in Table 4.1. Because the structure of [TMEDA-Ni^{II}(OTf)(OH)Fe^{III}] was not of sufficient quality, a high quality solid-state structure of the analogous compound [TMEDA-Ni^{II}(Br)(OH)Fe^{III}] was obtained.

In the three bimetallic complexes, the five-coordinate Fe^{III} centers adopted distorted trigonal bipyramidal (tbp) geometries (τ_5 = 0.864–0.892, where τ_5 = 1 for ideal tbp geometry and τ_5 = 0 for ideal square pyramidal geometry),[43] formed by N_4O primary coordination spheres from the N-donors of [MST]$^{3-}$ and the O-atom of the bridging hydroxido ligand. The six-coordinate M^{II}

centers had distorted octahedral geometry (λ_{oct} = 1.012–1.036, where λ_{oct} = 1 for ideal octahedral geometry and larger values indicate greater distortion)[44] with N_3O_2Y primary coordination spheres, derived from the S=O groups of $[MST]^{3-}$, the N-donors of TMEDA, the O-atom of the OTf^- ion or the Br-atom of the Br^- ion, and the O-atom of the bridging hydroxido ligand.

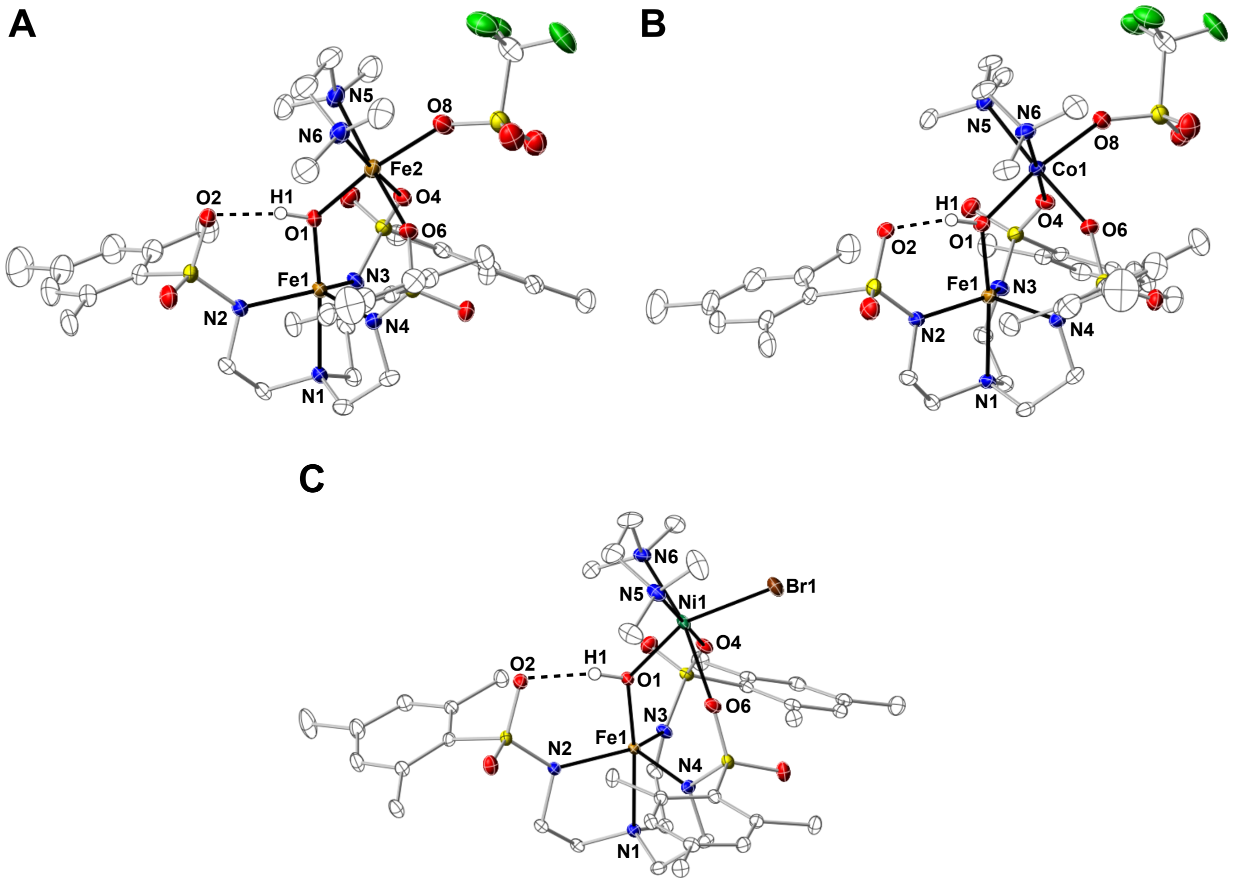

Figure 4.6. Thermal ellipsoid diagrams depicting the molecular structures of (**A**) [TMEDA-Fe^{II}(OTf)(OH)Fe^{III}] , (**B**) [TMEDA-Co^{II}(OTf)(OH)Fe^{III}], and (**C**) [TMEDA-Ni^{II}(Br)(OH)Fe^{III}]. Ellipsoids are drawn at the 50% probability level, and only the hydroxido H-atoms are shown for clarity.

The different ionic radii of the divalent metal ions are reflected most strongly in the bond distances to the N atoms of the TMEDA ligand. Fe^{II} has the largest ionic radius, and therefore [TMEDA-Fe^{II}(OTf)(OH)Fe^{III}] contains the longest average M^{II}–N_{TMEDA} bond distances (2.221(2) Å). In contrast, [TMEDA-Ni^{II}(OTf)(OH)Fe^{III}] has the shortest average M^{II}–N_{TMEDA} bond distances

(2.137(2) Å), reflecting the small ionic radius of Ni^{II}. These bond lengths are typical of M^{II}–TMEDA complexes, which are around 2.0–2.3 Å.[45–48]

A similar observation was made for the [TMTACN-M^{II}(OH)Fe^{III}]$^+$ complexes, where the average M^{II}–N$_{TMTACN}$ bond distances decreased with decreasing ionic radii. For smaller metal centers, the increased interaction with capping ligand donor atoms may be related to the strengthening of the ν(OH) observed by FTIR spectroscopy. Perhaps the metal center's stronger interaction with the N-atom donors decreases its interaction with the bridging hydroxido ligand, resulting in stronger O–H bonds.

Table 4.1. Selected metrical parameters for [TMEDA-M^{II}(X)(OH)Fe^{III}] (M^{II} (X$^-$) = Fe^{II} (OTf$^-$), Co^{II} (OTf$^-$), Ni^{II} (Br$^-$)) complexes.

[TMEDA-M^{II}(X)(OH)Fe^{III}]	M (Y) =		
	Fe2 (O8)	Co1 (O8)	Ni1 (Br1)
Bond distances (Å)			
Fe1–N1	2.227(2)	2.221(2)	2.258(2)
Fe1–N2	2.031(2)	2.035(2)	2.049(2)
Fe1–N3	2.001(2)	1.992(2)	1.995(2)
Fe1–N4	2.005(2)	1.994(2)	1.998(2)
Fe1–O1	1.855(2)	1.879(2)	1.893(1)
O1···O2	2.659	2.619	2.673
M–O1	1.928(2)	1.971(2)	1.987(1)
M–O4	2.207(2)	2.217(2)	2.172(1)
M–O6	2.147(2)	2.153(2)	2.620(1)
M–N5	2.211(2)	2.194(2)	2.129(2)
M–N6	2.231(2)	2.216(2)	2.144(2)
M–Y	2.086(2)	2.067(2)	2.451(3)
Fe1···Fe2	3.337	3.419	3.498
Avg. Fe1–N$_{eq\text{-}MST}$	2.012(2)	2.007(2)	2.014(2)
Avg. M–N$_{TMEDA}$	2.221(2)	2.205(2)	2.137(2)
d[Fe1–N$_{eq\text{-}MST}$][a]	0.357	0.351	0.393
Bond angles (˚)			
O1–Fe1–N1	175.20(8)	173.62(7)	174.09(6)
N2–Fe1–N3	121.10(9)	120.67(8)	117.40(6)
N2–Fe1–N4	121.72(9)	121.80(8)	120.55(6)
N3–Fe1–N4	107.86(8)	108.48(8)	110.87(7)

Fe1–O1–Fe2	126.40(9)	125.23(9)	128.72(7)
O1–Fe2–Y	171.04(8)	170.23(7)	156.12(4)
O4–Fe2–O6	96.13(7)	92.94(6)	103.61(5)
N5–Fe2–N6	82.76(9)	82.90(8)	85.23(7)
Calculated values			
τ_5[b]	0.891	0.864	0.892
V_{oct}[c]	12.8	12.8	14.6
λ_{oct}[d]	1.012	1.012	1.036

[a] distance of Fe1 from the plane formed by the equatorial nitrogen atoms N2, N3, and N4

[b] trigonality parameter, $\tau_5 = (\beta – a)/60$. β is the largest bond angle observed, and α is the second largest bond angle.[43]

[c] octahedral volume, calculated using the IVTON program.[49]

[d] mean oct quadratic elongation, $\lambda_{oct} = \Sigma_1^6(l_i/l_0)^2/6$. $\lambda_{oct} = 1$ for an ideal octahedron. l_0 represents the center-to-vertex distance of an octahedron with O_h symmetry whose volume is equal to that of the distorted octahedron with distances l_i.[44]

Electrochemical properties of [TMEDA-M^{II}(OTf)(OH)Fe^{III}] compounds

The electrochemical properties of the series of bimetallic compounds were probed using cyclic voltammetry (CV) (Figure 4.7). The three bimetallic complexes both exhibited a quasi-reversible one-electron reductive event which was assigned to the M^{II}Fe^{III}/M^{II}Fe^{II} couple. The M^{II}Fe^{III}/M^{II}Fe^{II} redox potential for [TMEDA-Fe^{II}(OTf)(OH)Fe^{III}] (–0.84 V versus the ferrocenium/ferrocene couple ([FeCp$_2$]$^{+/0}$)) and [TMEDA-Co^{II}(OTf)(OH)Fe^{III}] (–0.86 V versus [FeCp$_2$]$^{+/0}$) are comparable to those of [TMTACN-Fe^{II}(OH)Fe^{III}]$^+$ and [TMTACN-Co^{II}(OH)Fe^{III}]$^+$, (–0.86 V and –0.89 V versus [FeCp$_2$]$^{+/0}$ respectively).[38,39] The potential for the [TMEDA-Ni^{II}(OTf)(OH)Fe^{III}] species (–0.94 V versus [FeCp$_2$]$^{+/0}$) is cathodically shifted relative to the rest of the TMEDA series, and a similar shift was also observed for [TMTACN-Ni^{II}(OH)Fe^{III}]$^+$ (–0.99 V versus [FeCp$_2$]$^{+/0}$) when compared to the other complexes in the TMTACN series.[38,39] The reason for these shifts for the Ni^{II}-based compounds are unclear, as this reductive event does not directly involve the second metal center. This unusual redox behavior is illustrated by the fact that the M^{II}Fe^{II}/M^{II}Fe^{III} redox potentials for the other [TMTACN-M^{II}(OH)Fe^{III}]OTf compounds fell within a 0.04 V range.

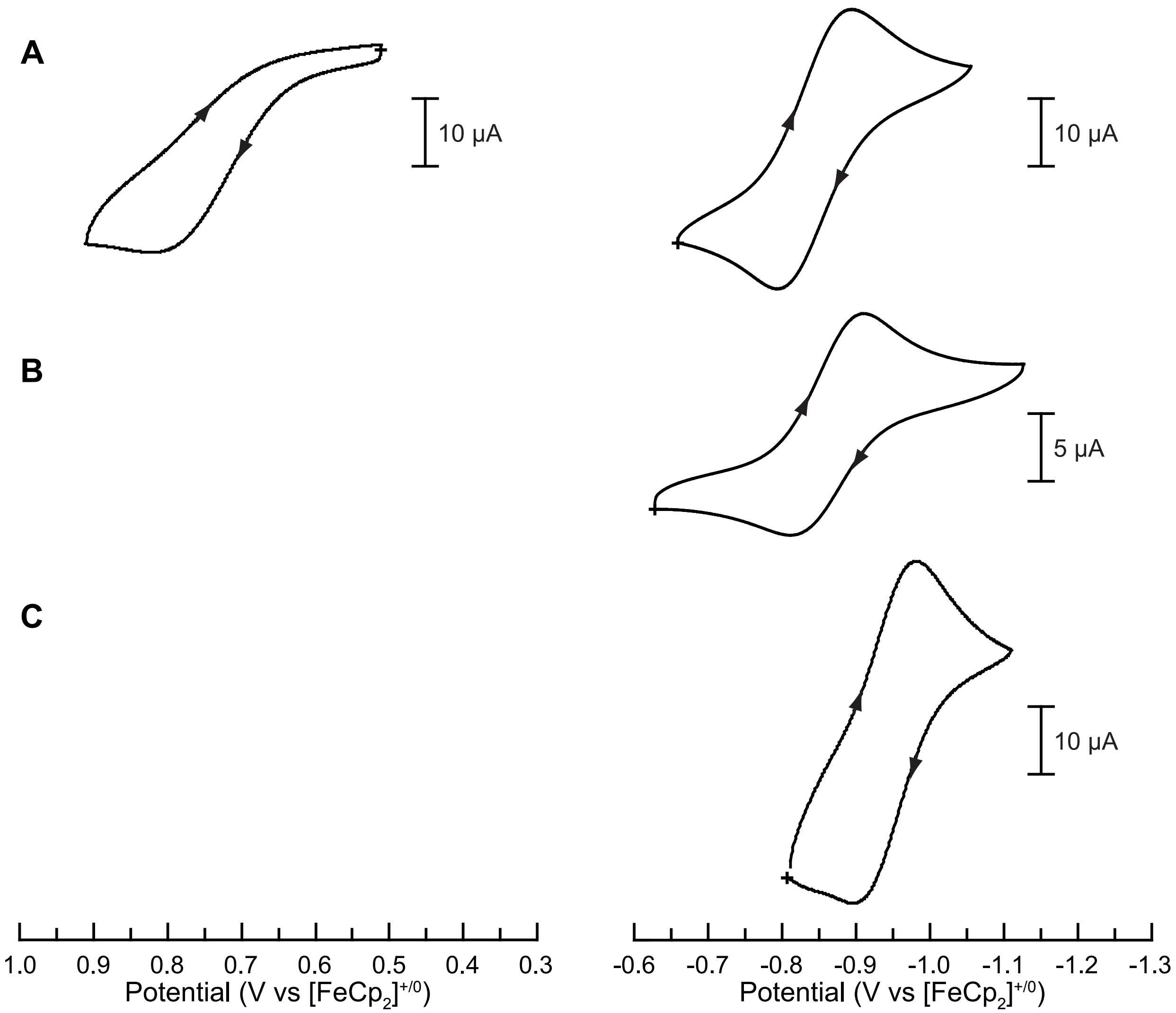

Figure 4.7. Cyclic voltammograms of (**A**) [TMEDA-Fe^{II}(OTf)(OH)Fe^{III}], (**B**) [TMEDA-Co^{II}(OTf)(OH)Fe^{III}], and (**C**) [TMEDA-Ni^{II}(OTf)(OH)Fe^{III}]. The cyclic voltammograms were collected at 100 mV s^{-1} in the presence of [FeCp$_2$].

The similarity in the reduction potentials of the TMEDA and TMTACN series of complexes suggests that in the TMEDA complexes, the OTf$^-$ ligand is not bound to the M^{II} center in solution. Formally neutral [TMEDA-M^{II}(OTf)(OH)Fe^{III}] species should be more difficult to reduce than the positively charged [TMTACN-M^{II}(OH)Fe^{III}]$^+$ complexes. However, since no major cathodic shift is observed for the TMEDA series of complexes, the overall charge of the two types of complexes should be the same, suggesting that [TMEDA-M^{II}(OH)Fe^{III}]$^+$, and not [TMEDA-M^{II}(OTf)(OH)Fe^{III}], is the dominant species in solution.

An irreversible oxidative feature was observable for the diiron compound (E_A = 0.82 V versus $[FeCp_2]^{+/0}$) and was assigned to the $Fe^{II}Fe^{III}/Fe^{III}Fe^{III}$ couple. No oxidative feature was observed for the heterobimetallic species. As late transition metal ions tend to have more positive oxidization potentials, the oxidation potentials of Co^{II} and Ni^{II} should be anodically shifted when compared to that of Fe^{II}. Thus, the $M^{II}Fe^{III}/M^{III}Fe^{III}$ couples were likely too positive to be detected.

EPR Spectra of [TMEDA-M^{II}(OTf)(OH)Fe^{III}] compounds

The magnetic properties of the [TMEDA-M^{II}(OTf)(OH)Fe^{III}] complexes were probed using X-band EPR spectroscopy. Previous studies with the TMTACN series of complexes revealed that antiferromagnetic coupling was observed between the two high-spin metal centers.[38,39]

[TMEDA-Fe^{II}(OTf)(OH)Fe^{III}] was likewise expected to exhibit antiferromagnetic coupling between the high-spin Fe^{III} center (S = 5/2) and Fe^{II} center (S = 2), resulting in a S = 1/2 ground-state. The rhombic perpendicular-mode EPR spectrum has signals centered around g = 2 (Figure 4.8A) was consistent with this spin-state, suggesting that antiferromagnetic coupling was also present in this series of compounds. As expected, [TMEDA-Ni^{II}(OTf)(OH)Fe^{III}] revealed a signal consistent with an S = 3/2 ground-state, derived from antiferromagnetic coupling between the high-spin Fe^{III} center (S = 5/2) and the Ni^{II} (S = 1) center. This observation of magnetic coupling indicates that these compounds remain assembled as bimetallic species in solution.

The signals from these two compounds are similar to those of their related TMTACN compounds (Figure 4.9). The differences in line shape may be attributed to differences in the primary coordination sphere of the divalent metal centers, as EPR spectroscopy is sensitive to geometric changes around metal centers.[50–52]

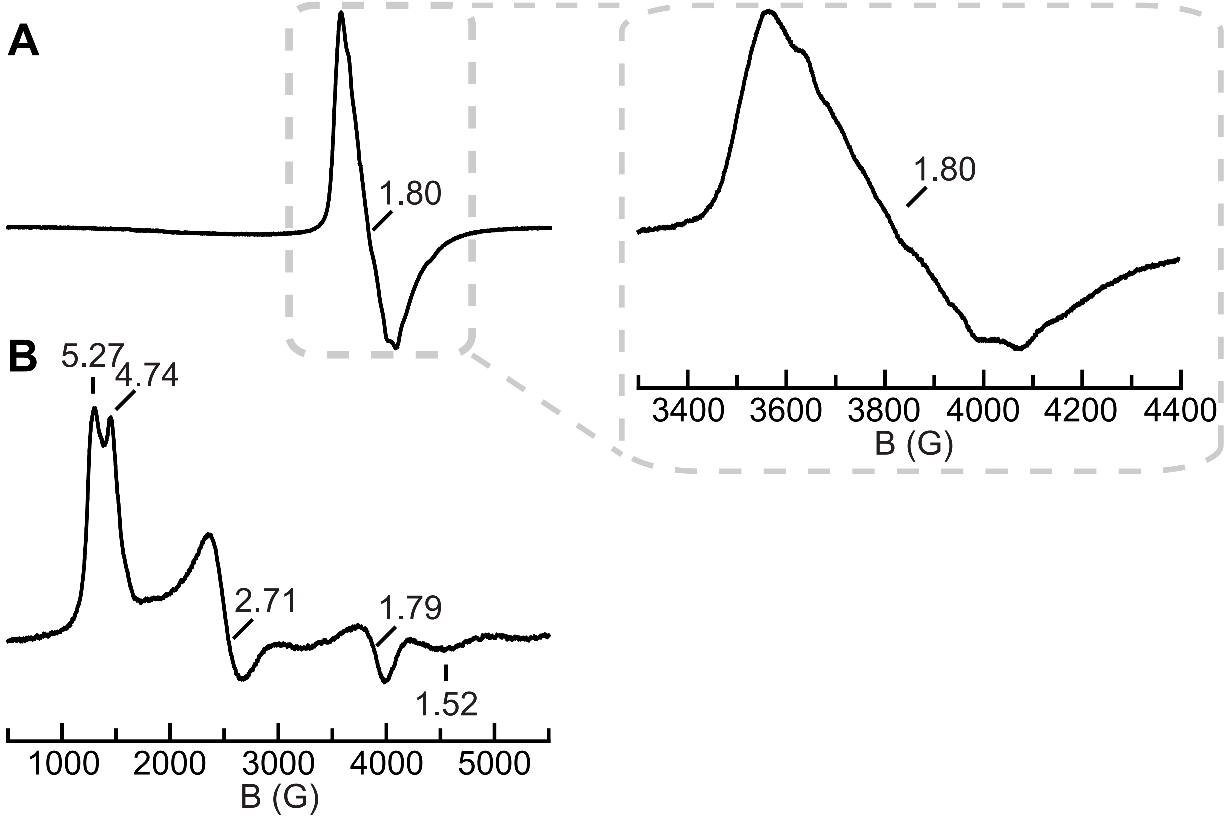

Figure 4.8. Perpendicular-mode EPR spectra for (**A**) [TMEDA-Fe^{II}(OTf)(OH)Fe^{III}] with zoomed inset and (**B**) [TMEDA-Ni^{II}(OTf)(OH)Fe^{III}], all collected at 10 K in CH_2Cl_2.

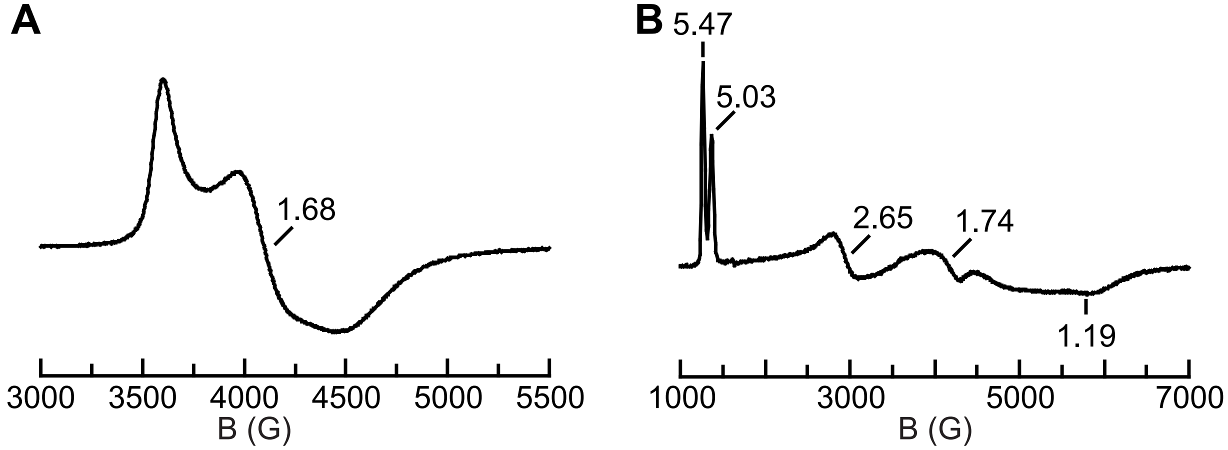

Figure 4.9. Perpendicular-mode EPR spectra for (**A**) [TMTACN-Fe^{II}(OH)Fe^{III}]OTf collected at 20 K in CH_2Cl_2 and (**B**) [TMTACN-Ni^{II}(OH)Fe^{III}]OTf collected at 11 K in CH_2Cl_2.[38,39]

No EPR signal was observed in either perpendicular- or parallel-mode for [TMEDA-Co^{II}(OTf)(OH)Fe^{III}]. However, antiferromagnetic coupling between the high-spin Fe^{III} center (S = 5/2) and the Co^{II} (S = 3/2) center should result in and S = 1 ground-state, and such signals are often difficult to observe. Evans' method[53] was used to determine the solution effective magnetic moment of [TMEDA-Co^{II}(OTf)(OH)Fe^{III}] at room temperature to be 5.8 μ_B. This value is consistent with the expected spin-only value for an S = 5/2 system of 5.9 μ_B, and not of an S = 1 system of 2.8 μ_B. This result shows that the coupling between the M^{II} and Fe^{III} centers is very weak at room temperature, unsurprising as strongly coupled EPR signals could not be observed at even 77 K for either [TMEDA-Fe^{II}(OTf)(OH)Fe^{III}] or [TMEDA-Ni^{II}(OTf)(OH)Fe^{III}].

Summary and Conclusions

This chapter presents the synthesis and characterization of a series of three new bimetallic compounds of the formulation [TMEDA-M^{II}(OTf)(OH)Fe^{III}], where M^{II} = Fe^{II}, Co^{II}, or Ni^{II}. All compounds in this series have similar optical, vibrational, and electrochemical properties. These physical properties are also similar to those of the related series of [TMTACN-M^{II}(OH)Fe^{III}]$^+$ complexes.[38,39]

The solid state structures determined by X-ray diffraction methods showed that all the compounds contain a M^{II}–(μ-OH)–Fe^{III} core. The two metal centers have different coordination environments, with the Fe^{III} centers having five-coordinate, distorted tbp primary coordination spheres and the M^{II} center having six-coordinate, distorted octahedral primary coordination spheres. Notably, the OTf^- counter anion occupies the sixth coordination site of the divalent metal centers. The metrical parameters of the Fe^{III} site remain consistent throughout the series, while the metrical parameters around the M^{II} site vary predictably depending on the ionic radii of the M^{II} center.

The magnetic properties of the complexes were investigated by EPR spectroscopy. The two high-spin metal centers exhibit antiferromagnetic coupling, allowing the series of complexes to access spin states ranging from S = 1/2 for [TMEDA-Fe^{II}(OTf)(OH)Fe^{III}] to S = 5/2 for [TMEDA-Ni^{II}(OTf)(OH)Fe^{III}]. These results also suggest that the compounds remain assembled as bimetallic species in solution. Having established that different M^{II} centers can be accommodated in this system, the ability to modulate the other key components of this system, namely the OTf^{-} ligand and capping ligand, will be explored in the following chapter.

Experimental

General Methods

All reagents were purchased from commercial sources and used as received, unless otherwise noted. Solvents were sparged with argon and dried over columns containing Q-5 and molecular sieves. Potassium hydride (KH) as a dispersion in mineral oil was filtered with a medium porosity glass-fritted funnel and washed 5 times each with pentane and diethyl ether (Et_2O). Solid KH was dried under vacuum and stored under inert atmosphere. The synthesis of the ligand was carried out in the air and the preparations of the metal complexes were conducted in a Vacuum Atmospheres, Co. drybox under an argon atmosphere. Dioxygen was dried on a Drierite gas purifier purchased from Fischer Scientific. TMEDA was distilled over CaO and KOH under static vacuum at 30 °C onto 4 Å molecular sieves and stored under inert atmosphere. Fe^{II}(OTf)$_2$·2MeCN,[54] Co^{II}(OTf)$_2$·2MeCN,[54] Ni^{II}(OTf)$_2$·5MeCN,[54] and NMe$_4$[Fe^{II}MST][37] were synthesized according to previous reports.

Complex Synthesis

[TMEDA-Fe^{II}(OTf)(OH)Fe^{III}]. This complex was prepared using literature procedures for the related salt [TMTACN-Fe^{II}(OH)Fe^{III}]OTf [38] using Fe^{II}(OTf)$_2$·2MeCN (46.1 mg, 106 mmol), TMEDA (13.2 mg, 114 mmol), and NMe$_4$[Fe^{II}MST] (86.6 mg, 106 mmol) to produce the desired complex in crystalline yields of 62–87%. Dark orange needle crystals of [TMEDA-Fe^{II}(OTf)(OH)Fe^{III}] suitable for X-ray diffraction were grown from a THF solution layered under pentane. Elemental analysis calcd. for [TMEDA-Fe^{II}(OTf)Fe^{III}]·0.5CH$_2$Cl$_2$, $C_{40.5}H_{63}ClF_3Fe_2N_6O_{10}S_4$: C, 43.19; H, 5.64; N, 7.46%, found: C, 42.89; H, 5.34; N, 7.34%. UV-vis (CH$_2$Cl$_2$, λ_{max}, nm (ε_{max}, M^{-1}cm^{-1})) 274(sh), 283(sh), 380(6800). FTIR (ATR, cm^{-1}, selected bands): 3272(OH), 2980, 2935, 2869, 1603, 1564, 1467, 1313, 1276, 1239, 1129, 1034, 953, 816, 662, 635, 609. (Nujol, cm^{-1}): 3260(OH). Exact mass calcd for [TMEDA-Fe^{II}(OH)Fe^{III}]$^+$, $C_{39}H_{62}Fe_2N_6O_7S_3$: 934.3 found: 934.2. $E_{1/2}$ (MeCN, V versus [FeCp$_2$]$^{+/0}$): –0.84. E_A (MeCN, V versus [FeCp$_2$]$^{+/0}$): 0.82.

[TMEDA-Co^{II}(OTf)(OH)Fe^{III}]. This complex was prepared using the method described above for [TMEDA-Fe^{II}(OTf)(OH)Fe^{III}] using Co^{II}(OTf)$_2$·2MeCN (39.2 mg, 0.0895 mmol), TMEDA (10.9 mg, 0.0936 mmol), and NMe$_4$[Fe^{II}MST] (73.2 mg, 0.0893 mmol) to produce the desired complex in crystalline yields of 62–85%. Dark orange needle crystals of [TMEDA-Co^{II}(OTf)(OH)Fe^{III}] suitable for X-ray diffraction were grown from a THF solution layered under pentane. Elemental analysis calcd. for [TMEDA-Co^{II}(OTf)(OH)Fe^{III}]·0.5C$_5$H$_{12}$, $C_{42.5}H_{68}CoF_3FeN_6O_{10}S_4$: C, 45.45; H, 6.10; N, 7.48%, found: C, 45.52; H, 5.96; N, 8.00%. UV-vis (CH$_2$Cl$_2$ solution λ_{max}/nm (ε_{max}/M^{-1}cm^{-1})) 275(sh), 387(4700). FTIR (ATR, cm^{-1}, selected bands): 3316(OH), 2975, 2935, 2871, 1603, 1467, 1311, 1278, 1239, 1220, 1129, 1073, 1037, 967, 953, 935, 851, 817, 662, 635, 609. (Nujol, cm^{-1}):

3312(OH). Exact mass calcd for [TMEDA-Co^{II}(OH)Fe^{III}]$^+$, $C_{39}H_{62}FeCoN_6O_7S_3$: 937.3 found: 937.1. $E_{1/2}$ (MeCN, V versus [FeCp$_2$]$^{+/0}$): –0.86. μ_{eff} (μ_B): 5.85.

[TMEDA-Ni^{II}(OTf)(OH)Fe^{III}]. This complex was prepared using the method described above for [TMEDA-Fe^{II}(OTf)(OH)Fe^{III}] using Ni^{II}(OTf)$_2$·5MeCN (50.2 mg, 0.0893 mmol), TMEDA (10.9 mg, 0.0936 mmol), and NMe$_4$[Fe^{II}MST] (73.6 mg, 0.0898 mmol) to produce the desired complex in crystalline yields of 60–67%. Dark orange block crystals of [TMEDA-Ni^{II}(OTf)(OH)Fe^{III}] suitable for X-ray diffraction were grown from a CH_2Cl_2 solution layered under pentane. Elemental analysis calcd. for [TMEDA-Ni^{II}(OTf)(OH)Fe^{III}]·0.5C_5H_{12}, $C_{42.5}H_{68}NiF_3FeN_6O_{10}S_4$: C, 45.46; H, 6.10; N, 7.48%, found: C, 45.74; H, 5.59; N, 7.96%. UV-vis (CH_2Cl_2 solution λ_{max}/nm (ε_{max}/M^{-1}cm^{-1})) 275(sh), 285(sh), 382(6500). FTIR (ATR, cm^{-1}, selected bands): 3341(OH), 2974, 2935, 2871, 2361, 1603, 1308, 1242, 1221, 1130, 1073, 1044, 968, 954, 936, 817, 648. (Nujol, cm^{-1}): 3341(OH). Exact mass calcd for [TMEDA-Ni^{II}(OH)Fe^{III}]$^+$, $C_{39}H_{62}FeNiN_6O_7S_3$: 936.3 found: 936.2. $E_{1/2}$ (MeCN, V versus [FeCp$_2$]$^{+/0}$): –0.94.

[TMEDA-Ni^{II}(Br)(OH)Fe^{III}]. This complex was prepared using the method described above for [TMEDA-Fe^{II}(OTf)(OH)Fe^{III}] using Ni^{II}Br$_2$ (73.5 mg, 0.0896 mmol), TMEDA (12.0 mg, 0.103 mmol), and NMe$_4$[Fe^{II}MST] (73.5 mg, 0.0896 mmol) to produce the desired complex in a crystalline yield of 47%. Dark orange block crystals of [TMEDA-Ni^{II}(OTf)(OH)Fe^{III}] suitable for X-ray diffraction were grown from a CH_2Cl_2 solution layered under pentane. UV-vis (CH_2Cl_2 solution λ_{max}/nm (ε_{max}/M^{-1}cm^{-1})) 275(sh), 285(sh), 387(6200). FTIR (ATR, cm^{-1}, selected bands): 3336(OH), 2973, 2912, 2866, 2361, 1601, 1562, 1465, 1308, 1269, 1130, 1072, 1051, 968, 953, 934, 818, 661.

(Nujol, cm^{-1}): 3345(OH). Exact mass calcd for $[TMEDA\text{-}Ni^{II}(OH)Fe^{III}]^+$, $C_{39}H_{62}FeNiN_6O_7S_3$: 936.3 found: 936.1. $E_{1/2}$ (MeCN, V versus $[FeCp_2]^{+/0}$): –0.94.

Physical Methods

Elemental analyses were performed on a Perkin-Elmer 2400 CHNS analyzer. UV-vis spectra were recorded with a Cary 50 spectrophotometer or an Agilent 8453 spectrophotometer equipped with an Unisoku Unispeks cryostat using either a 0.10 cm or 1.00 cm quartz cuvette. FTIR spectra were collected on a Varian 800 Scimitar Series FTIR spectrometer in air or a Thermo Scientific Nicolet iS5 spectrophotometer with an iD5 ATR attachment in a nitrogen filled glovebox. High-resolution mass spectra were collected using Waters Micromass LCT Premier Mass Spectrometer. CV experiments were conducted using a CH1600C electrochemical analyzer. A 2.0 mm glassy carbon electrode was used as the working electrode at scan velocities 0.1 V s^{-1}. $[FeCp_2]^{+/0}$ was used as an internal reference to monitor the reference electrode ($Ag^{0/+}$). Tetrabutylammonium hexafluorophosphate (TBAP) was use as the supporting electrolyte at a concentration of 0.1 M. Perpendicular-mode X-band EPR spectra were collected using a Bruker EMX spectrometer at 10 K using liquid helium. Solution effective magnetic moments were measured by Evans' method on a Bruker DRX500 spectrometer using flame sealed standard cores of 1:1 DMSO:DMSO-d_6 or 1:1 $CHCl_3$:$CDCl_3$.[53]

Crystallography

A Bruker SMART APEX II diffractometer and the APEX2 program package was used to determine the unit-cell parameters and for data collection. Crystallographic details are summarized in Appendix A.

References

(1) Jiang, W.; Yun, D.; Saleh, L.; Barr, E.; Xing, G.; Hoffart, L. M.; Maslak, M.-A.; Krebs, C.; Bollinger Jr., J. M. A manganese (IV)/iron (III) cofactor in Chlamydia trachomatis ribonucleotide reductase. *Science* **2007**, *316*, 1188–1191.

(2) Kurtz, D. M. Dioxygen-binding Proteins. In *Comprehensive Coordination Chemistry II*; Elsevier, 2003; pp 229–260.

(3) Fontecilla-Camps, J. C.; Volbeda, A. [NiFe]-Hydrogenases. *Encyclopedia of Metalloproteins*; Springer New York, 2013; pp 1535–1544.

(4) Schenk, G.; Mitić, N.; Gahan, L. R.; Ollis, D. L.; McGeary, R. P.; Guddat, L. W. Binuclear Metallohydrolases: Complex Mechanistic Strategies for a Simple Chemical Reaction. *Acc. Chem. Res.* **2012**, *45*, 1593–1603.

(5) Diril, H.; Chang, H. R.; Zhang, X.; Larsen, S. K.; Potenza, J. A.; Pierpont, C. G.; Schugar, H. J.; Isied, S. S.; Hendrickson, D. N. Binuclear Mixed-Valence $Mn^{II}Mn^{III}$ Complexes: Insight About the Resolution of Hyperfine Structure in the EPR Spectrum. *J. Am. Chem. Soc.* **1987**, *109*, 6207–6208.

(6) Borovik, A. S.; Papaefthymiou, V.; Taylor, L. F.; Anderson, O. P.; Que, Jr., L. Models for Iron-Oxo Proteins. Structures and Properties of $Fe^{II}Fe^{III}$, $Zn^{II}Fe^{III}$, and $Fe^{II}Ga^{III}$ Complexes with (μ-Phenoxo)bis(μ-carboxylato)dimetal Cores. *J. Am. Chem. Soc.* **1989**, *111*, 6183–6195.

(7) Buchanan, R. M.; Mashuta, M. S.; Richardson, J. F.; Webb, R. J.; Oberhausen, K. J.; Nanny, M. A.; Hendrickson, D. N. Synthesis, Structure, and Properties of a Novel Heterobimetallic $Fe^{III}Mn^{II}$ Complex Containing a Septadentate Polyimidazole Ligand. *Inorg. Chem.* **1990**, *29*, 1299–1301.

(8) Bossek, U.; Hummel, H.; Weyhermüller, T.; Bili, E.; Wieghardt, K. The First μ(OH)-Bridged Model Complex for the Mixed-Valent $Fe^{II}Fe^{III}$ Form of Hemerythrin. *Angew. Chem., Int. Ed. Engl.* **1996**, *34*, 2642–2645.

(9) Bossek, U.; Hummel, H.; Weyhermüller, T.; Wieghardt, K.; Russell, S.; van der Wolf, L.; Kolb, U. The$[Mn_2^{IV}(\mu\text{-}O)(\mu\text{-}PhBO_2)_2]^{2+}$ Unit: A New Structural Model for Manganese-Containing Metalloproteins. *Angew. Chemie Int. Ed. English* **1996**, *35*, 1552–1554.

(10) Ng, G. K. Y.; Ziller, J. W.; Borovik, A. S. Structural Diversity in Metal Complexes with a Dinucleating Ligand Containing Carboxyamidopyridyl Groups. *Inorg. Chem.* **2011**, *50*, 7922–7924.

(11) Ng, G. K.-Y.; Ziller, J. W.; Borovik, A. S. Preparation and structures of dinuclear complexes containing M^{II}–OH centers. *Chem. Commun.* **2012**, *48*, 2546–2548.

(12) Buchler, S.; Meyer, F.; Kaifer, E.; Pritzkow, H. Tunable TACN/pyrazolate hybrid ligands as dinucleating scaffolds for metallobiosite modeling—dinickel(II) complexes relevant to the urease active site. *Inorganica Chim. Acta* **2002**, *337*, 371–386.

(13) Isaac, J. A.; Gennarini, F.; López, I.; Thibon-Pourret, A.; David, R.; Gellon, G.; Gennaro, B.; Philouze, C.; Meyer, F.; Demeshko, S.; Le Mest, Y.; Réglier, M.; Jamet, H.; Le Poul, N.; Belle, C. Room-Temperature Characterization of a Mixed-Valent μ-Hydroxodicopper(II,III) Complex. *Inorg. Chem.* **2016**, *55*, 8263–8266.

(14) Dunn, T. J.; Ramogida, C. F.; Simmonds, C.; Paterson, A.; Wong, E. W. Y.; Chiang, L.; Shimazaki, Y.; Storr, T. Non-Innocent Ligand Behavior of a Bimetallic Ni Schiff-Base Complex Containing a Bridging Catecholate. *Inorg. Chem.* **2011**, *50*, 6746–6755.

(15) Clarke, R. M.; Hazin, K.; Thompson, J. R.; Savard, D.; Prosser, K. E.; Storr, T. Electronic Structure Description of a Doubly Oxidized Bimetallic Cobalt Complex with Proradical Ligands. *Inorg. Chem.* **2016**, *55*, 762–774.

(16) Alliger, G. E.; Müller, P.; Do, L. H.; Cummins, C. C.; Nocera, D. G. Family of Cofacial Bimetallic Complexes of a Hexaanionic Carboxamide Cryptand. *Inorg. Chem.* **2011**, *50*, 4107–4115.

(17) Neves, A.; Lanznaster, M.; Bortoluzzi, A. J.; Peralta, R. A.; Casellato, A.; Castellano, E. E.; Herrald, P.; Riley, M. J.; Schenk, G. An Unprecedented Fe^{III}(μ-OH)Zn^{II}Complex that Mimics the Structural and Functional Properties of Purple Acid Phosphatases. *J. Am. Chem. Soc.* **2007**, *129*, 7486–7487.

(18) de Souza, B.; Kreft, G. L.; Bortolotto, T.; Terenzi, H.; Bortoluzzi, A. J.; Castellano, E. E.; Peralta, R. A.; Domingos, J. B.; Neves, A. Second-Coordination-Sphere Effects Increase the Catalytic Efficiency of an Extended Model for $Fe^{III}M^{II}$ Purple Acid Phosphatases. *Inorg. Chem.* **2013**, *52*, 3594–3596.

(19) Wong, J. L.; Higgins, R. F.; Bhowmick, I.; Cao, D. X.; Szigethy, G.; Ziller, J. W.; Shores, M. P.; Heyduk, A. F.; Gagliardi, L.; Lu, C. C. Bimetallic iron–iron and iron–zinc complexes of the redox-active ONO pincer ligand. *Chem. Sci.* **2016**, *7*, 1594–1599.

(20) Rosenkoetter, K. E.; Ziller, J. W.; Heyduk, A. F. A Heterobimetallic W–Ni Complex Containing a Redox-Active $W[SNS]_2$ Metalloligand. *Inorg. Chem.* **2016**, *55*, 6794–6798.

(21) Rudd, P. A.; Liu, S.; Gagliardi, L.; Young, V. G.; Lu, C. C. Metal–Alane Adducts with Zero-Valent Nickel, Cobalt, and Iron. *J. Am. Chem. Soc.* **2011**, *133*, 20724–20727.

(22) Clouston, L. J.; Siedschlag, R. B.; Rudd, P. A.; Planas, N.; Hu, S.; Miller, A. D.; Gagliardi, L.; Lu, C. C. Systematic Variation of Metal-Metal Bond Order in Metal–Chromium Complexes. *J. Am. Chem. Soc.* **2013**, *135*, 13142–13148.

(23) Eisenhart, R. J.; Clouston, L. J.; Lu, C. C. Configuring Bonds between First-Row Transition Metals. *Acc. Chem. Res.* **2015**, *48*, 2885–2894.

(24) Serrano-Plana, J.; Garcia-Bosch, I.; Company, A.; Costas, M. Structural and Reactivity Models for Copper Oxygenases: Cooperative Effects and Novel Reactivities. *Acc. Chem. Res.* **2015**, *48*, 2397–2406.

(25) Delgado, M.; Ziegler, J. M.; Seda, T.; Zakharov, L. N.; Gilbertson, J. D. Pyridinediimine Iron Complexes with Pendant Redox-Inactive Metals Located in the Secondary Coordination Sphere. *Inorg. Chem.* **2016**, *55*, 555–557.

(26) Barton, B. E.; Rauchfuss, T. B. Hydride-Containing Models for the Active Site of the Nickel−Iron Hydrogenases. *J. Am. Chem. Soc.* **2010**, *132*, 14877–14885.

(27) Greenwood, B. P.; Forman, S. I.; Rowe, G. T.; Chen, C.-H.; Foxman, B. M.; Thomas, C. M. Multielectron Redox Activity Facilitated by Metal−Metal Interactions in Early/Late Heterobimetallics: Co/Zr Complexes Supported by Phosphinoamide Ligands. *Inorg. Chem.* **2009**, *48*, 6251–6260.

(28) Krogman, J. P.; Thomas, C. M. Metal–metal multiple bonding in C_3-symmetric bimetallic complexes of the first row transition metals. *Chem. Commun.* **2014**, *50*, 5115.

(29) Wu, B.; Wilding, M. J. T.; Kuppuswamy, S.; Bezpalko, M. W.; Foxman, B. M.; Thomas, C. M. Exploring Trends in Metal–Metal Bonding, Spectroscopic Properties, and Conformational Flexibility in a Series of Heterobimetallic Ti/M and V/M Complexes (M = Fe, Co, Ni, and Cu). *Inorg. Chem.* **2016**, *55*, 12137–12148.

(30) Lacy, D. C.; Park, Y. J.; Ziller, J. W.; Yano, J.; Borovik, A. S. Assembly and Properties of Heterobimetallic $Co^{II/III}/Ca^{II}$ Complexes with Aquo and Hydroxo Ligands. *J. Am. Chem. Soc.* **2012**, *134*, 17526–17535.

(31) Sickerman, N. S.; Henry, R. M.; Ziller, J. W.; Borovik, A. S. Preparation and structural properties of In^{III}–OH complexes. *Polyhedron* **2013**, *58*, 65–70.

(32) Sickerman, N. S.; Peterson, S. M.; Ziller, J. W.; Borovik, A. S.; Mäemets, V.; Leito, I.; Koppel, I. A.; Borovik, A. S. Synthesis, structure and reactivity of $Fe^{II}/^{III}$–NH_3 complexes bearing a tripodal sulfonamido ligand. *Chem. Commun.* **2014**, *50*, 2515.

(33) Cook, S. A.; Ziller, J. W.; Borovik, A. S. Iron(II) Complexes Supported by Sulfonamido Tripodal Ligands: Endogenous versus Exogenous Substrate Oxidation. *Inorg. Chem.* **2014**, *53*, 11029–11035.

(34) Lau, N.; Ziller, J. W.; Borovik, A. S. Sulfonamido tripods: Tuning redox potentials via ligand modifications. *Polyhedron* **2015**, *85*, 777–782.

(35) Lau, N.; Sano, Y.; Ziller, J. W.; Borovik, A. S. Terminal Ni^{II}−OH/−OH_2 complexes in trigonal bipyramidal geometries derived from H_2O. *Polyhedron* **2017**, *125*, 179–185.

(36) Park, Y. J.; Ziller, J. W.; Borovik, A. S. The Effects of Redox-Inactive Metal Ions on the Activation of Dioxygen: Isolation and Characterization of a Heterobimetallic Complex Containing a Mn^{III}–(μ-OH)–Ca^{II} Core. *J. Am. Chem. Soc.* **2011**, *133*, 9258–9261.

(37) Park, Y. J.; Cook, S. A.; Sickerman, N. S.; Sano, Y.; Ziller, J. W.; Borovik, A. S.

Heterobimetallic complexes with M^{III}-(μ-OH)-M^{II} cores (M^{III} = Fe, Mn, Ga; M^{II} = Ca, Sr, and Ba): structural, kinetic, and redox properties. *Chem. Sci.* **2013**, *4*, 717–726.

(38) Sano, Y.; Weitz, A. C.; Ziller, J. W.; Hendrich, M. P.; Borovik, A. S. Unsymmetrical Bimetallic Complexes with M^{II}–(μ-OH)–M^{III} Cores (M^{II}M^{III} = Fe^{II}Fe^{III}, Mn^{II}Fe^{III}, Mn^{II}Mn^{III}): Structural, Magnetic, and Redox Proper. *Inorg. Chem.* **2013**, *52*, 10229–10231.

(39) Sano, Y.; Lau, N.; Weitz, A. C.; Ziller, J. W.; Hendrich, M. P.; Borovik, A. S. Models for Unsymmetrical Active Sites in Metalloproteins: Structural, Redox, and Magnetic Properties of Bimetallic Complexes with M^{II}–(μ-OH)–Fe^{III} Cores. *Manuscript in preparation.*

(40) Aaron, H. S. Conformational Analysis of Intramolecular-Hydrogen-Bonded Compounds in Dilute Solution by Infrared Spectroscopy. John Wiley & Sons, Inc.; pp 1–52.

(41) Gellman, S. H.; Dado, G. P.; Liang, G. B.; Adams, B. R. Conformation-directing effects of a single intramolecular amide-amide hydrogen bond: variable-temperature NMR and IR studies on a homologous diamide series. *J. Am. Chem. Soc.* **1991**, *113*, 1164–1173.

(42) Shannon, R. D. Revised effective ionic radii and systematic studies of interatomic distances in halides and chalcogenides. *Acta Crystallogr. Sect. A* **1976**, *32*, 751–767.

(43) Addison, A. W.; Rao, T. N.; Reedijk, J.; van Rijn, J.; Verschoor, G. C. Synthesis, structure, and spectroscopic properties of copper(II) compounds containing nitrogen–sulphur donor ligands; the crystal and molecular structure of aqua[1,7-bis(N-methylbenzimidazol-2′-yl)-2,6-dithiaheptane]copper(II) perchlorate. *J. Chem. Soc. Dalt. Trans.* **1984**, No. 7, 1349.

(44) Robinson, K.; Gibbs, G. V.; Ribbe, P. H. Quadratic Elongation: A Quantitative Measure of Distortion in Coordination Polyhedra. *Science* **1971**, *172*, 567–570.

(45) Yoshida, T.; Suzuki, T.; Kanamori, K.; Kaizaki, S. Synthesis, Magnetic Properties, and Electronic Spectra of Octahedral Mixed-Ligand (beta-Diketonato)nickel(II) Complexes with a Chelated Nitronyl Nitroxide Radical. *Inorg. Chem.* **1999**, *38*, 1059–1068.

(46) Handley, D. A.; Hitchcock, P. B.; Leigh, G. J. Triangulo-pentahalotrimetal complexes of nickel(II) and cobalt(II) with *N,N,N′,N′,N*-tetramethylethane-1,2-diamine and related compounds. *Inorganica Chim. Acta* **2001**, *314*, 1–13.

(47) Amarasinghe, K. K. D.; Chowdhury, S. K.; Heeg, M. J.; Montgomery, J. Structure of an η1 Nickel O-Enolate: Mechanistic Implications in Catalytic Enyne Cyclizations. *Organometallics* **2001**, *20*, 370–372.

(48) Madhu, V.; Bolligarla, R.; Naik, I. K.; Mekala, R.; Das, S. K. A $\{Cu_4I_4\}$ Cluster Supported on a Metal-Dithiolato Complex Anion Causes its Conformational Change Leading to a Doubly-Bridged Curved Coordination Polymer and its Reactivity with a Diamine Resulting in the Emergence of a [M(diamine)(di. *Eur. J. Inorg. Chem.* **2016**, *2016*, 4257–4264.

(49) Balić Žunić, T.; Vicković, I.; IUCr. IVTON – a program for the calculation of geometrical aspects of crystal structures and some crystal chemical applications. *J. Appl. Crystallogr.* **1996**, *29*, 305–306.

(50) Garribba, E.; Micera, G. The Determination of the Geometry of Cu(II) Complexes: An EPR Spectroscopy Experiment. *J. Chem. Educ.* **2006**, *83*, 1229.

(51) Petasis, D. T.; Hendrich, M. P. Quantitative Interpretation of Multifrequency Multimode EPR Spectra of Metal Containing Proteins, Enzymes, and Biomimetic Complexes. 2015; pp 171–208.

(52) Mann, S. I.; Heinisch, T.; Weitz, A. C.; Hendrich, M. P.; Ward, T. R.; Borovik, A. S. Modular Artificial Cupredoxins. *J. Am. Chem. Soc.* **2016**, *138*, 9073–9076.

(53) Evans, D. F. 400. The determination of the paramagnetic susceptibility of substances in solution by nuclear magnetic resonance. *J. Chem. Soc.* **1959**, 2003–2005.

(54) Heintz, R. A.; Smith, J. A.; Szalay, P. S.; Weisgerber, A.; Dunbar, K. R. Homoleptic transition metal acetonitrile cations with tetrafluoroborate or trifluoromethanesulfonate anions. *Inorg. Synth.* **2002**, *33*, 75–83.

CHAPTER 5

Modular diiron complexes

Introduction

As mentioned in the previous chapter, bimetallic complexes are key targets for many synthetic inorganic groups due to their many attractive properties. For example, the presence of two metal centers in these systems can facilitate cooperative multielectron processes with earth abundant, first row transition metal ions.[1,2] In catalysis, bimetallic complexes can provide different reaction pathways, faster reaction rates, and greater selectivity than their monometallic counterparts.[3–5] In addition, it is possible to fine tune the physical properties of bimetallic complexes by independently modulating the two metal ions.[6]

Several ligand design approaches have been used to target bimetallic complexes. For instance, symmetrical dinucleating ligands have been designed to bind two metal centers in identical primary and secondary coordination spheres.[7–14] Often, such ligands are treated with a single metal ion to prepare symmetrical homobimetallic complexes, but some systems allow heterobimetallic complexes to be prepared *via* the stepwise addition of different metal ions.[15–17]

It is synthetically more challenging to synthesize systems capable of binding two metal centers in different primary and secondary coordination sphere environments, thus forming unsymmetrical bimetallic complexes. Some groups have designed “double-decker” ligands, which are dinucleating ligands with two different metal binding sites situated proximal to each other, and the close proximity of the metal centers often results in the formation of metal-metal bonds.[18–23] Another approach involves tethering two very different binding environments together to form unsymmetrical ligands, but this process often requires extensive ligand synthesis.[24–26]

The approach most relevant to the current work involves preparing unsymmetrical bimetallic complexes by combining two different monometallic complexes.[27–33] If one monometallic fragment contains a ligand capable of interacting with a second metal center, addition of a second monometallic fragment can result in the formation of unsymmetrical bimetallic complexes. Since the systematic substitution of starting complexes can allow for the preparation of families of related unsymmetrical bimetallic complexes, highly modular systems can be prepared with this method.

As mentioned in the last chapter, the Borovik group has used this approach to prepare a series of modular bimetallic compounds, using the tripodal ligand *N,N′,N″*-[2,2′,2″-nitrilotris(ethane-2,1-diyl)]tris(2,4,6-trimethylbenzenesulfonamido) ($[\mathrm{MST}]^{3-}$) as a scaffold.[34] The sulfonamido oxygen atoms are also able to interact with a second metal center, and can be used to prepare discretely bimetallic complexes of the formulation $[(\mathrm{L})\mathrm{M}^{\mathrm{II}}-(\mu\text{-OH})-\mathrm{M}^{\mathrm{III}}\mathrm{MST}]^{+}$ (Figure 5.1). Several different bimetallic complexes have be synthesized by this method, including certain combinations of M^{II} = $\mathrm{Ca}^{\mathrm{II}}$, $\mathrm{Sr}^{\mathrm{II}}$, $\mathrm{Ba}^{\mathrm{II}}$, $\mathrm{Mn}^{\mathrm{II}}$, $\mathrm{Fe}^{\mathrm{II}}$, $\mathrm{Co}^{\mathrm{II}}$, $\mathrm{Ni}^{\mathrm{II}}$, $\mathrm{Cu}^{\mathrm{II}}$, $\mathrm{Zn}^{\mathrm{II}}$ and $\mathrm{M}^{\mathrm{III}}$ = $\mathrm{Mn}^{\mathrm{III}}$, $\mathrm{Fe}^{\mathrm{III}}$, $\mathrm{Co}^{\mathrm{III}}$, $\mathrm{Ga}^{\mathrm{III}}$, $\mathrm{In}^{\mathrm{III}}$.[34–37]

The initial studies with these types of compounds involved the preparation of heterobimetallic complexes with redox inactive divalent metal ions (M^{II} = $\mathrm{Ca}^{\mathrm{II}}$, $\mathrm{Sr}^{\mathrm{II}}$, $\mathrm{Ba}^{\mathrm{II}}$) that were capped with crown ethers (L = 15-crown-5 or 18-crown-6) (Figure 5.1A).[36] Later, bimetallic complexes where both metal centers were transition metal ions were prepared using the nitrogen-based tridentate ligand 1,4,7-trimethyl-1,4,7-triazacyclononane (TMTACN) as the capping ligand (Figure 5.1B).[38,39] These compounds used ligands with relatively high denticity, resulting in the second divalent metal ion being coordinatively saturated. Therefore, a new series of bimetallic complexes were synthesized with low-denticity ligands bound to the second metal ion, most notably the bidentate ligand *N,N,N′,N′*-tetramethylethane-1,2-diamine (TMEDA). As discussed in the previous chapter, solid-state structures revealed that this series of complexes had the formulation [(TMEDA)M^{II}(OTf)–(μ-OH)–Fe^{III}MST] (M^{II} = Fe^{II}, Co^{II}, or Ni^{II}, denoted as [TMEDA-M^{II}(OTf)(OH)Fe^{III}]) (Figure 5.1C), in which a weakly binding trifluoromethanesulfonate (OTf^{-}) counter anion completes the primary coordination sphere of the M^{II} center. OTf^{-} ligands are known to weakly coordinate metal ions, prompting an investigation into the substitution chemistry of these complexes with other anions.

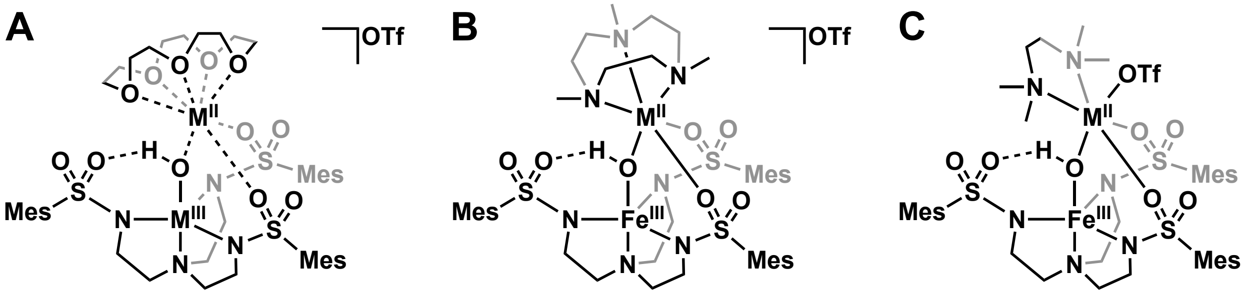

Figure 5.1. Specific examples of [MST]$^{3-}$ bimetallic complexes with (**A**) one transition metal ion (M^{III} = Mn^{III}, Fe^{III}) and one redox inactive metal ion (M^{II} = Ca^{II}, Sr^{II}, Ba^{II} (with 18-crown-6))[36] and (**B**) two transition metal ions where L = TMTACN, M^{III} = Fe^{III}, M^{II} = Mn^{II}, Fe^{II}, Co^{II}, Ni^{II}, Cu^{II}, or Zn^{II},[38,39] or (**C**) L = TMEDA, M^{III} = Fe^{III}, M^{II} = Fe^{II}, Co^{II}, or Ni^{II}.

In this chapter, the reactivity of the diiron complex [TMEDA-Fe^{II}(OTf)(OH)Fe^{III}] was investigated. The coordinating OTf^{-} ion is indeed substitutionally labile, demonstrated by the following preparation of two additional diiron compounds. Ligand substitution occurs if [TMEDA-Fe^{II}(OTf)(OH)Fe^{III}] is treated with the NMe$_4$X salts (X^{-} = NCS^{-} or N$_3$$^{-}$), as the metathesized product [TMEDA-Fe^{II}(X)(OH)Fe^{III}] is formed. [TMEDA-Fe^{II}(Br)(OH)Fe^{III}] can prepared if Fe^{II}Br$_2$ is used instead of Fe^{II}(OTf)$_2$·2MeCN in the initial synthesis.

These diiron compounds were characterized by X-ray diffraction methods, and the resulting structures show that the the different X^{-} ligands bind to the Fe^{II} centers in the solid-state. Though this series of complexes have similar optical spectra, they are differentiated using perpendicular mode X-band electronic paramagnetic (EPR) spectroscopy and Fourier transform infrared (FTIR) spectroscopy.

These results, along with those of the previous chapter, demonstrate the versatility of this system as both the M^{II} center and X^{-} ligand can be modulated. The substitution of the bidentate ligand on the second metal ion was also examined. Previous results showed that this system can accommodate different capping ligands, but direct substitutions of capping ligands were not attempted. Treatment of [TMEDA-Fe^{II}(OTf)(OH)Fe^{III}] with two equivalents of the less hindered bidentate ligand ethylenediamine (en) resulted in the formation of [(en)$_2$$Fe^{II}$−(μ-OH)−$Fe^{III}$MST]OTf (denoted as [(en)$_2$-Fe^{II}(OH)Fe^{III}]OTf). This new compound has a different primary coordination sphere around the Fe^{II} center when compared to either related TMEDA or TMTACN diiron analogue. Thus, three key components of the system can be modulated.

Results and Discussion

Preparation and characterization of [TMEDA-Fe^{II}(X)(OH)Fe^{III}] compounds

[TMEDA-Fe^{II}(OTf)(OH)Fe^{III}] was prepared by the preparative route described previously in Chapter 4 (Scheme 5.1). If $Fe^{II}Br_2$ was used instead of $Fe^{II}(OTf)_2\cdot 2MeCN$, [TMEDA-$Fe^{II}$(Br)(OH)$Fe^{III}$] was prepared. Crystals suitable for X-ray diffraction were obtained by layering a CH_2Cl_2 solution of [TMEDA-Fe^{II}(Br)(OH)Fe^{III}] under pentane, resulting in block crystals in yields ranging from 46–62 %. This result demonstrated that the diiron complexes could be prepared with different types of anionic ligands bound to the Fe^{II} center, hinting that other ligands could also bind at this sixth coordination site.

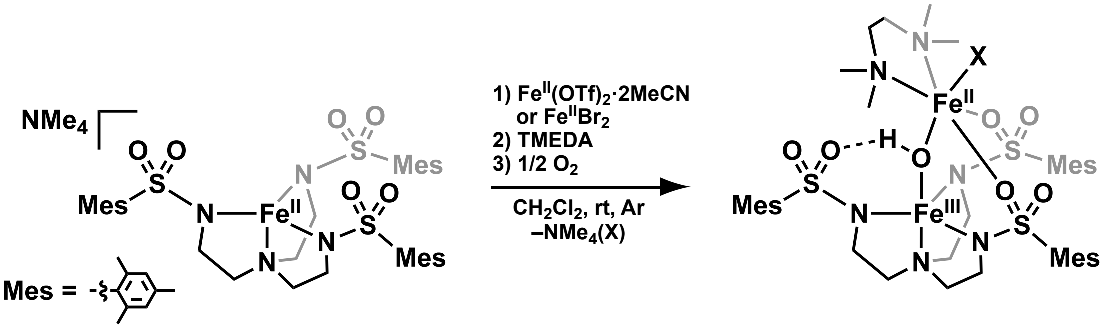

Scheme 5.1. Preparation of [TMEDA-Fe^{II}(X)(OH)Fe^{III}] complexes (X$^-$ = OTf$^-$, Br$^-$).

The lability of the coordinated OTf$^-$ ion was probed by conducting metathesis reactions with other anions. In these reactions, salts with SCN$^-$ or N$_3^-$ anions were used because these anions have distinct vibrational features. The availability of a spectroscopic handle allowed the success of these reactions to be quickly assessed by FTIR spectroscopy. Treating the bimetallic complex [TMEDA-Fe^{II}(OTf)(OH)Fe^{III}] with NMe$_4$(X) (X$^-$ = SCN$^-$, N$_3^-$) in THF resulted in the precipitation of solid NMe$_4$(OTf) from the dark orange solutions (Scheme 5.2). After filtration, the filtrates were dried under vacuum. The resulting orange powders were redissolved in CH$_2$Cl$_2$ and layered under pentane to afford block or needle-shaped crystals in yields ranging from 48–78%.

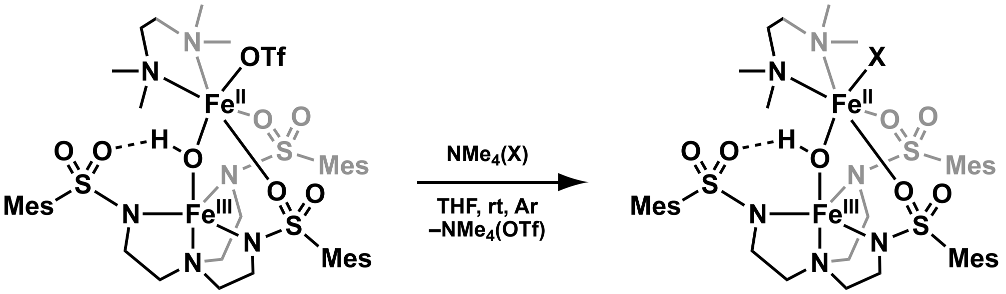

Scheme 5.2. Preparation of [TMEDA-Fe^{II}(X)(OH)Fe^{III}] complexes (X$^-$ = NCS$^-$, N$_3^-$) *via* metathesis with NMe$_4$(X) salts.

FTIR spectroscopy on these putative [TMEDA-Fe^{II}(X)(OH)Fe^{III}] products revealed characteristic bands for the NCS^{-} (2064 cm^{-1}) and N$_3^{-}$ (2069 cm $^{-1}$) ligands (Figure 5.2C). These bands were at higher energy than the analogous bands in NMe$_4$(SCN) (2058 cm $^{-1}$)[40] and NMe$_4$(N$_3$) (1998 cm^{-1}),[41] suggesting that that these anions are coordinated to the Fe^{II} center.[41] Additionally, the loss of bands at 1239, 1034, 635 cm $^{-1}$ suggest that OTf^{-} ligand is substituted in these reactions, as such bands are associated with the OTf^{-} ion.[42]

The four diiron compounds otherwise have similar vibrational properties. Each has a ν(OH) band observed around 3200–3300 cm^{-1} (Figure 5.2A), where the broadness of these bands suggest the presence of intramolecular H-bonding between the bridging hydroxido ligands and one of the sulfonamido oxygen atoms from [MST]$^{3-}$.[43,44]

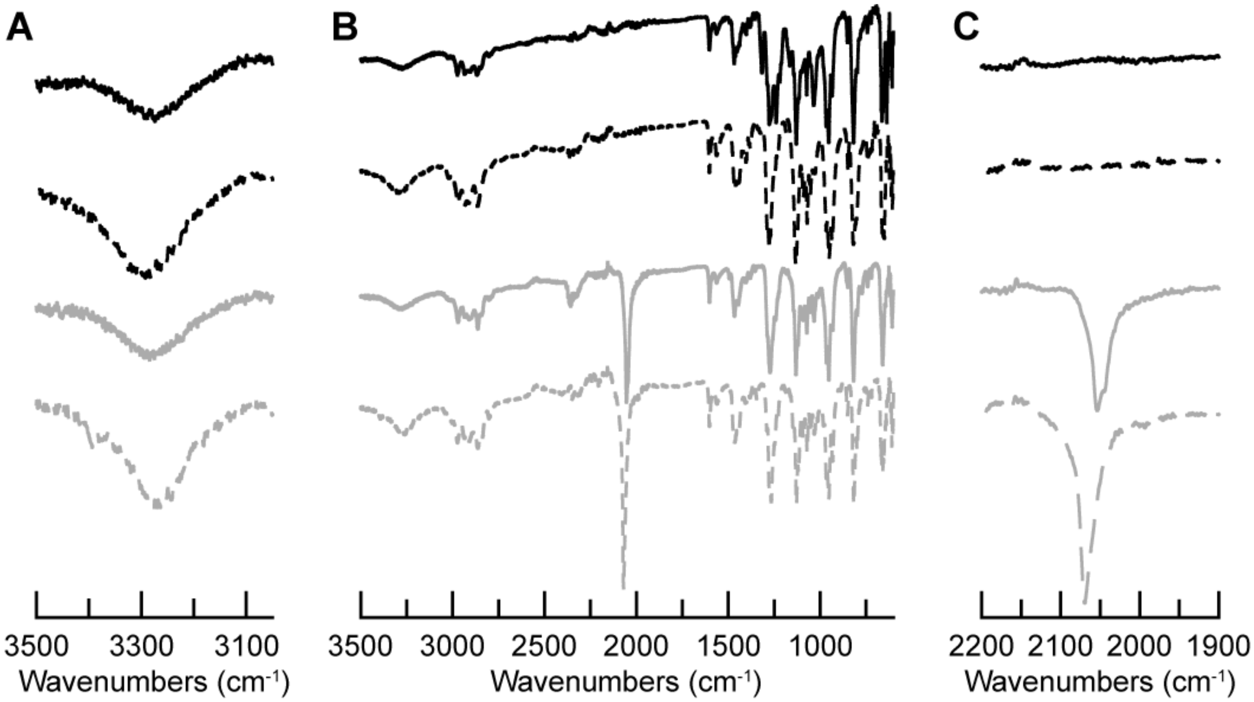

Figure 5.2. FTIR spectra of [TMEDA-Fe^{II}(OTf)(OH)Fe^{III}] (solid black), [TMEDA-Fe^{II}(Br)(OH)Fe^{III}] (dashed black), [TMEDA-Fe^{II}(NCS)(OH)Fe^{III}] (solid grey), and [TMEDA-Fe^{II}(OTf)(OH)Fe^{III}] (dashed grey), showing (**A**) the expanded region around ν(OH), (**B**) the full spectra, and (**C**) the region around ν(SCN) and ν(N$_3$). All spectra were collected by attenuated total reflectance (ATR).

The bimetallic formulation of the four crystalline [TMEDA-Fe^{II}(X)(OH)Fe^{III}] compounds was further supported by electrospray ionization mass spectrometry (ESI-MS), in which the m/z of the molecular ion and experimental isotope patterns matched those calculated for [TMEDA-Fe^{II}(OH)Fe^{III}]$^{+}$. Since these complexes only ionize as [TMEDA-Fe^{II}(OH)Fe^{III}]$^{+}$, the identity of the X^{-} ligand could not be determined by positive mode ESI-MS. The series of compounds all have similar optical properties, as each have a characteristic absorption band at λ_{max} = 380–392 nm (ε = 6100–7000 M^{-1}cm^{-1}) (Figure 5.3). These optical features are similar to the previously reported bands observed for the related [(TMTACN)M^{II}–(μ-OH)–Fe^{III}MST]$^{+}$ complexes (M^{II} = Mn^{II}, Fe^{II}, Co^{II}, Ni^{II}, Cu^{II}, or Zn^{II}, denoted as [TMTACN-M^{II}(OH)Fe^{III}]$^{+}$)(see Chapter 4).[38,39]

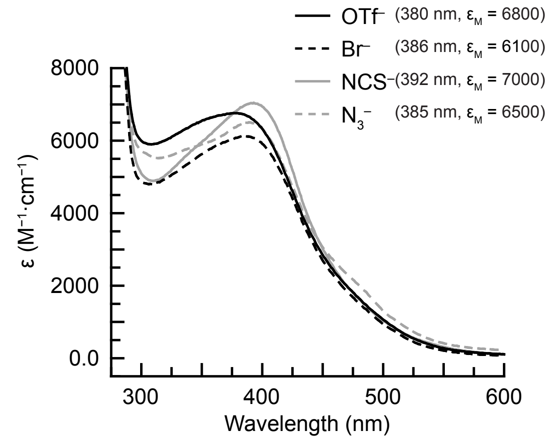

Figure 5.3. UV-visible (UV-vis) spectra for diiron compounds [TMEDA-Fe^{II}(X)(OH)Fe^{III}] with X^{-} ligand specified. All spectra were collected on 0.1 mM CH_2Cl_2 solutions at 25 ˚C.

Solid-state molecular structures of [TMEDA-Fe^{II}(X)(OH)Fe^{III}] compounds

The molecular structures of the [TMEDA-Fe^{II}(X)(OH)Fe^{III}] complexes were determined by X-ray diffraction methods and revealed the expected bimetallic structures (Figure 5.4). Selected metrical parameters and calculated values are shown in Table 4.1.

The five-coordinate Fe^{III} centers contain a N_4O primary coordination sphere formed by the [MST]$^{3-}$ ligand and bridging hydroxido ligand, and adopts a distorted trigonal bipyramidal (tbp) geometry based on the structural parameter τ_5 = 0.854–0.914 (see Chapter 4).[45] The six-coordinate Fe^{II} centers have a N_3O_2Y (Y = O (OTf^-), Br (Br^-), N (NCS^- and N_3^-)) primary coordination sphere that adopt a distorted octahedral coordination geometry based on the octahedral quadratic elongation parameter λ_{oct} = 1.012–1.036 (see Chapter 4).[46] The equatorial plane is formed by the SO_2Mes groups of $[MST]^{3-}$ and the TMEDA ligand, while the bridging hydroxido ligand and the X^- ligand are *trans* to each other (175.38(5)–173.49(5)°) and occupy the axial positions.

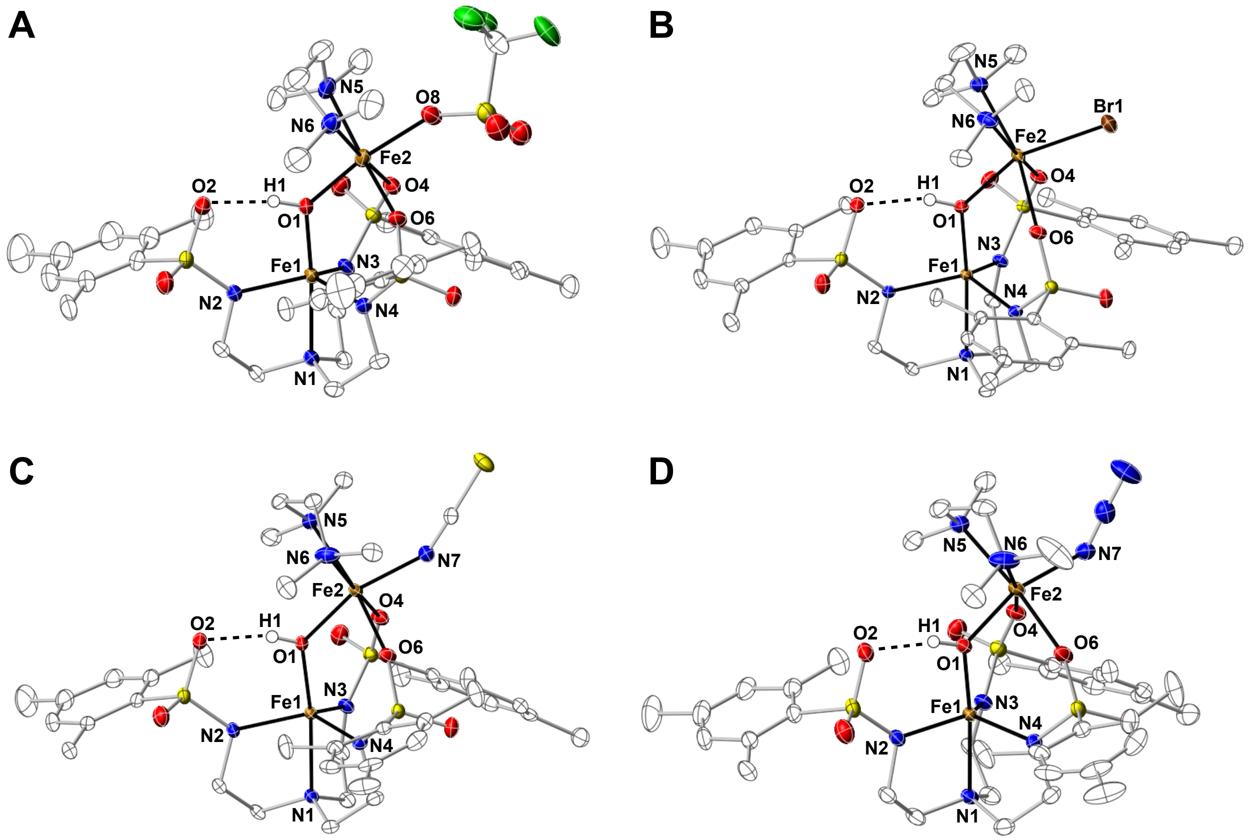

Figure 5.4. Thermal ellipsoid diagrams depicting the molecular structures of (**A**) [TMEDA-Fe^{II}(OTf)(OH)Fe^{III}], (**B**) [TMEDA-Fe^{II}(Br)(OH)Fe^{III}], (**C**) [TMEDA-Fe^{II}(NCS)(OH)Fe^{III}], and (**D**) [TMEDA-Fe^{II}(N_3)(OH)Fe^{III}]. Ellipsoids are drawn at the 50% probability level, and only the hydroxido H atoms are shown for clarity.

The Fe1–Y distances reflect the different bound atoms of the various counter anions. The longest bond is from Fe1–Br1, which is expected as the bromide ion has the largest ionic radius of the different binding atoms of the anionic ligands.[47] This long bond distance causes the greatest octahedral distortion of this series of compounds. The Fe1–Y bond distances for the NCS$^-$ and N$_3^-$ compounds are similar, suggesting that the thiocyanate ligand is not bound through the S-atom, but rather through the N-atom.

Table 5.1. Selected metrical parameters for [TMEDA-Fe^{II}(X)(OH)Fe^{III}] (X$^-$ = OTf$^-$, Br$^-$, NCS$^-$, N$_3^-$) complexes.

[TMEDA-Fe^{II}(X)(OH)Fe^{III}]	X$^-$ (Y) =			
	OTf$^-$ (O8)	Br$^-$ (Br1)	NCS$^-$ (N7)	N$_3^-$ (N7)
Bond distances (Å)				
Fe1–N1	2.227(2)	2.251(1)	2.220(1)	2.232(2)
Fe1–N2	2.031(2)	2.043(1)	2.032(1)	2.030(2)
Fe1–N3	2.001(2)	1.997(1)	1.997(1)	2.017(2)
Fe1–N4	2.005(2)	2.003(1)	2.016(1)	1.994(2)
Fe1–O1	1.855(2)	1.888(1)	1.886(1)	1.887(2)
O1···O2	2.659	2.658	2.611	2.617
Fe2–O1	1.928(2)	1.983(1)	1.962(1)	1.983(2)
Fe2–O4	2.207(2)	2.276(1)	2.402(1)	2.293(2)
Fe2–O6	2.147(2)	2.499(1)	2.283(1)	2.404(2)
Fe2–N5	2.211(2)	2.263(2)	2.277(2)	2.236(2)
Fe2–N6	2.231(2)	2.238(2)	2.236(2)	2.262(2)
Fe2–Y	2.086(2)	2.479(3)	2.040(2)	2.058(2)
Fe1···Fe2	3.337	3.482	3.458	3.482
Avg. Fe1–N$_{eq\text{-}MST}$	2.012(2)	2.014(1)	2.015(1)	2.013(2)
Avg. Fe2–N$_{TMEDA}$	2.221(2)	2.251(2)	2.257(2)	2.249(2)
d[Fe1–N$_{eq\text{-}MST}$]^{a}	0.357	0.387	0.363	0.371
Bond angles (˚)				
O1–Fe1–N1	175.20(8)	175.38(5)	173.49(5)	174.72(7)
N2–Fe1–N3	121.10(9)	117.31(6)	117.74(6)	121.29(8)
N2–Fe1–N4	121.72(9)	120.49(6)	122.27(6)	117.55(7)
N3–Fe1–N4	107.86(8)	111.35(6)	110.40(6)	111.18(8)
Fe1–O1–Fe2	126.40(9)	128.09(7)	127.94(7)	128.24(8)
O1–Fe2–Y	171.04(8)	157.19(4)	160.78(6)	158.44(7)
O4–Fe2–O6	96.13(7)	108.73(4)	103.07(4)	104.32(6)
N5–Fe2–N6	82.76(9)	81.53(6)	81.48(6)	81.31(8)
Calculated values				
τ_5^{b}	0.891	0.914	0.854	0.891
V_{oct}^{c}	12.8	15.3	13.7	13.7
λ_{oct}^{d}	1.012	1.036	1.029	1.034

[a] distance of Fe1 from the plane formed by the equatorial nitrogen atoms N2, N3, and N4

[b] trigonality parameter, $\tau_5 = (\beta - a)/60$. β is the largest bond angle observed, and α is the second largest bond angle.[45]
[c] octahedral volume, calculated using the IVTON program.[48]
[d] mean oct quadratic elongation, $\lambda_{oct} = \Sigma_1^6 (l_i/l_0)^2/6$. $\lambda_{oct} = 1$ for an ideal octahedron. l_0 represents the center-to-vertex distance of an octahedron with O_h symmetry whose volume is equal to that of the distorted octahedron with distances l_i. λ'_{oct} is the oct quadratic elongation toward one axis.[46]

The distances between the O1···O6 atoms, ranging from 2.611–2.659 Å, are suggestive of intramolecular H-bonds formed between the hydrogen atom of the bridging hydroxido ligand and a sulfonamido oxygen atom of the $[MST]^{3-}$ ligand.[49] These distances are shorter than the reported distances for the related heterobimetallic complexes $[L\supset M^{II}–(\mu\text{-OH})–M^{III}MST]^+$ ($L\supset M^{II}$ = 15-crown-5$\supset$Ca^{II}, 15-crown-5$\supset$Sr^{II}, or 18-crown-6$\supset$Ba^{II}, M^{III} = Mn^{III} or Fe^{III}), which have O1···O6 distances ranging from 2.685–2.700 Å.[36] These distances suggest that the H-bonding is stronger in the diiron complexes. The Fe^{II} ion has a smaller ionic radius than any of the redox inactive metal ions and should therefore be the best Lewis acid. Thus, the diiron complexes should have weaker O–H bonds in the bridging hydroxido ligands then those complexes with alkaline earth metals, which explains the difference in H-bonding strength.

Electrochemical properties of [TMEDA-Fe^{II}(X)(OH)Fe^{III}] compounds

The electrochemical properties of the series of bimetallic complexes were probed using cyclic voltammetry (CV) (Table 5.2). All the diiron compounds exhibited a one-electron reductive event that was assigned to the Fe^{II}Fe^{III}/Fe^{II}Fe^{II} couple (Figure 5.5). In general, the redox potentials of the [TMEDA-Fe^{II}(X)(OH)Fe^{III}] compounds were similar to that of [TMTACN-Fe^{II}(OH)Fe^{III}]OTf, which has a Fe^{II}Fe^{III}/Fe^{II}Fe^{II} couple at –0.86 V versus the ferrocenium/ferrocene ($[FeCp_2]^{+/0}$) couple.[38] The voltammograms for the compounds with OTf$^-$, Br$^-$, and NCS$^-$ were quasi-reversible, with Fe^{II}Fe^{II}/Fe^{II}Fe^{III} redox potentials ranging from –0.84 to –0.89 V versus $[FeCp_2]^{+/0}$, but the voltammogram of the N_3^- compound was irreversible with an E_C = –0.99 V versus $[FeCp_2]^{+/0}$. The compounds with NCS^- and N_3^- were slightly cathodically shifted compare to those with OTf^- and Br^-.

Table 5.2. Electrochemical data for the [TMEDA-Fe^{II}(X)(OH)Fe^{III}] compounds in MeCN.

X^- =	$E_{1/2}$($Fe^{II}Fe^{III}/Fe^{II}Fe^{II}$, V versus $[FeCp_2]^{+/0}$)	E_A($Fe^{II}Fe^{III}/Fe^{III}Fe^{III}$, V versus $[FeCp_2]^{+/0}$)
OTf^-	–0.84	0.82
Br^-	–0.84	0.84
NCS^-	–0.89	0.98
N_3^-	–0.99*	0.84

*E_C, not $E_{1/2}$

An irreversible oxidative feature was also observable for the four diiron compounds, assigned to the $Fe^{II}Fe^{III}/Fe^{III}Fe^{III}$ couple. They occur at similar potentials, except for that of the NCS^- complex which is anodically shifted. These potentials are all anodically shifted relative to that of [TMTACN-Fe^{II}(OH)Fe^{III}]OTf (0.35 V versus $[FeCp_2]^{+/0}$.[38]

These results reinforce the hypothesis from Chapter 4 that the X^- ligands do not remain bound in solution. Since the reduction potentials are all very similar, the overall charge of the two series of complexes should be the same, suggesting that [TMEDA-M^{II}(OH)Fe^{III}]$^+$ is the dominant species in these experiments. The anodic shift in the oxidation potentials of the TMEDA complexes relative to that of the TMTACN complex is also explained by this hypothesis. Formally neutral [TMEDA-Fe^{II}(OTf)(OH)Fe^{III}] complexes should easier to oxidize than the positively charged [TMTACN-Fe^{II}(OH)Fe^{III}]$^+$ complex, resulting in cathodically shifted oxidation potentials. However, the opposite effect is observed. Furthermore, the five-coordinate Fe^{II} centers of putative [TMEDA-Fe^{II}(OH)Fe^{III}]$^+$ complexes should have less electron density than the six-coordinate Fe^{II} center of [TMTACN-Fe^{II}(OH)Fe^{III}]$^+$. Therefore, the [TMEDA-Fe^{II}(OH)Fe^{III}]$^+$ complexes should be harder to oxidize than [TMTACN-Fe^{II}(OH)Fe^{III}]$^+$, explaining the observed anodic shift.

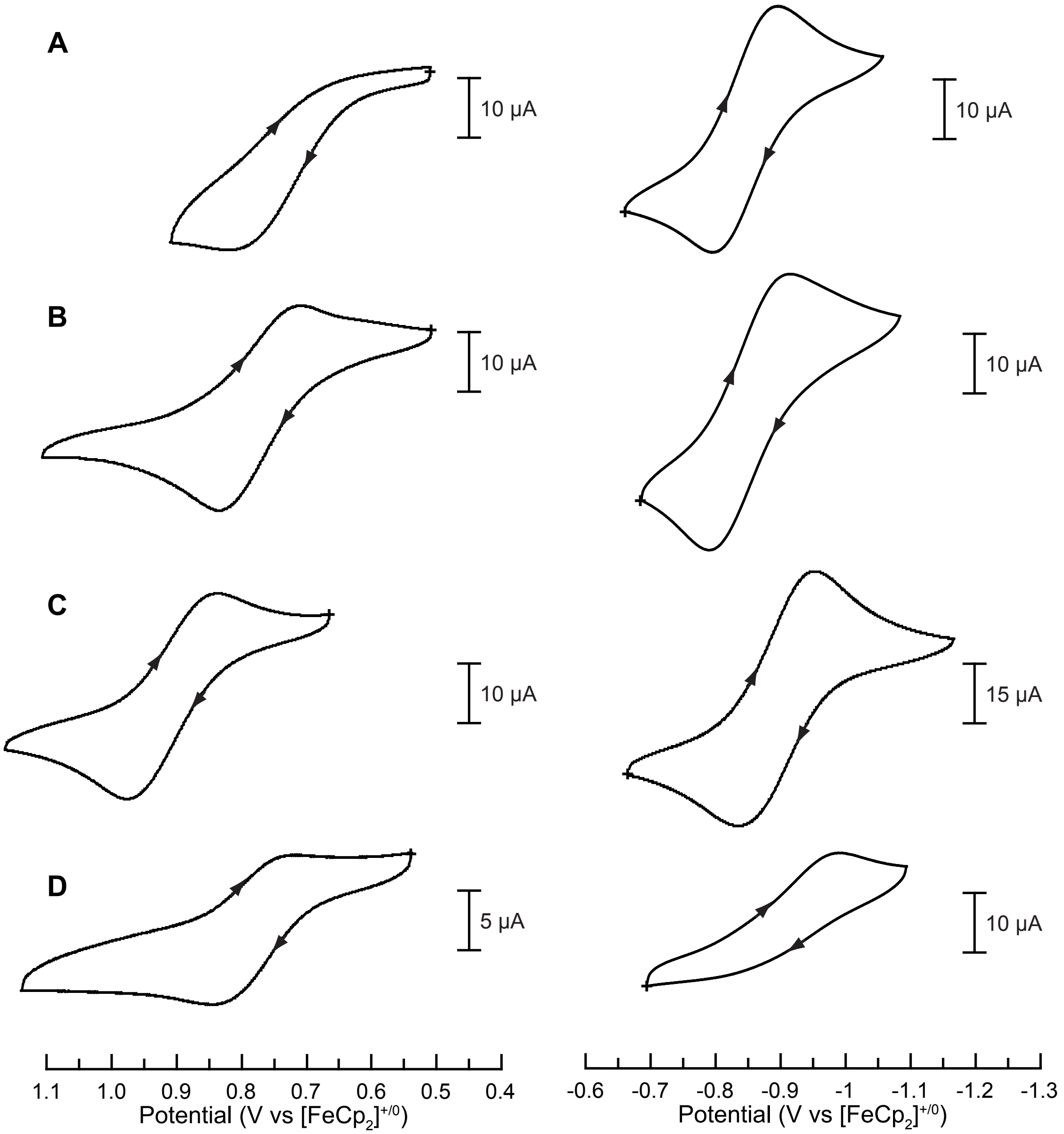

Figure 5.5. Cyclic voltammograms of (**A**) [TMEDA-Fe^{II}(OTf)(OH)Fe^{III}], (**B**) [TMEDA-Fe^{II}(Br)(OH)Fe^{III}], (**C**) [TMEDA-Fe^{II}(NCS)(OH)Fe^{III}], and (**D**) [TMEDA-Fe^{II}(N$_3$)(OH)Fe^{III}]. The cyclic voltammograms were collected at 100 mV s^{-1} in the presence of [FeCp$_2$].

EPR spectra of [TMEDA-Fe^{II}(X)(OH)Fe^{III}] compounds

The magnetic properties of the [TMEDA-Fe^{II}(X)(OH)Fe^{III}] complexes were probed using X-band EPR spectroscopy. Previous studies with both the TMEDA and TMTACN series of complexes revealed that antiferromagnetic coupling was observed between the two metal centers, both of which were found in the high-spin state.[38,39] The series of [TMEDA-Fe^{II}(X)(OH)Fe^{III}] complexes likewise exhibited this type of coupling, as rhombic perpendicular-mode EPR spectra centered around g = 2 were observed for the four compounds (Figure 5.6). These signals were consistent with an S = 1/2 spin- state resulting antiferromagnetic coupling between the high-spin Fe^{III} center (S = 5/2) and Fe^{II} center (S = 2). The line shapes of these signals were all different from each other, and also different from that of $[TMTACN\text{-}Fe^{II}(OH)Fe^{III}]^+$ (see Chapter 4). As the line shape of EPR spectroscopy is sensitive to geometric changes around metal centers, this result could suggest that the anionic sixth ligands remained bound to the complexes in solution, although this notion is disputed by the conclusions drawn by the previous discussions of CV results.[50–52]

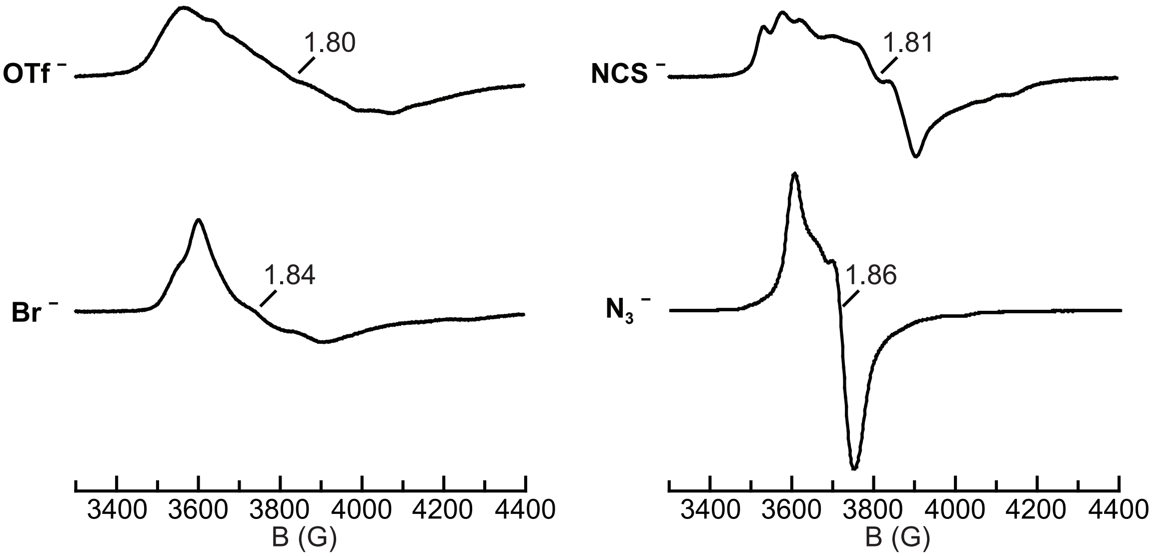

Figure 5.6. Perpendicular-mode EPR spectra for $[TMEDA\text{-}Fe^{II}(X)(OH)Fe^{III}]$ with the X^- ligand specified in the figure, all collected at 10 K in CH_2Cl_2.

Preparation and characterization of $[(en)_2\text{-}Fe^{II}(OH)Fe^{III}]OTf$

Considering the ability of the $[TMEDA\text{-}M^{II}(X)(OH)Fe^{III}]$ system to accommodate different M^{II} centers and X^- ligands, the ability to modulate the capping ligand was explored. Preparation of complexes with other bidentate capping ligands were attempted, by using different bidentate ligands besides TMEDA in Scheme 5.1. Though en, symmetric *N,N′*-dimethylethylenediamine, unsymmetric *N,N*-dimethylethylenediamine, and 2,2'-bipyridine were all attempted, only en produced a well-defined bimetallic product.

A CH_2Cl_2 solution of en, $NMe_4[Fe^{II}MST]$, and $Fe^{II}(OTf)_2 \cdot 2MeCN$ was treated with 0.5 equivalents of O_2 for 1 h. After workup, needle crystals suitable for X-ray diffraction were obtained by layering a THF solution of the product under pentane. The solid-state structure revealed a discretely bimetallic product, though this structure differed significantly from any previous bimetallic compound prepared with $[MST]^{3-}$. The compound maintained a $Fe^{II}(OH)Fe^{III}$ bimetallic core, but instead of a single capping ligand, two en ligands were bound to the Fe^{II} center, resulting in a salt with the formulation $[(en)_2\text{-}Fe^{II}(OH)Fe^{III}]OTf$ (Figure 5.7).

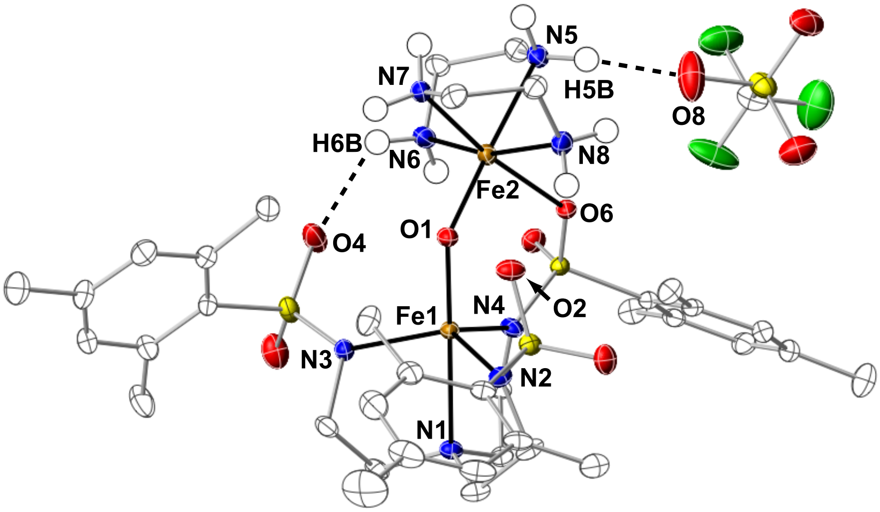

Figure 5.7. Thermal ellipsoid diagram depicting the molecular structure of $[(en)_2\text{-}Fe^{II}(OH)Fe^{III}]OTf$. Ellipsoids are drawn at the 50% probability level, and only the en H-atoms are shown for clarity.

Selected metrical parameters and calculated values are shown in Table 5.3. The N_4O_2 primary coordination sphere of the Fe^{II} center is composed of four N-donors from the two en ligands, one O-donor from the bridging hydroxido ligand, and one O-donor from a sulfonamido arm of $[MST]^{3-}$. The primary coordination sphere of the Fe^{II} center in $[(en)_2\text{-}Fe^{II}(OH)Fe^{III}]OTf$ is thus different from those of all other examples of bimetallic compounds with $[MST]^{3-}$, which have two

O-atoms from the sulfonamido moieties bound. The remaining two sulfonamido arms in [(en)$_2$-Fe^{II}(OH)Fe^{III}]OTf form intramolecular H-bonds with either the bridging hydroxido ligand (O1···O2 = 2.936 Å) or an NH group of one of the en ligands (N6···O4 = 2.831 Å).[49] Additionally, a third intermolecular H-bond is observed between the one of the en ligands and the OTf^{-} counter anion (N5···O8 = 2.971 Å). The introduction of the en ligands thus creates a more complicated H-bonding network in [(en)$_2$-Fe^{II}(OH)Fe^{III}]OTf than in the other related bimetallic compounds.

Table 5.3. Selected metrical parameters for [(en)$_2$-Fe^{II}(OH)Fe^{III}]OTf.

[(en)$_2$-Fe^{II}(OH)Fe^{III}]OTf			
Bond distances (Å)		*Bond angles (˚)*	
Fe1–N1	2.329(2)	O1–Fe1–N1	177.20(8)
Fe1–N2	2.024(2)	N2–Fe1–N3	118.35(9)
Fe1–N3	2.018(2)	N2–Fe1–N4	112.30(9)
Fe1–N4	2.038(2)	N3–Fe1–N4	116.84(9)
Fe1–O1	1.792(2)	Fe1–O1–Fe2	138.40(1)
O1···O2	2.936	O1–Fe2–O6	92.32(9)
Fe2–O1	1.806(2)	N5–Fe2–N6	78.09(8)
Fe2···O4	3.791	N7–Fe2–N8	81.62(9)
Fe2–O6	2.111(2)		
Fe2–N5	2.236(2)	*Calculated values*	
Fe2–N6	2.166(2)	τ_5[b]	0.981
Fe2–N7	2.165(2)	V_{oct}[c]	12.3
Fe2–N8	2.152(2)	λ_{oct}[d]	1.013
Fe1···Fe2	3.363		
Avg. Fe1–N$_{eq\text{-}MST}$	2.027(2)		
Avg. Fe2–N$_{en}$	2.180(2)		
d[Fe1–N$_{eq\text{-}MST}$][a]	0.419		

Revising the stoichiometry of the preparation of [(en)$_2$-Fe^{II}(OH)Fe^{III}]OTf allowed this product to be formed in crystalline yields of 63–87%. It could also be prepared by treating [TMEDA-Fe^{II}(OTf)(OH)Fe^{III}] with two equivalents of en (Scheme 5.3), a process that was monitored by UV-vis spectroscopy (Figure 5.8A). The final trace of this process was identical to the UV-vis spectrum of the independently prepared [(en)$_2$-Fe^{II}(OH)Fe^{III}]OTf.

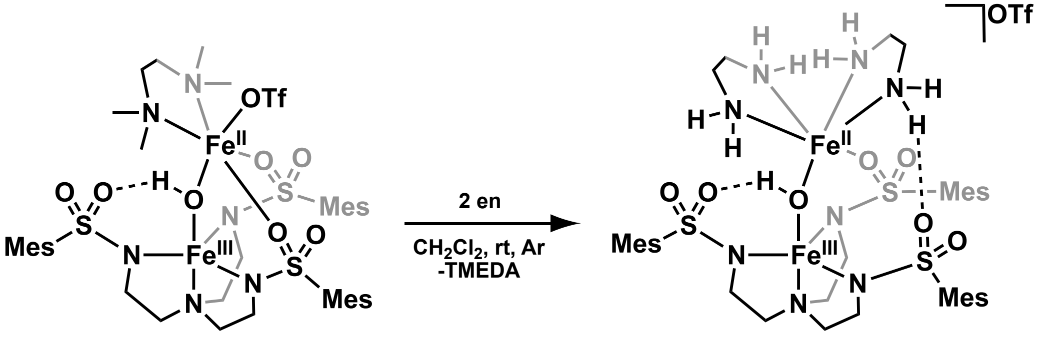

Scheme 5.3. Preparation of $[(en)_2\text{-Fe}^{II}(OH)Fe^{III}]OTf$ from $[TMEDA\text{-Fe}^{II}(OTf)(OH)Fe^{III}]$.

The other physical properties of $[(en)_2\text{-Fe}^{II}(OH)Fe^{III}]OTf$ were similar to that of the related $[TMEDA\text{-Fe}^{II}(X)(OH)Fe^{III}]$ compounds. New vibrational bands that were close in energy to the NH vibrations of free en were observed in the FTIR spectrum of $[(en)_2\text{-Fe}^{II}(OH)Fe^{III}]OTf$, consistent with its formulation (Figure 5.8B). The rest of the spectrum was similar to those of $[TMEDA\text{-Fe}^{II}(X)(OH)Fe^{III}]$. As with the $[TMEDA\text{-Fe}^{II}(X)(OH)Fe^{III}]$ complexes, perpendicular-mode EPR spectroscopy on $[(en)_2\text{-Fe}^{II}(OH)Fe^{III}]OTf$ revealed an $S = 1/2$ signal that had a line shape that was different than any of the other diiron compounds (Figure 5.9). CV studies revealed an irreversible one-electron reductive event at –1.1 V versus $[FeCp_2]^{+/0}$ that was assigned to the $Fe^{II}Fe^{II}/Fe^{II}Fe^{III}$ couple, as well as an irreversible one-electron oxidative event at 0.82 V versus $[FeCp_2]^{+/0}$ (Figure 5.10). Finally, the experimental isotope patterns of the ESI-MS spectrum was one mass unit less than those calculated for $[(en)_2\text{-Fe}^{II}(OH)Fe^{III}]^+$, which could be attributed to a putative $[(en)_2\text{-Fe}^{III}(O)Fe^{III}]^+$ species.

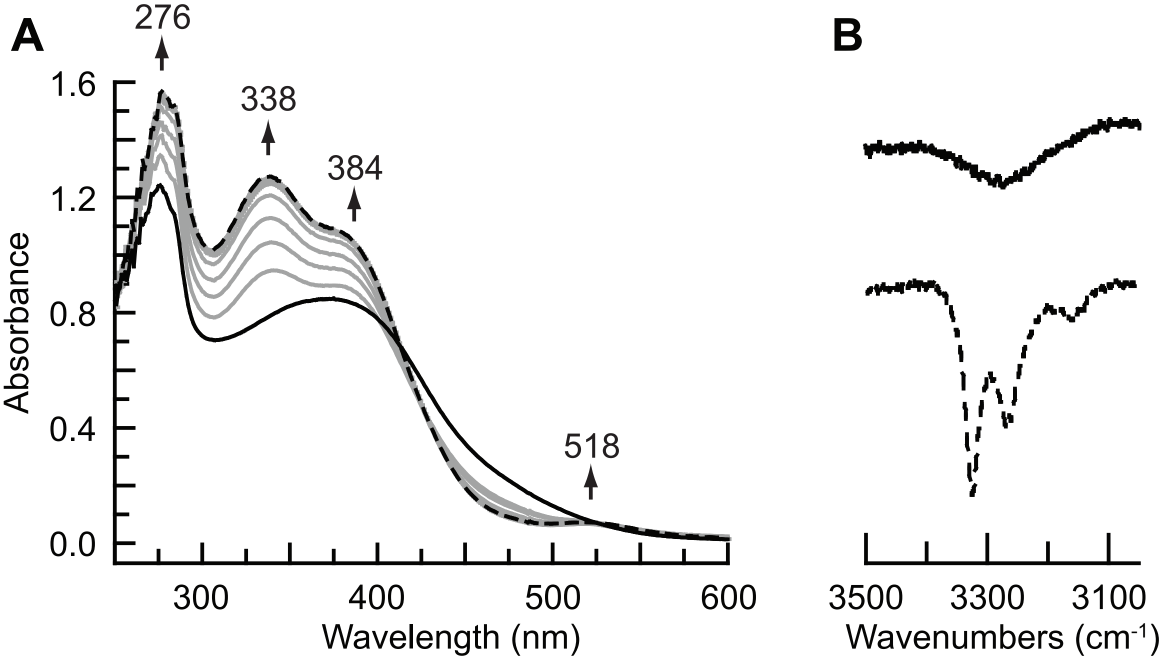

Figure 5.8. (**A**) UV-vis spectra for the substitution of TMEDA for en in a 0.1 mM CH_2Cl_2 solution of [TMEDA-$Fe^{II}(OTf)(OH)Fe^{III}$] at 25 °C, showing the conversion of [TMEDA-$Fe^{II}(OTf)(OH)Fe^{III}$] (solid black) to $[(en)_2$-$Fe^{II}(OH)Fe^{III}]OTf$ (dashed black) after 42 min. (**B**) FTIR spectra of [TMEDA-$Fe^{II}(OTf)(OH)Fe^{III}$] (solid black) and $[(en)_2$-$Fe^{II}(OH)Fe^{III}]OTf$ (solid black), showing the expanded region around ν(OH) collected by ATR.

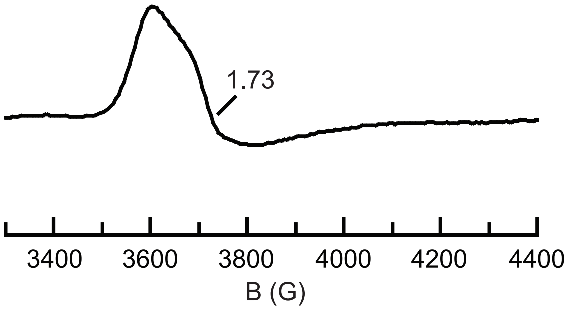

Figure 5.9. Perpendicular-mode EPR spectrum of $[(en)_2$-$Fe^{II}(OH)Fe^{III}]OTf$ collected at 10 K in CH_2Cl_2.

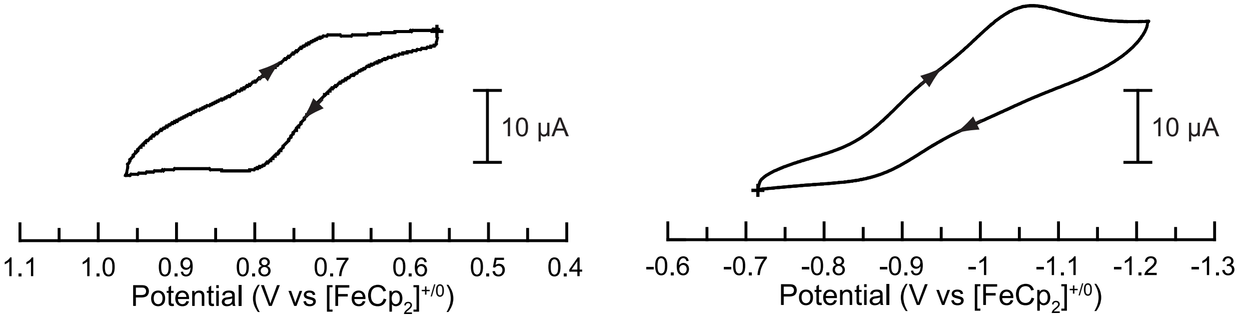

Figure 5.10. Cyclic voltammograms of $[(en)_2$-$Fe^{II}(OH)Fe^{III}]OTf$. The cyclic voltammograms were collected at 100 mV s^{-1} in the presence of $[FeCp_2]$.

Summary and Conclusions

This chapter has described the substitution chemistry of the bimetallic complex [TMEDA-Fe^{II}(OTf)(OH)Fe^{III}], which can be used as a synthon to modulate many key components. [TMEDA-Fe^{II}(OTf)(OH)Fe^{III}] contains a OTf^{-} ligand that is substitutionally labile. This feature was used to prepare two new diiron complexes, [TMEDA-Fe^{II}(X)(OH)Fe^{III}] (X^{-} = NCS^{-} or N_3^{-}). Additionally, modifying the initial preparation of [TMEDA-Fe^{II}(OTf)(OH)Fe^{III}] with $Fe^{II}Br_2$ allowed for the preparation of [TMEDA-Fe^{II}(Br)(OH)Fe^{III}]. The four diiron compounds all have S = 1/2 perpendicular-mode EPR signals, though the line shapes are different. This may suggest that the X^{-} ligand remain bound in solution, but this conclusion is disputed by electrochemical data. The other physical properties of the series of compounds are similar.

In addition to altering the X^{-} ligand, modification of the capping ligand was also attempted. The related compound [$(en)_2$-Fe^{II}(OH)Fe^{III}]OTf was prepared by treating [TMEDA-Fe^{II}(OTf)(OH)Fe^{III}] with 2 equivalents of en. The solid-state structure of this complex revealed that two en ligands are bound to the Fe^{II} center, in contrast to the single capping ligand observed for all other bimetallic complexes prepared with $[MST]^{3-}$. The primary and secondary coordination spheres of [$(en)_2$-Fe^{II}(OH)Fe^{III}]OTf are different from the related diiron compound with TMEDA, as one sulfonamido ligand arm no longer binds to the Fe^{II} center. Instead, it is involved in H-bonding with one NH groups of the en ligands. This result stresses the importance of the identity of the capping ligand in these types of compounds, and emphasizes the high degree of flexibility observed in this bimetallic system.

Experimental

General Methods

All reagents were purchased from commercial sources and used as received, unless otherwise noted. Solvents were sparged with argon and dried over columns containing Q-5 and molecular sieves. Potassium hydride (KH) as a dispersion in mineral oil was filtered with a medium porosity glass-fritted funnel and washed 5 times each with pentane and diethyl ether (Et_2O). Solid KH was dried under vacuum and stored under inert atmosphere. The synthesis of the ligand was carried out in the air and the preparations of the metal complexes were conducted in a Vacuum Atmospheres, Co. drybox under an argon atmosphere. Dioxygen was dried on a Drierite gas purifier purchased from Fischer Scientific. TMEDA and en were distilled over CaO and KOH under static vacuum at 30 °C onto 4 Å molecular sieves and stored under inert atmosphere. $Fe^{II}(OTf)_2 \cdot 2MeCN$,[53] $NMe_4[Fe^{II}MST]$,[36] $NMe_4(SCN)$,[40] and $NMe_4(N_3)$[41] were synthesized according to previous reports.

Preparation of Complexes

[TMEDA-Fe^{II}(OTf)(OH)Fe^{III}]. This complex was prepared using literature procedures for the related salt [TMTACN-$Fe^{II}(OH)Fe^{III}$]OTf [38] using $Fe^{II}(OTf)_2 \cdot 2MeCN$ (46.1 mg, 106 mmol), TMEDA (13.2 mg, 114 mmol), and $NMe_4[Fe^{II}MST]$ (86.6 mg, 106 mmol) to produce the desired complex in crystalline yields of 62–87%. Dark orange needle crystals of [TMEDA-$Fe^{II}(OTf)(OH)Fe^{III}$] suitable for X-ray diffraction were grown from a THF solution layered under pentane. Elemental analysis calcd. for [TMEDA-$Fe^{II}(OTf)Fe^{III}$]$\cdot 0.5CH_2Cl_2$, $C_{40.5}H_{63}ClF_3Fe_2N_6O_{10}S_4$: C, 43.19; H, 5.64; N, 7.46%, found: C, 42.89; H, 5.34; N, 7.34%. UV-vis (CH_2Cl_2, λ_{max}, nm (ε_{max}, $M^{-1}cm^{-1}$)) 274(sh), 283(sh),

380(6800). FTIR (ATR, cm^{-1}, selected bands): 3272(OH), 2980, 2935, 2869, 1603, 1564, 1467, 1313, 1276, 1239, 1129, 1034, 953, 816, 662, 635, 609. (Nujol, cm^{-1}): 3260(OH). Exact mass calcd for [TMEDA-Fe^{II}(OH)Fe^{III}]$^+$, $C_{39}H_{62}Fe_2N_6O_7S_3$: 934.3 found: 934.2. $E_{1/2}$ (MeCN, V versus [FeCp$_2$]$^{+/0}$): –0.84. E_A (MeCN, V versus [FeCp$_2$]$^{+/0}$): 0.82.

[TMEDA-Fe^{II}(Br)(OH)Fe^{III}]. This complex was prepared using the method described above for [TMEDA-Fe^{II}(OTf)(OH)Fe^{III}] using Fe^{II}Br$_2$ (20.5 mg, 0.0951 mmol), TMEDA (10.5 mg, 0.0902 mmol), and NMe$_4$[Fe^{II}MST] (73.2 mg, 0.0893 mmol) to produce the desired complex in crystalline yields of 46–62%. Dark orange block crystals of [TMEDA-Fe^{II}(Br)(OH)Fe^{III}] suitable for X-ray diffraction were grown from a CH_2Cl_2 solution layered under pentane. Elemental analysis calcd. for [TMEDA-Fe^{II}(Br)(OH)Fe^{III}]·0.5CH_2Cl_2, $C_{39.5}H_{63}ClBrFe_2N_6O_7S_3$: C, 44.63; H, 5.81; N, 7.97%, found: C, 44.88; H, 6.01; N, 7.95%. UV-vis (CH_2Cl_2, λ_{max}, nm (ε_{max}, M^{-1}cm^{-1})) 276(sh), 284(sh), 386(6100). FTIR (ATR, cm^{-1}, selected bands): 3286(OH), 2981, 2933, 2893, 2865, 1602, 1562, 1464, 1277, 1126, 1071, 953, 935, 818, 660. (Nujol, cm^{-1}): 3288(OH). Exact mass calcd for [TMEDA-Fe^{II}(OH)Fe^{III}]$^+$, $C_{39}H_{62}Fe_2N_6O_7S_3$: 934.3 found: 934.1. $E_{1/2}$ (MeCN, V versus [FeCp$_2$]$^{+/0}$): –0.85. E_A (MeCN, V versus [FeCp$_2$]$^{+/0}$): 0.84.

[TMEDA-Fe^{II}(NCS)(OH)Fe^{III}]. A solution of [TMEDA-Fe^{II}(OTf)(OH)Fe^{III}] (88.0 mg, 0.0812 mmol) in THF (10 mL) was treated with NMe$_4$(SCN) (10.9 mg, 0.0824 mmol) and stirred for 1 h. The solvent was removed under vacuum, then the resulting solid was redissolved in CH_2Cl_2 then filtered through a medium porosity glass-fritted funnel to remove the insoluble NMe$_4$(OTf). The filtrate was layered under pentane, and dark orange block crystals suitable for X-ray diffraction were

obtained. The crystals were collected on a medium porosity glass-fritted funnel and dried under vacuum, resulting in crystalline yields of 58–78%. Elemental analysis calcd. for [TMEDA-Fe^{II}(NCS)(OH)Fe^{III}]·CH_2Cl_2, $C_{41}H_{64}Cl_2Fe_2N_7O_7S_4$: C, 45.69; H, 5.99; N, 9.10%, found: C, 45.45; H, 6.04; N, 9.01%. UV-vis (CH_2Cl_2, λ_{max}, nm (ε_{max}, $M^{-1}cm^{-1}$)) 275(sh), 285(sh), 392(7000). FTIR (ATR, cm^{-1}, selected bands): 3278(OH), 2978, 2912, 2886, 2860, 2056(CN), 1603, 1564, 1470, 1456, 1350, 1259, 1102, 962, 817, 657, 638. (Nujol, cm^{-1}): 3271(OH), 2064(CN). Exact mass calcd for [TMEDA-Fe^{II}(OH)Fe^{III}]$^+$, $C_{39}H_{62}Fe_2N_6O_7S_3$: 934.3 found: 934.2. $E_{1/2}$ (MeCN, V versus $[FeCp_2]^{+/0}$): –0.89. E_A (MeCN, V versus $[FeCp_2]^{+/0}$): 0.98.

[TMEDA-Fe^{II}(N_3)(OH)Fe^{III}]. This complex was prepared using the method described above for [TMEDA-Fe^{II}(NCS)(OH)Fe^{III}] using [TMEDA-Fe^{II}(OTf)(OH)Fe^{III}] (100. mg, 0.925 mmol) and $NMe_4(N_3)$ (11.1 mg, 0.955 mmol) to produce the desired complex in crystalline yields of 48–58%. Dark orange block crystals of [TMEDA-Fe^{II}(N_3)(OH)Fe^{III}] suitable for X-ray diffraction were grown from a CH_2Cl_2 solution layered under pentane. Elemental analysis calcd. for [TMEDA-Fe^{II}(N_3)(OH)Fe^{III}]·CH_2Cl_2, $C_{40}H_{64}Cl_2Fe_2N_9O_7S_3$: C, 45.25; H, 6.08; N, 11.87%, found: C, 45.55; H, 6.10; N, 12.15%. UV-vis (CH_2Cl_2, λ_{max}, nm (ε_{max}, $M^{-1}cm^{-1}$)) 275(sh), 285(sh), 389(6500). FTIR (ATR, cm^{-1}, selected bands): 3270(OH), 2913, 2938, 2909, 2863, 2842, 2069 (N_3), 1602, 1562, 1465, 1339, 1276, 1130, 1093, 1070, 1051, 952, 933, 850, 818, 661. (Nujol, cm^{-1}): 3271(OH), 2080(N_3). Exact mass calcd for [TMEDA-Fe^{II}(OH)Fe^{III}]$^+$, $C_{39}H_{62}Fe_2N_6O_7S_3$: 934.3 found: 934.2. E_c (MeCN, V versus $[FeCp_2]^{+/0}$): –0.99. E_A (MeCN, V versus $[FeCp_2]^{+/0}$): –0.99. E_A (MeCN, V versus $[FeCp_2]^{+/0}$): 0.84.

$[(en)_2$-$Fe^{II}(OH)Fe^{III}]OTf$. Method A. This complex was prepared using the method described above for the [TMEDA-Fe^{II}(OTf)(OH)Fe^{III}] using $Fe^{II}(OTf)_2\cdot 2MeCN$ (39.0 mg, 0.0894 mmol), en (10.8 mg, 0.180 mmol), and $NMe_4[Fe^{II}MST]$ (73.1 mg, 0.0892 mmol) to produce the desired complex in crystalline yield of 63–87%. Dark orange needle crystals of $[(en)_2$-$Fe^{II}(OH)Fe^{III}]OTf$ suitable for X-ray diffraction were grown from a THF solution layered under methylcyclohexane. Elemental analysis calcd. for $[(en)_2$-$Fe^{II}(OH)Fe^{III}]OTf\cdot C_5H_{12}$, $C_{43}H_{74}F_3Fe_2N_8O_{10}S_4$: C, 44.52; H, 6.43; N, 9.66%, found: C, 44.84; H, 6.13; N, 9.78%. UV-vis (CH_2Cl_2, λ_{max}, nm (ε_{max}, $M^{-1}cm^{-1}$)) 274(sh), 283(sh), 339(9500), 382(sh), 524(50.). FTIR (ATR, cm^{-1}, selected bands): 3325(NH), 3268(NH), 3159(NH), 2962, 2934, 2862, 1603, 1449, 1253, 1225, 1153, 1135, 1082, 1028, 968, 939, 822, 797, 656, 637. (Nujol, cm^{-1}): 3235(NH), 3265(NH), 3160(NH). Exact mass calcd for $[(en)_2$-$Fe^{III}(O)Fe^{III}]^+$, $C_{37}H_{61}Fe_2N_8O_7S_3$: 937.4 found: 937.3. E_C (MeCN, V versus $[FeCp_2]^{+/0}$): –1.06. E_A (MeCN, V versus $[FeCp_2]^{+/0}$): 0.82.

Method B. A solution of [TMEDA-Fe^{II}(OTf)(OH)Fe^{III}] (88.0 mg, 0.0812 mmol) in CH_2Cl_2 (10 mL) was treated with en (10.9 mg, 0.0824 mmol) and stirred for 2 h. The solvent was removed under vacuum, then the resulting solid was redissolved in THF. This THF solution was layered under pentane to produce the desired complex with a crystalline yield of 31–39%. This reaction could also be monitored by UV-vis spectroscopy, conducted in an Agilent 8453 equipped with an Unisoku Unispeks cryostat. In an Ar-filled drybox, a 3 mL DCM solution of [TMEDA-Fe^{II}(OTf)(OH)Fe^{III}] (0.3 µmol, 0.1 mM) was transferred to a 1.0 cm quartz cuvette, which was sealed by a rubber septum. This cuvette was removed from the drybox and placed in the spectrophotometer. 2 equivalents of en (0.6 µmol, 30 mM), also prepared in the drybox, were injected to the cuvette *via* a gas-tight syringe and the spectral changes monitored every 120 s. The spectroscopic properties of the dark orange, needle crystals prepared by Method B are the same as those obtained for [(en)$_2$-Fe^{II}(OH)Fe^{III}]OTf prepared by Method A.

Physical Methods

Elemental analyses were performed on a Perkin-Elmer 2400 CHNS analyzer. UV-vis spectra were recorded with a Cary 50 spectrophotometer or an Agilent 8453 spectrophotometer equipped with an Unisoku Unispeks cryostat using either a 0.10 cm or 1.00 cm quartz cuvette. FTIR spectra were collected on a Varian 800 Scimitar Series FTIR spectrometer in air or a Thermo Scientific Nicolet iS5 spectrophotometer with an iD5 ATR attachment in a nitrogen filled glovebox. High-resolution mass spectra were collected using Waters Micromass LCT Premier Mass Spectrometer. Cyclic voltammetry (CV) experiments were conducted using a CH1600C electrochemical analyzer. A 2.0 mm glassy carbon electrode was used as the working electrode at scan velocities 0.1 V s^{-1}. A [FeCp$_2$]$^{+/0}$ couple was used as an internal reference to monitor the reference electrode (Ag$^{0/+}$). Tetrabutylammonium hexafluorophosphate (TBAP) was use as the supporting electrolyte at a concentration of 0.1 M. Perpendicular-mode X-band EPR spectra were collected using a Bruker EMX spectrometer at 10 K using liquid helium.

Crystallography

A Bruker SMART APEX II diffractometer and the APEX2 program package was used to determine the unit-cell parameters and for data collection. Crystallographic details are summarized in Appendix A.

References

(1) McCollum, D. G.; Yap, G. P. A.; Liable-Sands, L.; Rheingold, A. L. Bimetallic Reactivity . Oxo Transfer Reactions with a Heterobimetallic Complex of Iron(II) and Vanadium(III). *Inorg. Chem.* **1997**, *36*, 2230–2235.

(2) Incarvito, C.; Rheingold, A. L.; Gavrilova, A. L.; Qin, C. J.; Bosnich, B. Bimetallic reactivity. One-site addition two-metal oxidation reactions using a Di-Co(II) complex of a binucleating ligand with 5- and 6-coordinate sites. *Inorg. Chem.* **2001**, *40*, 4101–4108.

(3) Shibasaki, M.; Yamamoto, Y. Preface. In *Multimetallic Catalysts in Organic Synthesis*; Shibasaki, M., Yamamoto, Y., Eds.; Wiley-VCH, 2004; pp XI–XII.

(4) Powers, D. C.; Benitez, D.; Tkatchouk, E.; Goddard, W. A.; Ritter, T. Bimetallic Reductive Elimination from Dinuclear Pd(III) Complexes. *J. Am. Chem. Soc.* **2010**, *132*, 14092–14103.

(5) Shibasaki, M.; Kanai, M.; Matsunaga, S.; Kumagai, N. Multimetallic Multifunctional Catalysts for Asymmetric Reactions. In *Bifunctional Molecular Catalysis*; Springer Berlin Heidelberg, 2011; pp 1–30.

(6) Mankad, N. P. Selectivity Effects in Bimetallic Catalysis. *Chem. Eur. J.* **2016**, *22*, 5822–5829.

(7) Ng, G. K. Y.; Ziller, J. W.; Borovik, A. S. Structural Diversity in Metal Complexes with a Dinucleating Ligand Containing Carboxyamidopyridyl Groups. *Inorg. Chem.* **2011**, *50*, 7922–7924.

(8) Ng, G. K.-Y.; Ziller, J. W.; Borovik, A. S. Preparation and structures of dinuclear complexes containing M^{II}–OH centers. *Chem. Commun.* **2012**, *48*, 2546–2548.

(9) Kremer, A. B.; Osten, K. M.; Yu, I.; Ebrahimi, T.; Aluthge, D. C.; Mehrkhodavandi, P. Dinucleating Ligand Platforms Supporting Indium and Zinc Catalysts for Cyclic Ester Polymerization. *Inorg. Chem.* **2016**, *55*, 5365–5374.

(10) Buchler, S.; Meyer, F.; Kaifer, E.; Pritzkow, H. Tunable TACN/pyrazolate hybrid ligands as dinucleating scaffolds for metallobiosite modeling—dinickel(II) complexes relevant to the urease active site. *Inorganica Chim. Acta* **2002**, *337*, 371–386.

(11) Isaac, J. A.; Gennarini, F.; López, I.; Thibon-Pourret, A.; David, R.; Gellon, G.; Gennaro, B.; Philouze, C.; Meyer, F.; Demeshko, S.; Le Mest, Y.; Réglier, M.; Jamet, H.; Le Poul, N.; Belle, C. Room-Temperature Characterization of a Mixed-Valent μ-Hydroxodicopper(II,III) Complex. *Inorg. Chem.* **2016**, *55*, 8263–8266.

(12) Dunn, T. J.; Ramogida, C. F.; Simmonds, C.; Paterson, A.; Wong, E. W. Y.; Chiang, L.; Shimazaki, Y.; Storr, T. Non-Innocent Ligand Behavior of a Bimetallic Ni Schiff-Base Complex Containing a Bridging Catecholate. *Inorg. Chem.* **2011**, *50*, 6746–6755.

(13) Clarke, R. M.; Hazin, K.; Thompson, J. R.; Savard, D.; Prosser, K. E.; Storr, T. Electronic Structure Description of a Doubly Oxidized Bimetallic Cobalt Complex with Proradical Ligands. *Inorg. Chem.* **2016**, *55*, 762–774.

(14) Alliger, G. E.; Müller, P.; Do, L. H.; Cummins, C. C.; Nocera, D. G. Family of Cofacial

Bimetallic Complexes of a Hexaanionic Carboxamide Cryptand. *Inorg. Chem.* **2011**, *50*, 4107–4115.

(15) Borovik, A. S.; Que, L.; Papaefthymiou, V.; Münck, E.; Taylor, L. F.; Anderson, O. P. Heterobimetallic complexes with (μ-phenoxo)bis(μ-carboxylato) cores. *J. Am. Chem. Soc.* **1988**, *110*, 1986–1988.

(16) Borovik, A. S.; Papaefthymiou, V.; Taylor, L. F.; Anderson, O. P.; Que, Jr., L. Models for Iron-Oxo Proteins. Structures and Properties of $Fe^{II}Fe^{III}$, $Zn^{II}Fe^{III}$, and $Fe^{II}Ga^{III}$ Complexes with (μ-Phenoxo)bis(μ-carboxylato)dimetal Cores. *J. Am. Chem. Soc.* **1989**, *111*, 6183–6195.

(17) Blusch, L. K.; Mitevski, O.; Martin-Diaconescu, V.; Pröpper, K.; DeBeer, S.; Dechert, S.; Meyer, F. Selective Synthesis and Redox Sequence of a Heterobimetallic Nickel/Copper Complex of the Noninnocent Siamese-Twin Porphyrin. *Inorg. Chem.* **2014**, *53*, 7876–7885.

(18) Rudd, P. A.; Liu, S.; Gagliardi, L.; Young, V. G.; Lu, C. C. Metal–Alane Adducts with Zero-Valent Nickel, Cobalt, and Iron. *J. Am. Chem. Soc.* **2011**, *133*, 20724–20727.

(19) Clouston, L. J.; Siedschlag, R. B.; Rudd, P. A.; Planas, N.; Hu, S.; Miller, A. D.; Gagliardi, L.; Lu, C. C. Systematic Variation of Metal-Metal Bond Order in Metal–Chromium Complexes. *J. Am. Chem. Soc.* **2013**, *135*, 13142–13148.

(20) Eisenhart, R. J.; Clouston, L. J.; Lu, C. C. Configuring Bonds between First-Row Transition Metals. *Acc. Chem. Res.* **2015**, *48*, 2885–2894.

(21) Greenwood, B. P.; Forman, S. I.; Rowe, G. T.; Chen, C.-H.; Foxman, B. M.; Thomas, C. M. Multielectron Redox Activity Facilitated by Metal−Metal Interactions in Early/Late Heterobimetallics: Co/Zr Complexes Supported by Phosphinoamide Ligands. *Inorg. Chem.* **2009**, *48*, 6251–6260.

(22) Krogman, J. P.; Thomas, C. M. Metal–metal multiple bonding in C_3-symmetric bimetallic complexes of the first row transition metals. *Chem. Commun.* **2014**, *50*, 5115.

(23) Wu, B.; Wilding, M. J. T.; Kuppuswamy, S.; Bezpalko, M. W.; Foxman, B. M.; Thomas, C. M. Exploring Trends in Metal–Metal Bonding, Spectroscopic Properties, and Conformational Flexibility in a Series of Heterobimetallic Ti/M and V/M Complexes (M = Fe, Co, Ni, and Cu). *Inorg. Chem.* **2016**, *55*, 12137–12148.

(24) Serrano-Plana, J.; Garcia-Bosch, I.; Company, A.; Costas, M. Structural and Reactivity Models for Copper Oxygenases: Cooperative Effects and Novel Reactivities. *Acc. Chem. Res.* **2015**, *48*, 2397–2406.

(25) Das, B.; Daver, H.; Singh, A.; Singh, R.; Haukka, M.; Demeshko, S.; Meyer, F.; Lisensky, G.; Jarenmark, M.; Himo, F.; Nordlander, E. A Heterobimetallic FeIIIMn II Complex of an Unsymmetrical Dinucleating Ligand: A Structural and Functional Model Complex for the Active Site of Purple Acid Phosphatase of Sweet Potato. *Eur. J. Inorg. Chem.* **2014**, *2014*, 2204–2212.

(26) Delgado, M.; Ziegler, J. M.; Seda, T.; Zakharov, L. N.; Gilbertson, J. D. Pyridinediimine Iron Complexes with Pendant Redox-Inactive Metals Located in the Secondary Coordination

Sphere. *Inorg. Chem.* **2016**, *55*, 555–557.

(27) Lawrence, J. D.; Li, H.; Rauchfuss, T. B.; Bénard, M.; Rohmer, M.-M. Diiron Azadithiolates as Models for the Iron-Only Hydrogenase Active Site: Synthesis, Structure, and Stereoelectronics. *Angew. Chemie* **2001**, *113*, 1818–1821.

(28) Barton, B. E.; Rauchfuss, T. B. Hydride-Containing Models for the Active Site of the Nickel−Iron Hydrogenases. *J. Am. Chem. Soc.* **2010**, *132*, 14877–14885.

(29) Li, Y.; Rauchfuss, T. B. Synthesis of Diiron(I) Dithiolato Carbonyl Complexes. *Chem. Rev.* **2016**, *116*, 7043–7077.

(30) Evans, W. J.; Lee, D. S.; Ziller, J. W. Reduction of Dinitrogen to Planar Bimetallic $M_2(\mu\text{-}\eta^2\text{:}\eta^2\text{-}N_2)$ Complexes of Y, Ho, Tm, and Lu Using the $K/Ln[N(SiMe_3)_2]_3$ Reduction System. **2003**.

(31) Evans, W. J.; Kozimor, S. A.; Ziller, J. W. Synthesis of heteroleptic uranium compounds including an asymmetric, sterically unsaturated, bimetallic, organouranium(IV) halide: $(C_5Me_5)(C_8H_8)ClU(\mu\text{-}Cl)U(C_8H_8)(C_5Me_5)$. *Polyhedron* **2006**, *25*, 484–492.

(32) Wong, J. L.; Higgins, R. F.; Bhowmick, I.; Cao, D. X.; Szigethy, G.; Ziller, J. W.; Shores, M. P.; Heyduk, A. F.; Gagliardi, L.; Lu, C. C. Bimetallic iron–iron and iron–zinc complexes of the redox-active ONO pincer ligand. *Chem. Sci.* **2016**, *7*, 1594–1599.

(33) Rosenkoetter, K. E.; Ziller, J. W.; Heyduk, A. F. A Heterobimetallic W–Ni Complex Containing a Redox-Active $W[SNS]_2$ Metalloligand. *Inorg. Chem.* **2016**, *55*, 6794–6798.

(34) Lacy, D. C.; Park, Y. J.; Ziller, J. W.; Yano, J.; Borovik, A. S. Assembly and Properties of Heterobimetallic $Co^{II/III}/Ca^{II}$ Complexes with Aquo and Hydroxo Ligands. *J. Am. Chem. Soc.* **2012**, *134*, 17526–17535.

(35) Park, Y. J.; Ziller, J. W.; Borovik, A. S. The Effects of Redox-Inactive Metal Ions on the Activation of Dioxygen: Isolation and Characterization of a Heterobimetallic Complex Containing a Mn^{III}–(μ-OH)–Ca^{II} Core. *J. Am. Chem. Soc.* **2011**, *133*, 9258–9261.

(36) Park, Y. J.; Cook, S. A.; Sickerman, N. S.; Sano, Y.; Ziller, J. W.; Borovik, A. S. Heterobimetallic complexes with M^{III}-(μ-OH)-M^{II} cores (M^{III} = Fe, Mn, Ga; M^{II} = Ca, Sr, and Ba): structural, kinetic, and redox properties. *Chem. Sci.* **2013**, *4*, 717–726.

(37) Sickerman, N. S.; Henry, R. M.; Ziller, J. W.; Borovik, A. S. Preparation and structural properties of In^{III}–OH complexes. *Polyhedron* **2013**, *58*, 65–70.

(38) Sano, Y.; Weitz, A. C.; Ziller, J. W.; Hendrich, M. P.; Borovik, A. S. Unsymmetrical Bimetallic Complexes with M^{II}–(μ-OH)–M^{III} Cores ($M^{II}M^{III}$ = $Fe^{II}Fe^{III}$, $Mn^{II}Fe^{III}$, $Mn^{II}Mn^{III}$): Structural, Magnetic, and Redox Proper. *Inorg. Chem.* **2013**, *52*, 10229–10231.

(39) Sano, Y.; Lau, N.; Weitz, A. C.; Ziller, J. W.; Hendrich, M. P.; Borovik, A. S. Models for Unsymmetrical Active Sites in Metalloproteins: Structural, Redox, and Magnetic Properties of Bimetallic Complexes with M^{II}–(μ-OH)–Fe^{III} Cores. *Manuscript in preparation.*

(40) Shurdha, E.; Moore, C. E.; Rheingold, A. L.; Lapidus, S. H.; Stephens, P. W.; Arif, A. M.; Miller, J. S. First Row Transition Metal(II) Thiocyanate Complexes, and Formation of 1-, 2-

, and 3-Dimensional Extended Network Structures of $M(NCS)_2(Solvent)_2$ (M = Cr, Mn, Co) Composition. *Inorg. Chem.* **2013**, *52*, 10583–10594.

(41) Christe, K. O.; Wilson, W. W.; Bau, R.; Bunte, S. W. New synthesis, crystal structure, and vibrational spectra of tetramethylammonium azide and reactions of the fluoride anion with hydrazoic acid and of the azide anion with hydrogen fluoride. *J. Am. Chem. Soc.* **1992**, *114*, 3411–3414.

(42) Johnston, D. H.; Shriver, D. F. Vibrational study of the trifluoromethanesulfonate anion: unambiguous assignment of the asymmetric stretching modes. *Inorg. Chem.* **1993**, *32*, 1045–1047.

(43) Gellman, S. H.; Dado, G. P.; Liang, G. B.; Adams, B. R. Conformation-directing effects of a single intramolecular amide-amide hydrogen bond: variable-temperature NMR and IR studies on a homologous diamide series. *J. Am. Chem. Soc.* **1991**, *113*, 1164–1173.

(44) Aaron, H. S. Conformational Analysis of Intramolecular-Hydrogen-Bonded Compounds in Dilute Solution by Infrared Spectroscopy. John Wiley & Sons, Inc.; pp 1–52.

(45) Addison, A. W.; Rao, T. N.; Reedijk, J.; van Rijn, J.; Verschoor, G. C. Synthesis, structure, and spectroscopic properties of copper(II) compounds containing nitrogen–sulphur donor ligands; the crystal and molecular structure of aqua[1,7-bis(N-methylbenzimidazol-2′-yl)-2,6-dithiaheptane]copper(II) perchlorate. *J. Chem. Soc. Dalt. Trans.* **1984**, No. 7, 1349.

(46) Robinson, K.; Gibbs, G. V.; Ribbe, P. H. Quadratic Elongation: A Quantitative Measure of Distortion in Coordination Polyhedra. *Science* **1971**, *172*, 567–570.

(47) Shannon, R. D. Revised effective ionic radii and systematic studies of interatomic distances in halides and chalcogenides. *Acta Crystallogr. Sect. A* **1976**, *32*, 751–767.

(48) Balić Žunić, T.; Vicković, I.; IUCr. IVTON – a program for the calculation of geometrical aspects of crystal structures and some crystal chemical applications. *J. Appl. Crystallogr.* **1996**, *29*, 305–306.

(49) Emsley, J. Very strong hydrogen bonding. *Chem. Soc. Rev.* **1980**, *9*, 91.

(50) Garribba, E.; Micera, G. The Determination of the Geometry of Cu(II) Complexes: An EPR Spectroscopy Experiment. *J. Chem. Educ.* **2006**, *83*, 1229.

(51) Petasis, D. T.; Hendrich, M. P. Quantitative Interpretation of Multifrequency Multimode EPR Spectra of Metal Containing Proteins, Enzymes, and Biomimetic Complexes. 2015; pp 171–208.

(52) Mann, S. I.; Heinisch, T.; Weitz, A. C.; Hendrich, M. P.; Ward, T. R.; Borovik, A. S. Modular Artificial Cupredoxins. *J. Am. Chem. Soc.* **2016**, *138*, 9073–9076.

(53) Heintz, R. A.; Smith, J. A.; Szalay, P. S.; Weisgerber, A.; Dunbar, K. R. Homoleptic transition metal acetonitrile cations with tetrafluoroborate or trifluoromethanesulfonate anions. *Inorg. Synth.* **2002**, *33*, 75–83.

APPENDIX A

Crystallography

Chapter 2

Table A.1. Crystallographic data for $NMe_4[Fe^{II}RST(OH_2)]$ salts.

$NMe_4[Fe^{II}RST(OH_2)]$	R = $-CF_3$	$-Cl$	$-H$	$-CH_3$	$-OCH_3$
formula	$C_{31}H_{38}F_9FeN_5O_7S_3\bullet½(CH_2Cl_2)$	$C_{29}H_{42}Cl_5FeN_5O_8S_3$	$C_{28}H_{41}FeN_5O_7S_3$	$C_{32}H_{51}Cl_2FeN_5O_8S_3$	$C_{31}H_{47}FeN_5O_{10}S_3$
fw	958.15	917.95	711.69	856.70	801.76
T (K)	88(2)	143(2)	88(2)	143(2)	88(2)
crystal system	Triclinic	Triclinic	Monoclinic	Triclinic	Monoclinic
space group	$P\bar{1}$	$P\bar{1}$	$P2_1/n$	$P\bar{1}$	Pc
a (Å)	9.3473(4)	9.8185(5)	8.8715(4)	9.7228(10)	18.489(3)
b (Å)	13.7450(6)	11.9558(7)	19.4880(9)	11.9881(12)	10.8005(15)
c (Å)	31.0075(14)	18.9546(10)	18.8873(8)	19.114(2)	18.417(3)
α (deg)	98.6366(6)	97.3441(6)	90	73.7474(12)	90
β (deg)	91.6897(6)	100.9682(6)	98.7312(6)	78.9829(12)	92.9591(19)
γ (deg)	96.5594(6)	114.2141(6)	90	66.5432(12)	90
Z	4	2	4	2	4
V ($Å^3$)	3908.4(3)	1938.84(18)	3227.5(2)	1954.1(3)	3672.8(9)
δ_{calc} (mg/m^3)	1.628	1.572	1.465	1.456	1.450
indep. reflections	15932	8937	8250	9015	16272
R1	0.0612	0.0356	0.0301	0.0410	0.0443
wR2	0.1605	0.0994	0.0755	0.1034	0.0910
Goof	1.018	1.052	1.022	1.041	0.983
CCDC#	982221	982222	982223	982224	982225

$R1 = \Sigma||F_o|-|F_c|| / \Sigma|F_o|$

$wR2 = [\Sigma[w(F_o^2-F_c^2)^2] / \Sigma[w(F_o^2)^2]]^{1/2}$

Goof = $S = [\Sigma[w(F_o^2-F_c^2)^2] / (n-p)]^{1/2}$ where n is the number of reflections and p is the total number of parameters refined.

Structure of[$NMe_4[Fe^{II}F_3ST(OH_2)]$]. A colorless crystal of approximate dimensions 0.272 x 0.185 x 0.050 mm was mounted on a glass fiber and transferred to a Bruker SMART APEX II diffractometer. The APEX2[1] program package was used to determine the unit-cell parameters and for data collection (90 sec/frame scan time for a sphere of diffraction data). The raw frame data was processed using SAINT[2] and SADABS[3] to yield the reflection data file. Subsequent calculations were carried out using the SHELXTL[4] program. There were no systematic absences nor any diffraction symmetry other than the Friedel condition. The centrosymmetric triclinic space group $P\bar{1}$ was assigned and later determined to be correct.

The structure was solved by direct methods and refined on F^2 by full-matrix least-squares techniques. The analytical scattering factors[5] for neutral atoms were used throughout the analysis. H(1)-H(4) were located from a difference-Fourier map and refined (x,y,z and U_{iso}). All other hydrogen atoms were included using a riding model. There was half a disordered dichloromethane molecule per formula unit which was included using multiple components with partial site-occupancy-factors. C(59)-C(62) and F(10)-F(12) were also disordered and included using multiple components with partial site-occupancy-factors.

At convergence, wR2 = 0.1605 and Goof = 1.018 for 1054 variables refined against 15932 data (0.8 Å), R1 = 0.0612 for those 12825 data with $I > 2.0\sigma(I)$.

Structure of $NMe_4[Fe^{II}CST(OH_2)]$. A colorless crystal of approximate dimensions 0.337 x 0.246 x 0.143 mm was mounted on a glass fiber and transferred to a Bruker SMART APEX II diffractometer. The APEX2[6] program package was used to determine the unit-cell parameters and for data collection (20 sec/frame scan time for a sphere of diffraction data). The raw frame data was processed using SAINT[7] and SADABS[3] to yield the reflection data file. Subsequent calculations were carried out using the SHELXTL[4] program. There were no systematic absences nor any diffraction symmetry other than the Friedel condition. The centrosymmetric triclinic space group $P\bar{1}$ was assigned and later determined to be correct.

The structure was solved by direct methods and refined on F^2 by full-matrix least-squares techniques. The analytical scattering factors[5] for neutral atoms were used throughout the analysis. H(1) and H(2) were located from a difference-Fourier map and refined (x,y,z and U_{iso}). H(3) and H(4) were also located from a difference Fourier map and did not refine well , so they were restrained during refinement and the O(8)-H(3) and O(8)-H(4) distances were fixed at 0.8 Å. All other hydrogen atoms were included using a riding model. There was one molecule of dichloromethane per formula unit and one water molecule per formula unit.

At convergence, wR2 = 0.0994 and Goof = 1.052 for 478 variables refined against 8937 data (0.75 Å), R1 = 0.0356 for those 7745 data with $I > 2.0\sigma(I)$.

Structure of $NMe_4[Fe^{II}PST(OH_2)]$. A colorless crystal of approximate dimensions 0.257 x 0.239 x 0.068 mm was mounted on a glass fiber and transferred to a Bruker SMART APEX II diffractometer. The APEX2[1] program package was used to determine the unit-cell parameters and for data collection (20 sec/frame scan time for a sphere of diffraction data). The raw frame data was processed using SAINT[2] and SADABS[3] to yield the reflection data file. Subsequent calculations were carried out using the SHELXTL[4] program. The diffraction symmetry was 2/*m* and the systematic absences were consistent with the monoclinic space group $P2_1/n$ that was later determined to be correct.

The structure was solved by direct methods and refined on F^2 by full-matrix least-squares techniques. The analytical scattering factors[6] for neutral atoms were used throughout the analysis. Hydrogen atoms were located from a difference-Fourier map and refined (x,y,z and U_{iso}).

At convergence, wR2 = 0.0755 and Goof = 1.022 for 561 variables refined against 8250 data (0.73 Å), R1 = 0.0301 for those 6897 data with I > 2.0σ(I).

Structure of $NMe_4[Fe^{II}TST(OH_2)]$. A colorless crystal of approximate dimensions 0.286 x 0.260 x 0.159 mm was mounted on a glass fiber and transferred to a Bruker SMART APEX II diffractometer. The APEX2[6] program package was used to determine the unit-cell parameters and for data collection (15 sec/frame scan time for a sphere of diffraction data). The raw frame data was processed using SAINT[7] and SADABS[8] to yield the reflection data file. Subsequent calculations were carried out using the SHELXTL[9] program. There were no systematic absences nor any diffraction symmetry other than the Friedel condition. The centrosymmetric triclinic space group $P\bar{1}$ was assigned and later determined to be correct.

The structure was solved by direct methods and refined on F^2 by full-matrix least-squares techniques.[4] The analytical scattering factors[8] for neutral atoms were used throughout the analysis. There was one water molecule and one disorder dichloromethane solvent molecule present. The dichloromethane molecule was included using multiple components with partial site-occupancy-factors. The water protons H(1)-H(4) were allowed to freely refine (x,y,z and U_{iso}). The remaining hydrogen atoms were included using a riding model.

At convergence, wR2 = 0.1034 and Goof = 1.041 for 510 variables refined against 9015 data (0.74 Å), R1 = 0.0410 for those 6664 data with I > 2.0σ(I).

Structure of $NMe_4[Fe^{II}MOST(OH_2)]$. A colorless crystal of approximate dimensions 0.230 x 0.210 x 0.184 mm was mounted in a cryo loop and transferred to a Bruker SMART APEX II diffractometer. The APEX2[1] program package was used to determine the unit-cell parameters and for data collection (20 sec/frame scan time for a sphere of diffraction data). The raw frame data was processed using SAINT[2] and SADABS[3] to yield the reflection data file. Subsequent calculations were carried out using the SHELXTL[4] program. The diffraction symmetry was 2/*m* and the systematic absences were consistent with the monoclinic space groups *Pc and P*2*/c*. It was later determined that space group *Pc* was correct.

The structure was solved by direct methods and refined on F^2 by full-matrix least-squares techniques. The analytical scattering factors[2] for neutral atoms were used throughout the analysis. H(1)–H(4) were located from a difference-Fourier map and refined (x,y,z and U_{iso}). All other hydrogen atoms were included using a riding model. There were two molecules of the formula-unit present (Z = 4).

At convergence, wR2 = 0.0910 and Goof = 0.983 for 931 variables refined against 16272 data (0.75 Å), R1 = 0.0443 for those 13641 data with I > 2.0σ(I). The absolute structure was assigned by refinement of the Flack parameter.[10]

Chapter 3

Table A.2. Crystallographic data for $K_2[Ni^{II}H_3buea(OH)]$ and $NMe_4[Ni^{II}MST(OH_2)]$ salts.

	$K_2[Ni^{II}H_3buea(OH)]$	$NMe_4[Ni^{II}MST(OH_2)]$
formula	$[C_{27}H_{57}K_2N_9NiO_6 \bullet \frac{1}{2}(C_4H_{10}O)]_\infty$	$C_{37}H_{59}N_5NiO_7S_3$
fw	777.78	840.78
T (K)	88(2)	88(2)
crystal system	Triclinic	Monoclinic
space group	$P\bar{1}$	*C*2/*c*
a (Å)	11.7237(8)	26.5309(11)
b (Å)	13.5910(9)	9.6415(4)
c (Å)	14.5409(9)	31.6736(13)
α (deg)	88.9341(8)	90

β (deg)	68.6217(7)	90.3364(7)
γ (deg)	70.7167(8)	90
Z	2	8
V (Å^3)	2022.7(2)	8101.9(6)
δ_{calc} (mg/m^3)	1.277	1.379
indep. reflections	8869	9750
R1	0.0318	0.0436
wR2	0.0822	0.1017
Goof	1.032	1.013
CCDC#	1501483	1501484

Structure of $K_2[Ni^{II}H_3buea(OH)]$. A green crystal of approximate dimensions 0.252 x 0.465 x 0.803 mm was mounted on a glass fiber and transferred to a Bruker SMART APEX II diffractometer. The APEX2[11] program package was used to determine the unit-cell parameters and for data collection (60 sec/frame scan time for a sphere of diffraction data). The raw frame data was processed using SAINT[12] and SADABS[13] to yield the reflection data file. Subsequent calculations were carried out using the SHELXTL[14] program. There were no systematic absences nor any diffraction symmetry other than the Friedel condition. The centrosymmetric triclinic space group $P\bar{1}$ was assigned and later determined to be correct.

The structure was solved by direct methods and refined on F^2 by full-matrix least-squares techniques. The analytical scattering factors[5] for neutral atoms were used throughout the analysis. Hydrogen atoms H(1), H(5), H(6) and H(7) were located from a difference-Fourier map and refined (x,y,z and U_{iso}). The remaining hydrogen atoms were included using a riding model. The molecule was polymeric repeating about inversion centers. Atoms C(22), C(23), C(24) and N(8) were disordered and included using multiple components with partial site-occupancy-factors. There was one half molecule of diethylether present. The solvent was located on an inversion center and was disordered.

At convergence, wR2 = 0.0863 and Goof = 1.032 for 506 variables refined against 8869 data (0.78Å), R1 = 0.0318 for those 7775 data with I > 2.0σ(I).

Structure of $NMe_4[Ni^{II}MST(OH_2)]$. A green crystal of approximate dimensions 0.254 x 0.083 x 0.073 mm was mounted in a cryoloop and transferred to a Bruker SMART APEX II diffractometer. The APEX2[11] program package was used to determine the unit-cell parameters and for data collection (90 sec/frame scan time for a sphere of diffraction data). The raw frame data was processed using SAINT[12] and SADABS[13] to yield the reflection data file. Subsequent calculations were carried out using the SHELXTL[14] program. The diffraction symmetry was 2/*m* and the systematic absences were consistent with the monoclinic space groups *Cc* and *C*2/*c*. It was later determined that space group *C*2/*c* was correct.

The structure was solved by direct methods and refined on F^2 by full-matrix least-squares techniques. The analytical scattering factors[5] for neutral atoms were used throughout the analysis. Hydrogen atoms H1A and H1B on O1 were located from a difference-Fourier map and refined (x,y,z and U_{iso}). The remaining hydrogen atoms were included using a riding model. The NMe_4^+ counterion was disordered and included using multiple components with partial site-occupancy-factors.

At convergence, wR2 = 0.1017 and Goof = 1.013 for 494 variables refined against 9750 data (0.75 Å), R1 = 0.0436 for those 7238 data with I > 2.0σ(I).

Table A.3. Crystallographic data for [(TMEDA)M^{II}(OTf)–(μ-OH)–Fe^{III}MST] compounds (M^{II} = Fe^{II}, Co^{II}, or Ni^{II}).

	[(TMEDA)Fe^{II}(OTf) –(μ-OH)–Fe^{III}MST]	[(TMEDA)Co^{II}(OTf) –(μ-OH)–Fe^{III}MST]	[(TMEDA)Ni^{II}(Br) –(μ-OH)–Fe^{III}MST]
formula	$[C_{40}H_{62}F_3Fe_2N_6O_{10}S_4]$	$C_{40}H_{62}CoF_3FeN_6O_{10}S_4$	$C_{39}H_{62}BrFeN_6NiO7S_3 \bullet CH_2Cl_2$
fw	1083.89	1086.97	1102.52
T (K)	133(2)	133(2)	88(2)
crystal system	Monoclinic	Monoclinic	Monoclinic
space group	*C2/c*	*C2/c*	$P2_1/c$
a (Å)	39.226(3)	39.277(5)	21.8160(18)
b (Å)	16.9526(13)	16.972(2)	13.1714(11)
c (Å)	18.8719(14)	18.844(2)	17.6057(14)
α (°)	90	90	90
β (°)	110.8868(9)	110.7870(15)	107.5355(10)
γ (°)	90	90	90
Z	8	8	4
V (Å^3)	11724.9(15)	11744(2)	4823.9(7)
δ_{calc} (mg/m^3)	1.228	1.230	1.518
indep. reflections	14240	12057	12122
R1	0.0459	0.0396	0.0307
wR2	0.1302	0.0974	0.0833
Goof	1.025	1.032	1.036
CCDC#	1554807	1554810	1554811

Structure of [(TMEDA)Fe^{II}(OTf)–(μ-OH)–Fe^{III}MST]. A red crystal of approximate dimensions 0.176 x 0.203 x 0.399 mm was mounted in a cryoloop and transferred to a Bruker SMART APEX II diffractometer. The APEX2[15] program package was used to determine the unit-cell parameters and for data collection (30 sec/frame scan time for a sphere of diffraction data). The raw frame data was processed using SAINT[7] and SADABS[8] to yield the reflection data file. Subsequent calculations were carried out using the SHELXTL[9] program. The diffraction symmetry was 2/*m* and the systematic absences were consistent with the monoclinic space groups *Cc* and *C*2/*c*. It was later determined that space group *C*2/*c* was correct.

The structure was solved by dual space methods and refined on F^2 by full-matrix least-squares techniques. The analytical scattering factors[5] for neutral atoms were used throughout the analysis. Hydrogen atom H(1) was located from a difference-Fourier map and refined (x,y,z and riding U_{iso}) with d(O-H) = 0.85Å. The remaining hydrogen atoms were included using a riding model.

At convergence, wR2 = 0.1302 and Goof = 1.025 for 602 variables refined against 14240 data (0.74Å), R1 = 0.0459 for those 9978 data with $I > 2.0\sigma(I)$.

There were several high residuals present in the final difference-Fourier map. It was not possible to determine the nature of the residuals although it was probable that tetrahydrofuran and/or pentane solvents were present. The SQUEEZE[16a] routine in the PLATON[16b] program package was used to account for the electrons in the solvent accessible voids.

Structure of [(TMEDA)Co^{II}(OTf)–(μ-OH)–Fe^{III}MST]. An orange crystal of approximate dimensions 0.102 x 0.177 x 0.342 mm was mounted in a cryoloop and transferred to a Bruker SMART APEX II diffractometer. The APEX2[15] program package was used to determine the unit-cell parameters and for data collection (60 sec/frame scan time). The raw frame data was processed using SAINT[7] and SADABS[8] to yield the reflection data file. Subsequent calculations were carried out using the SHELXTL[9] program. The diffraction symmetry was 2/*m* and the systematic absences were consistent with the monoclinic space groups *Cc* and *C*2/*c*. It was later determined that space group *C*2/*c* was correct.

The structure was solved by dual space methods and refined on F^2 by full-matrix least-squares techniques. The analytical scattering factors[5] for neutral atoms were used throughout the analysis. Hydrogen atom H(1) was located from a difference-Fourier map and refined (x,y,z and riding U_{iso}) with d(O-H) = 0.85Å. The remaining hydrogen atoms were included using a riding model.

At convergence, wR2 = 0.0974 and Goof = 1.032 for 603 variables refined against 12057 data (0.80Å), R1 = 0.0396 for those 9013 data with $I > 2.0\sigma(I)$.

There were several high residuals present in the final difference-Fourier map. It was not possible to determine the nature of the residuals although it was probable that tetrahydrofuran and/or pentane solvents were present. The SQUEEZE[16a] routine in the PLATON[16b] program package was used to account for the electrons in the solvent accessible voids.

Chapter 5

Table A.4. Crystallographic data for [(TMEDA)Fe^{II}(X)−(μ-OH)−Fe^{III}MST] compounds (X^- = Br^-, NCS^-, N_3^-) and [$(en)_2Fe^{II}$−(μ-OH) −Fe^{III}MST]OTf.

	[(TMEDA)Fe^{II}(Br) −(μ-OH)−Fe^{III}MST]	[(TMEDA)Fe^{II}(NCS) −(μ-OH)−Fe^{III}MST]	[(TMEDA)Fe^{II}(N_3) −(μ-OH)−Fe^{III}MST]	[$(en)_2Fe^{II}$−(μ-OH) −Fe^{III}MST]OTf
formula	$C_{40}H_{64}BrCl_2Fe_2N_6O_7S_3$	$C_{40}H_{62}Fe_2N_7O_7S_4$	$C_{39}H_{62}Fe_2N_9O_7S_3$	$C_{46}H_{78}Cl_2F_3Fe_2N_8O_{10}S_4$
fw	1099.66	992.90	976.85	1271.00
T (K)	88(2)	88(2)	88(2)	133(2)
crystal system	Monoclinic	Trigonal	Trigonal	Triclinic
space group	$P2_1/c$	$R\bar{3}$	$R\bar{3}$	$P\bar{1}$
a (Å)	21.7773(13)	34.669(3)	34.1173(18)	9.0701(8)
b (Å)	13.2666(8)	34.669(3)	34.1173(18)	17.9865(15)
c (Å)	17.6201(11)	20.8648(16)	21.137(11)	18.8049(16)
α (°)	90	90	90	107.8561(11)
β (°)	107.4513(8)	90	90	94.8064(12)
γ (°)	90	120	120	97.9985(10)
Z	4	18	18	2
V ($Å^3$)	4856.3(5)	21183(2)	21183(2)	2865.5(4)
δ_{calc} (mg/m^3)	1.504	1.366	1.378	1.473
indep. reflections	12173	10658	10386	12888
R1	0.0290	0.0290	0.0358	0.0474
wR2	0.0712	0.0781	0.0969	0.1326
Goof	1.038	1.041	1.019	1.041

CCDC#	1554806	1554808	1554809	1554812

Structure of [(TMEDA)Fe^{II}(Br)−(μ-OH)−Fe^{III}MST]. A red crystal of approximate dimensions 0.395 x 0.298 x 0.256 mm was mounted in a cryoloop and transferred to a Bruker SMART APEX II diffractometer. The APEX2[15] program package was used to determine the unit-cell parameters and for data collection (25 sec/frame scan time for a sphere of diffraction data). The raw frame data was processed using SAINT[7] and SADABS[8] to yield the reflection data file. Subsequent calculations were carried out using the SHELXTL[9] program. The diffraction symmetry was 2/*m* and the systematic absences were consistent with the monoclinic space group $P2_1/c$ that was later determined to be correct.

The structure was solved by dual space methods and refined on F^2 by full-matrix least-squares techniques. The analytical scattering factors[5] for neutral atoms were used throughout the analysis. Hydrogen atom H1 was located from a difference-Fourier map and refined (x,y,z and U_{iso}). The remaining hydrogen atoms were included using a riding model. There was one molecule of dichloromethane present that was disordered over two positions (0.50:0.50). The tetramethylethylenediamine ligand was disordered over two positions (0.7:0.3).

At convergence, wR2 = 0.0745 and Goof = 1.039 for 613 variables refined against 12173 data (0.73 Å), R1 = 0.0290 for those 10639 data with $I > 2.0\sigma(I)$.

Structure of [(TMEDA)Fe^{II}(NCS)−(μ-OH)−Fe^{III}MST]. An orange crystal of approximate dimensions 0.152 x 0.196 x 0.305 mm was mounted in a cryoloop and transferred to a Bruker SMART APEX II diffractometer. The APEX2[15] program package was used to determine the unit-cell parameters and for data collection (25 sec/frame scan time for a sphere of diffraction data).

The raw frame data was processed using SAINT[7] and SADABS[8] to yield the reflection data file. Subsequent calculations were carried out using the SHELXTL[9] program. The systematic absences were consistent with the hexagonal space groups $R3$ and $R\bar{3}$. The centrosymmetric space group $R\bar{3}$ was assigned and later determined to be correct.

The structure was solved by dual space methods and refined on F^2 by full-matrix least-squares techniques. The analytical scattering factors[5] for neutral atoms were used throughout the analysis. Hydrogen atoms H(1) was located from a difference-Fourier amp and refined (x,y,z and U_{iso}) with d(O-H) = 0.85Å. The remaining hydrogen atoms were included using a riding model. Atoms C(36) and C(37) were disordered and including using multiple components with partial site-occupancies-factors.

At convergence, wR2 = 0.0.0969 and Goof = 1.019 for 576 variables refined against 10386 data (0.78 Å), R1 = 0.0358 for those 8242 data with $I > 2.0\sigma(I)$.

There were several high residuals present in the final difference-Fourier map. It was not possible to determine the nature of the residuals although it was probable that pentane and/or dichloromethane solvents were present. The SQUEEZE[16a] routine in the PLATON[16b] program package was used to account for the electrons in the solvent accessible voids.

Structure of [(TMEDA)Fe^{II}(N$_3$)−(μ-OH)−Fe^{III}MST]. A red crystal of approximate dimensions 0.158 x 0.159 x 0.352 mm was mounted in a cryoloop and transferred to a Bruker SMART APEX II diffractometer. The APEX2[15] program package was used to determine the unit-cell parameters and for data collection (30 sec/frame scan time for a sphere of diffraction data). The raw frame data was processed using SAINT[7] and SADABS[8] to yield the reflection data file. Subsequent calculations were carried out using the SHELXTL[9] program. The systematic absences were consistent with the hexagonal space groups R3 and $R\bar{3}$. The centrosymmetric space group $R\bar{3}$ was assigned and later determined to be correct.

The structure was solved by dual space methods and refined on F^2 by full-matrix least-squares techniques. The analytical scattering factors[5] for neutral atoms were used throughout the analysis. Hydrogen atom H(1) was located from a difference-Fourier map and refined (x,y,z and U_{iso}). The remaining hydrogen atoms were included using a riding model. Atoms C(34), C(36), C(37) and C(39) were disordered and included using multiple components with partial site-occupancy-factors.

At convergence, wR2 = 0.0781 and Goof = 1.041 for 596 variables refined against 10658 data (0.78 Å), R1 = 0.0290 for those 9003 data with $I > 2.0\sigma(I)$.

There were several high residuals present in the final difference-Fourier map. It was not possible to determine the nature of the residuals although it was probable that pentane and/or dichloromethane was present. The SQUEEZE[16a] routine in the PLATON[16b] program package was used to account for the electrons in the solvent accessible voids.

Structure of $[(en)_2Fe^{II}-(\mu\text{-}OH)-Fe^{III}MST]OTf$. A red crystal of approximate dimensions 0.152 x 0.209 x 0.285 mm was mounted in a cryoloop and transferred to a Bruker SMART APEX II diffractometer. The APEX2[1] program package was used to determine the unit-cell parameters and for data collection (60 sec/frame scan time for a sphere of diffraction data). The raw frame data was processed using SAINT[2] and SADABS[3] to yield the reflection data file. Subsequent calculations were carried out using the SHELXTL[4] program. There were no systematic absences nor any diffraction symmetry other than the Friedel condition. The centrosymmetric triclinic space group $P\bar{1}$ was assigned and later determined to be correct.

The structure was solved by dual space methods and refined on F^2 by full-matrix least-squares techniques. The analytical scattering factors[5] for neutral atoms were used throughout the analysis. Hydrogen atoms were included using a riding model. The hydrogen associated with O(1) was not located or included in the refinement. In addition to the triflate anion, there was one molecule of dichloromethane and one molecule of methylcyclohexane present per formula-unit.

At convergence, wR2 = 0.1326 and Goof = 1.029 for 686 variables refined against 12888 data (0.75 Å), R1 = 0.0474 for those 10581 data with $I > 2.0\sigma(I)$.

References

(1) APEX2 Version 2013.6-2, Bruker AXS, Inc.; Madison, WI **2013**.

(2) SAINT Version 8.32b, Bruker AXS, Inc.; Madison, WI **2012**.

(3) Sheldrick, G. M. SADABS, Version 2012/1, Bruker AXS, Inc.; Madison, WI **2012**.

(4) Sheldrick, G. M. SHELXTL, Version 2013/3, Bruker AXS, Inc.; Madison, WI **2013**.

(5) International Tables for X-Ray Crystallography 1992, Vol. C., Dordrecht: Kluwer Academic Publishers.

(6) APEX2 Version 2011.4-1, Bruker AXS, Inc.; Madison, WI **2011**.

(7) SAINT Version 7.68a, Bruker AXS, Inc.; Madison, WI **2009**.

(8) Sheldrick, G. M. SADABS, Version 2008/1, Bruker AXS, Inc.; Madison, WI **2008**.

(9) Sheldrick, G. M. SHELXTL, Version 2008/4, Bruker AXS, Inc.; Madison, WI **2008**.

(10) Flack, H. D., Parsons, S. Acta. Cryst., A60, s61, **2004**.

(11) APEX2 Version 2014.11-0, Bruker AXS, Inc.; Madison, WI **2014.**

(12) SAINT Version 8.34a, Bruker AXS, Inc.; Madison, WI **2013.**

(13) Sheldrick, G. M. SADABS, Version 2014/5, Bruker AXS, Inc.; Madison, WI **2014.**

(14) Sheldrick, G. M. SHELXTL, Version 2014/7, Bruker AXS, Inc.; Madison, WI **2014.**

(15) APEX2 Version 2010.3-0, Bruker AXS, Inc.; Madison, WI **2010.**

(16) (a) Spek, A.L. SQUEEZE, Acta Cryst. **2015**, C71, 9-19., (b) Spek, A. L. PLATON, Acta. Cryst. **2009**, D65, 148-155